UNIVERSITÀ DI PARMA

UNIVERSITA' DEGLI STUDI DI PARMA

DOTTORATO DI RICERCA IN
Medicina Molecolare

CICLO XXXII

GCN5 contributes to intracellular lipid accumulation in human primary cardiac fibroblasts in Arrhythmogenic Cardiomyopathy

Coordinatore:
Chiar.mo Prof. Stefania Conti

Tutore:
Chiar.mo Prof. Donatella Stilli
Dr. Alessandra Rossini

Dottorando: Alessandra Pagliaro

Anni 2016/2019

Al vostro dolce sorriso, che non si spegnerà mai.

A nonna Adele e nonno Giuseppe

This doctoral thesis is subjected to a 36-months embargo period

Abstract

Arrhythmogenic cardiomyopathy (ACM) is a genetic disorder due to mutations in desmosomal genes, showing low penetrance and variable expressivity. It is phenotypically characterized by progressive myocardial fibro-fatty replacement, ventricular arrhythmias and sudden death. Arrhythmias can be treated by the implantation of a cardioverter device, while for the fibro-fatty degeneration no conventional therapies exist except for heart transplantation in patients with end-stage heart failure.

For years, ACM has been considered as a cardiomyocyte disease, though recent evidences underline a role of cardiac stromal cells (CStCs) as a source of adipocytes in ACM hearts. Therefore, in this study CStCs have been used as *in vitro* model for the investigation of ACM. CStCs are cells of mesenchymal origin particularly abundant in the myocardium, and involved in many aspects of cardiac functions, such as synthesis and deposition of extra cellular matrix (ECM), cell-cell communication, intercellular signaling and production of growth factors and cytokines. They also have a potential to differentiate into several other cell types, including adipocytes.

Several studies demonstrate that histone acetyltransferase GCN5 facilitates adipogenesis through the regulation of PPARγ, master gene of adipogenesis. The aim of this work is to evaluate whether GCN5 is involved in intracellular lipid accumulation in human primary ventricular CStCs obtained from ACM patients and healthy donors (NON ACM).

Therefore, CStCs have been isolated from ventricular samples obtained from patients undergoing biopsies for diagnostic reasons at the Centro Cardiologico Monzino (Milano, Italy). CStCs are cultured, amplified in basal medium (BM) and characterized by flow cytometry. Western Blot analysis show that, when cultured in BM, ACM CStCs express higher GCN5 protein levels compared to NON ACM CStCs. Interestingly, we observe that GCN5 down-modulation by shRNA silencing significantly reduce intracellular lipid accumulation in ACM CStCs when exposed to an adipogenic milieu (AM). In addition, when CStCs are treated with 200 μmol/L MB-3, a specific inhibitor of GCN5, we also observe a dramatic reduction of lipid accumulation in ACM CStCs. Therefore, we try to investigate the mechanisms involved in the reduction of lipid accumulation after GCN5 inhibition/knockdown. A preliminary RNAseq analysis of ACM CStCs exposed to adipogenic medium and adipogenic medium in presence of MB-3, reveal the modulation of several interesting classes of genes, namely those associated with extracellular matrix re-organization, metabolic processes and redox balance. These evidences should be considered

as preliminary and further analysis are required to confirm the data. However, in agreement with the transcriptome preliminary evidence, MB-3 administration is able to restore mitochondrial ROS concentration that results upregulated in ACM CStCs compared to NON ACM. We have also collected preliminary data regarding the respiratory activity of NON ACM CStCs and ACM CStCs after the exposure to adipogenic medium, observing an increased oxidative phosphorylation in ACM CStCs. Taken together, all these observations, sustain a possible role of mitochondria in ACM pathogenesis. Finally, we also have evidences of GCN5 expression in *ex-vivo* samples: approximately the 30% of spindle fibroblast-like cells present in the region of fatty substitution of three ACM human right ventricles samples show increased positivity for GCN5 evaluated by immunohistochemistry evaluation.

The collected results indicate that GCN5 inhibition might reduce fat accumulation of ACM CStCs, possibly by modulating intracellular redox processes. Further experiments are mandatory to elucidate GCN5 function and its downstream players in the onset of the disease. These results might pave the way for the identification of possible new target for pharmacological interventions.

Contents

Index of Figures

Index of tables

Abbreviations

α -sma: α-smooth muscle actin
Ab: abnormalities
ACM: Arrythmogenic Cardiomyopythay
AM: Adipogenic Medium
AD: Autosomal Dominant
ADP: Adenosine diphosphate
AG: angiography
AKRs: Aldo-Keto Reductases
ALDH2: Aldehyde dehydrogenase 2
Alpha T-cat: alpha t catenin
AM: Adipogenic Medium
Ama: Antimycin
APC: Adenomatous Polyposis Coli
AR: Autosomal Recessive
ARVC: Arrhyhmogenic Right Ventricular Cardiomyopathy
ARVD: Arrhyhmogenic Right Ventricular Dysplasia
ATP: Adenosine triphosphate
β-cat: beta catenin
BCA: BiCinchoninic Acid
bFGF: basic fibroblast growth factor
BM: Basal Medium
BMCStC: Bone Marrow Mesenchymal Cells
BSA:Bovine Serum Albumin
cAMP: Cyclic adenosine monophosphate
C/EBPalpa:CCAAT/enhancer-binding protein alplha
C/EBPbeta:CCAAT/enhancer-binding proteins beta
C/EBPdelta:CCAAT/enhancer-binding proteins delta
CBP: Cre-binding protein
CCCP: carbonyl cyanide m-chlorophenyl hydrazone
cGMP: cyclic guanosine monophosphate
CK1: Casein Kinase 1
CMR: cardiac magnetic resonance
CMs:cardiomyocytes
CPVT:Catecholaminergic polymorphic ventricular tachycardia
CStC: Cardiac Stromal Cell
CTNNA3: αT-catenin
DCM: Dilated Cardiomyopathy
DES: Desmin
DMSO: dimethyl sulfoxide
DSC2: Desmocollin 2
DSG2: Desmoglein 2
Dsh: Disheveled
DSP: Desmoplakin
DTT; Dithiothreitol
EAM: electroanatomic voltage mapping
ECG:electrocardiogram
ECL: Enhanced ChemiLuminescence
ECM: Extracellular Matrix
EDTA: Ethylenediaminetetraacetic acid
EGTA: ethylene glycol tetra-acetic acid
EMB: endomyocardial biopsy
EMS: Emergency Medical Service
ETS: electron transfer system
FADH2: flavin adenine dinucleotide
FBS: Foetal Bovine Serum
FITC: Fluorescein isothiocyanate,
FLNC: Filamin C
FZD: Frizzled receptors
G: GLutammate
GCN5: General Control of Amino Acid Synthesis Protein 5-Like 2
GDP: Guanosine Diphosphate
GFP: Green Fluorescent Protein
GNATs: GCN5-related N-acetyltransferases
GSH: Glutathione
GSK3: Glycogen Synthase Kinase 3
GSSH: Glutathione Sintethase
GTP: Guanosine Triphosphate
H_2O_2: Hydrogen Peroxide
H3K27ac: H3lysines 27 acetilation
H3K9ac: H3lysines 9 acetilation
HATs: histone acetyltransferases
HBSS: Hank's Balanced Salt Solution
HCM: Hypertrophic Cardiomyopathy
HDACs: histone deacetylases
HRP: horseradish peroxidase
HSC: Hematopoietic Stem Cells
IBMX: 3-isobutyl-1-methylxanthine
ICD: Cardioverter Defibrillator
ID: Intercalate disc
ILK: Integrin Linked Kinase
IMDM: Iscove's Modified Dulbecco's Medium
iPSC: Induced Pluripotent Stem Cells
iPSC-CMs: Induced Pluripotent Stem Cells derived Cardiomyocytes
ISCT: International Society for Cellular Therapy
JUP: Junction Plakoglobin
LATS1: Large tumor suppressor 1
LATS2: Large tumor suppressor 2
L-Glu: L-Glutamine
LDS: Lithium Dodecyl Sulfate
LMNA: Laminin A
LPR5: low-density lipoprotein-receptor-related protein 5
LPR6: low-density lipoprotein-receptor-related protein 6
LV: Left Ventricle

M: malate
MB-3: (2R,3S)-rel-4-Methylene-5-oxo-2-propyltetrahydrofuran-3-carboxylic acid
MiR05: mitochondrial respiration medium
MitoSox: Mitochondrial Superoxide Indicator
MLC: myosin light chain
MOI: multiplicity of infection
MRTF/SRF: myocardiac related transcription factor A/serum response transcription factor
MSC: Mesenchymal stem cells
MST1: mammalian sterile 20-related kinase 1
MST2: mammalian sterile 20-related kinase 2
MStCs: Mesenchymal or Marrow Stromal Cells
MYPT: myosin phosphatase targeting protein
MYST: MOZ, Ybf2/Sas3, Sas2 and Tip60'-related HATs
NAC: N-acetylcysteine
NaCl: Sodium Cloride
NAD+: Nicotinamide adenine dinucleotide
NADPH: Nicotinamide adenine dinucleotide phosphate
NF2: Neurofibromin 2
NOS: Nitric oxide synthases
NP-40: Igepal
NQO1: Quinone reductase
OsO4: osmium tetroxide
OXPHOS: Oxidative phosphorilation
Pai1: Plasminogen activator inhibitor-1
PBS: Phosphate-Buffered Saline
PBS-T: Phosphate-Buffered Saline Tween
PCAF: P300/CBP-associated factor
Pen/strep: Penicillin/ Streptomycin
PFA: paraformaldehyde
PG: Plakoglobin
PGC1-alpha: proliferator-activated receptor gamma coactivator 1-alpha
PKA: phosphodiesterases
PKC-a: Protein Kinase C-α
PKP2: Plakophilin 2
PLIN-1: Perilipin-1
PLN: Phospholamban
PNLPA2: Patatin Like Phospholipase Domain Containing 2
PPAR: peroxisome proliferator-activated receptors
PPARy: Peroxisome Proliferator Activated Receptor Gamma
PPP1R13: Protein Phosphatase 1 Regulatory Subunit 13 Like
PVC: Premature Ventricular Contraction
PVDF: polyvinylidene fluoride
QPc: ubiquinone binding protein
qPCR: Reverse transcription polymerase chain reaction
RCM: Restrective Cardiomyopathy
RISP: Rieske iron sulfur protein
ROCK: Rho kinases
ROS: Reactive Oxygen Species
Rot: Rotenone
ROX state: residual oxygen consumption
RT: Room Temperature
RV: Right Ventricle
RYR2: Ryanodine Receptor 2
S: Succinate
SAGA: Spt-Ada-Gcn5 acetyltransferase
SCD: Sudden Cardiac Death
SCN5A: Sodium Channel Alpha Subunit 5
SDS: Sodium Dodecyl Sulfate
SDS-PAGE: Sodium Dodecyl Sulfate–polyacrylamide gel electrophoresis
SIRT1: Sirtuin 1
SRC3: Nuclear hormone-related HATs SRC1 and ACTR
SUIT: substrate uncoupler inhibitor titration
TAF: General transcription factor HATs including the TFIID subunit TBP-associated factor-1
TAZ: transcriptional co-activators with a PDZ-binding motif
TCF/LEF:T-cell factor/lymphoid enhancing factor
TEAD: TEA domain transcription factors family
TEM: Transmission Electron Microscopy
TGFβ: Transforming growth factor beta
TGFβ1: Transforming growth factor beta 1
TGFβ2: Transforming growth factor beta 2
TGFβ3: Transforming growth factor beta 3
TGFβR:Transforming Growth Factor Receptor
TJP1: Zonula Occludens 1
TMEM43: Transmembrane Protein 43
TP63: Tumor Protein 63
TTN:Titin
VT: Ventricular Tachicardia
WB: Western Blot
YAP: Yes-associated protein

1 Introduction

1.1 Sudden Cardiac Death and cardiomyopathies: an overview.

Sudden cardiac death (SCD) is defined as "sudden and unexpected death occurring within one hour of the onset of symptoms or occurring in patients found dead within 24 hours of being asymptomatic and presumably due to a cardiac arrhythmia or hemodynamic catastrophe". SCD is the leading cause of death in the United States, responsible for 170.000 to 450.000 deaths annually [1]. According to the Emergency Medical Service (EMS), the incidence of SCD is lower in Asia (52.5 cases per 100000 persons per year) than Europe (86.4 cases per 100000 persons per year), while in United States, Ireland and Netherlands the incidence corresponds to 40-100 cases per 100000 people in the general population [2]. SCD generally develops in elderly due to ventricular fibrillation in the context of coronary heart disease [3]. However, in people under the age of 60 years the leading cause of SCD are cardiomyopathies [4].

A detailed classification of cardiomyopathies has been suggested by Elliot and his colleagues [5, 6]. Primary cardiomyopathies are a group of alterations in the structure and in the function of myocardium [7], which cannot be included in the set of artery diseases, valvular heart diseases, hypertension or congenital heart diseases. They can be genetic, nongenetic or acquired, and are all characterized by being solely or predominantly confined to heart muscle. Secondary cardiomyopathies show pathological myocardial involvement as part of a multiorgan disorders [7].

The most common primary cardiomyopathies are: Dilated Cardiomyopathy (DCM), Hypertrophic Cardiomyopathy (HCM), Arrhythmogenic Cardiomyopathy (ACM), and Restrictive Cardiomyopathy (RCM) [5].

1.2 Arrhythmogenic Cardiomyopathy

1.2.1 Definition and history

Arrhythmogenic Cardiomyopathy (ACM) is a genetically transmitted cardiac disorder of the heart, phenotypically characterized by structural and functional alterations, which mainly involve the right ventricle (RV) [8]. ACM is characterized by a progressive loss of cardiomyocytes, followed by fibro-fatty replacement of the myocardium [9]. The disruption of the myocardial architecture leads to an alteration of the normal electrical impulse conduction, increasing the risk of ventricular arrythmias and SCD [10].

The pathology was described for the first time in 1736 by Giovanni Maria Lancisi, Pope's physician and Professor of Anatomy in Rome, in a book entitled "*De Motu Cordis et Aneurysmatibus*", in which he described the history of a family with disease recurrence in four generations. The disease was characterized by symptoms as palpitations and dilatations of the RV, heart failure and SCD [11]. Later in 1819, the pathology was described more in detail by Laennec, who introduced for the first time the concept of the fat accumulation in the heart [6]. In 1982, Marcus and Fontaine reported the first comprehensive clinical description of the disease and they used for the first time the term "Arrhythmogenic Right Ventricular Dysplasia" (ARVD). They described a clinical condition observed in 24 patients with ventricular tachyarrhythmias of left bundle branch block morphology [12].

Nowadays, the pathology is no longer considered as a dysplastic disorder but as a cardiomyopathy, and therefore the name has been changed in "Arrhythmogenic Right Ventricular Cardiomyopathy" (ARVC). [13]. However, the increasing evidences of the involvement of the both ventricles led to the broader term "Arrhythmogenic Cardiomyopathy" [14] [15].

1.2.2 Incidence

ACM is an autosomal dominant disease with an estimated incidence of 1:5000 cases in the worldwide population [16]. Interestingly, the disease shows a higher prevalence in the northeast of Italy, where it reaches an incidence of 1:2000 [17]. The disease is one of the most common causes of SCD in young people (< 35 years) and it accounts for the 10% of deaths of undiagnosed cardiac diseases in patients under 65 years [18, 19]. Data from literature underline that 11-22% of SCD in young athletes occurring during physical exercise, is due to undiagnosed ACM [20]. Specifically, in Italy and in Denmark, ACM represents the most frequent cause of SCD in young athletes (25% higher than other industrialized countries) [21].

A possible explanation could be that exercise may precipitate cardiac arrhythmias, because of myocardial stretch and sympathetic overactivity. ACM affects more men than women with a ratio of 3:1 [15], probably due to more intense physical exercise and biological factors, as estrogens in women, able to prevent apoptosis of myocardial cells [22]. The onset of the disease generally occurs in adolescent and in young age, but in some cases the manifestation can occur also later [23]. However, many cases are asymptomatic or clinically silent and they are not diagnosed or, even worst, they are mistakenly classified. It has also been demonstrated that in the 50% of ACM patients, SCD is the first manifestation of the

pathology [24],[25]. Therefore, the exact prevalence of the disease could be even higher [24].

1.2.3 Pathology

Although ACM shows a spectrum of different phenotypes, ranging from the involvement of only one of the two ventricles to bi-ventricular forms up to different nature of the myocardium replacement in the heart, the natural course of the disease can be subdivided in four phases [26]:

1. *Concealed phase,* characterized by minimal structural abnormalities of the RV with or without ventricular arrhythmias. This phase is generally asymptomatic, and the cardiac arrest could be the first and, paradoxically, also the last manifestation of the disease, especially in young athletes during physical exercise. In the early phases, the fibro-fatty replacement starts at the level of the so-called ´triangle of dysplasia´ that consists of inflow, outflow and apical regions of the RV and then the substitution can extend to the left ventricle (LV) [54].
2. *Over arrhythmic phase*, characterized by palpitations, syncope, right ventricular arrythmias, which can vary from premature ventricular beats, to non-sustained ventricular tachycardia up to ventricular fibrillation leading to cardiac arrest. Generally this phase is associated with functional and structural abnormalities in RV, detectable by imaging [27];
3. *Global right ventricular dysfunction phase,* showing a complete involvement of all the right ventricular myocardium, leading to impaired contractility and isolated right heart failure. In this stage the activity and the function of the LV are still preserved;
4. *Final phase,* characterized by a biventricular alterations and it generally leads to heart failure [19].

The frequent and sometimes predominant involvement of the LV suggests that ACM is a complex disease, with a broad spectrum of phenotypes and three main possible patterns of expressions have been identified:

- *Classic form (39% of cases)* is characterized by an increased ratio of RV to LV volume, with a more severe involvement of the RV, while the LV is only involved in the late stage of the disease. Clinical hallmarks of this pattern are negative anterior T waved and ventricular arrhythmia with left bundle branch block morphology [19]*;*
- *Left dominant form, (5% of cases),* which shows an involvement of the LV and is characterized by one or more, at the same time, of the following features: LV wall

abnormalities, chamber dilatation and systolic impairment. Clinical hallmarks are ventricular arrhythmias of right bundle branch block morphology and infero-lateral T wave inversion at electrocardiogram [19];

- *Biventricular form (56% of cases)* is defined by early and parallel involvement of RV and LV. When the disease is already in an advanced state, a biventricular dilatation and systolic impairment is observable

In two-third of ACM cases, another pathological marker is the infiltration of inflammatory cells, CD43 positive T-lymphocytes, associated with focal myocyte necrosis. Considering that the regeneration of cardiac myocytes is limited, fibrofatty replacement is stimulated. However, it is not clear if inflammation is caused by cardiomyocyte death or whether it results from viral infections or immune reaction [28-30].

1.2.4 Genetics

ACM is a genetic disorder, inherited with an autosomal dominant transmission, incomplete penetrance [12, 31, 32] and extremely variable expressivity [26], since, among the carriers of the same causative mutations the phenotype can be highly variable. This suggests that not only genetics, but also epigenetic, lifestyle and environmental factors, as physical exercise might have a role in the development of ACM [32].

ACM has been initially described as a disease of the cardiac desmosomes [33]. Desmosomes are complex structures localized at the level of plasma membrane and involved in the cell-cell adhesion and tissue integrity**.** Their function is fundamental especially in tissues subjected to mechanical stress, as skin and heart [34]. Approximately 50% of symptomatic individuals harbor a mutation in one of the five major components of the cardiac desmosome [35]: *DSP* (desmoplakin) [36], *JUP* (plakoglobin) [37], *PKP2* (plakophilin 2) [38], *DSG2* (desmoglein 2) [39], and *DSC2* (desmocollin 2) [40], with *PKP2* mutations being the most prevalent and making up 30% of the cases [41].

The *JUP* gene codes for the plakoglobin (PG) also called y-catenin; it is a member of the armadillo family and it has been described as the first causative gene associated to ACM. The armadillo family includes also β-catenin, the main player of the Wnt pathway, already associated to ACM pathogenesis (see the dedicated chapter below). The *PKP2* gene is expressed in the heart [38] and encodes the plakophilin-2 protein belonging to the Armadillo family, which interacts with plakoglobin and desmoplakin [42]. *DSG2* and *DSC2* genes code for desmoglein 2 and desmocollin 2 proteins, respectively. Both proteins belong to the cadherin family [43]. The *DSP* gene encodes desmoplakin , which is a member of plakin

family and it is a protein of the cytoplasmic desmosomal plaque, responsible for the link between desmosomes and intermediate filaments [32].

More recently, ACM has been described as a disease of the intercalated discs (ID, [44]), complex structures located in the myocardium at the end to end site of contact between cardiomyocytes (CMs). Cardiac intercalated discs provide mechanical and electro-metabolic coupling among cells. Mechanical communication is guaranteed by the interaction of desmosomes and *adherens junctions* in the so-called *area composita* [45]. Adherens junctions are essential for the transmission of force between cells, necessary for synchronous contraction [46]. The main transmembrane component of the cardiac adherens juctions is N-cadherin **(**NCad) [47]. Attached to the cytoplasmatic tail of the cadherins, there are β-catenin (β-cat) and PG both bound to αT-catenin (αT-Cat), which directly interacts with sarcomeric actin microfilaments [26].

Electro-metabolic coupling between adjacent cardiac cells depends on gap junctions [48]. *Gap junctions* were discovered in 1967 by Revel and Karnovsky [49], who observed that the membranes of two different cells were in contact, but not fused, and separated by a gap with interposed junctions. Gap junctions are composed of molecules belonging to the connexin family, among which the most important subtype in the heart Connexin 43, 45 and 40 [50]. Of interest, it has been shown that gap junctions and the voltage-gated sodium channel complex interact amongst each other in an area called cardiac *connexome* [51], in which also desmosomal proteins are present [52]. In Fig. 1 a schematic illustration of the intercalated disc is reported.

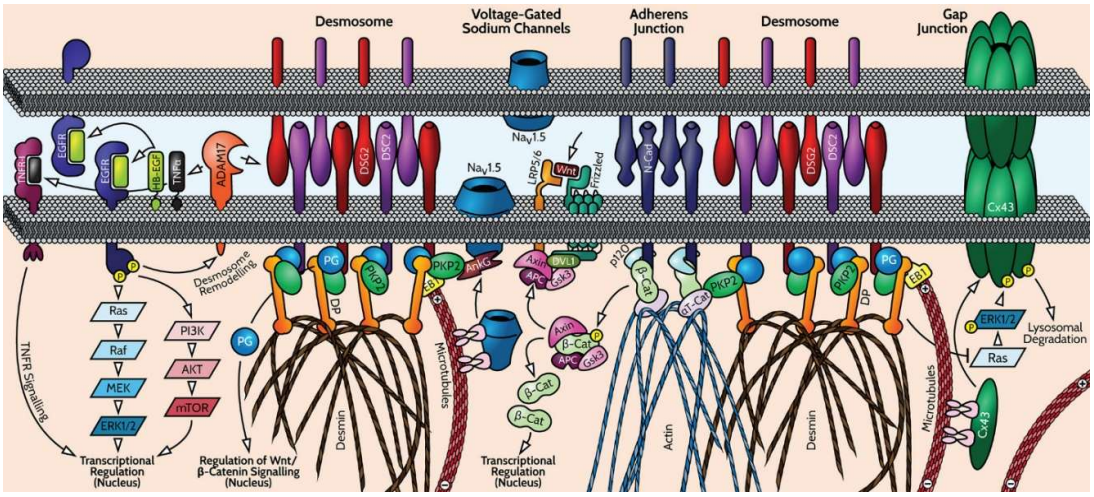

Figure 1. Complex integration of mechanical and electrochemical signaling at cardiac intercalated discs. Abbreviations: **PG:** Plakoglobin, **DSP:** Desmoplakin, **PKP2:** Plakophilin 2, **DSC2:** Desmocollin, **NCad:** N-cadherin, **β -cat:** beta-Catenin, **p120:** p 120 catenin, **αT-Cat:** alpha T-catenin, **Cx43:** connexin-43, **Ank G:** adaptor protein ankyrin G. **Elliott P. et al., 2019.**

In the last years, novel putative causative mutations have been identified in genes encoding proteins of *area composita* and *connexome*, as *CTNNA3* [53], *CDH2* [54], *SCN5A* [55] and *TJP1* [56].

Notably, also mutations in non-ID genes have been associated with the disease, as *TMEM43* [57], *TGFβ3* [58], *DES* [59], *LMNA* [60], *PLN* [61] , *TP63* [62], *ILK* [63], *FLNC* [64] and *PPP1R13 [65]*.

Moreover, mutations in *RYR2* were thought to cause ACM, but the phenotype suggests a phenocopy of polymorphic ventricular tachycardia (CPVT) [66] [67]. The Table 1 reports a list of the 20 genes which have been associated with ACM.

Table 1. List of genes associated with ACM. AR = Autosomal Recessive; AD = Autosomal Dominant.

Gene	Protein	Mode of inheritance
JUP	Plakoglobin	AR/AD
RYR2	Ryanodine Receptor 2	AR/AD
DSP	Desmoplakin	AR/AD
PKP2	Plakophilin-2	AD
TGFβ3	Transforming Growth Factor β3	AD
DSG	Desmoglein-2	AR/AD
DSC2	Desmocollin-2	AD/AR
TMEM43	Transmembrane Protein 43	AD
DES	Desmin	AD
TTN	Titin	AD
LMNA	Lamin A/C	AD
PLN	Phospholamban	AD
CTNNA3	αT-catenin	AD
FLNC	Filamin C	AD
SCN5A	Sodium Channel Alpha Subunit 5	AD
CDH2	N-Cadherin	AD
TJP1	Zonula Occludens 1	AD
TP63	Tumor Protein 63	AD
ILK	Integrin Linked Kinase	AD
PPP1R13	Protein Phosphatase 1 Regulatory Subunit 13 Like	AD

Although the principal trend of the transmission is the autosomal one, recessive variant forms have been reported. One of these forms is the Naxos disease, caused by a two-base pair deletion in *JUP* gene, corresponding to a frameshift and a premature termination of the protein. Phenotypically Naxos disease is associated to cutaneous manifestations, as non-epidermolytic palmoplantar keratosis and wooly hair, coupled with cardiac disorders with a penetrance nearly to 100% [26]. The name is due to the fact that this form was for the first time described in some families who lived in the homonymous island in Greece [68]. Another form transmitted with a recessive mode was described in 1990, and it was named Carvajal Syndrome [69] phenotypically similar to Naxos disease, but with also a left sided dilated cardiomyopathy and transmitted with a recessive inheritance. The mutation (c.7901delG) in the *DSP* gene was for the first time described mapping three Ecuadorian families with the Carvajal syndrome [32]. The association between skin and heart manifestations of this form of ACM could be explained by the similar junction apparatus (desmosome), responsible for cell-to-cell adhesion, present both in epidermal cells and myocytes. Other homozygous mutations have been found to be responsible of ACM, and these forms display only a cardiac-restricted phenotype, without evidences of hair or skin irregularities. Three mutations involve the gene encoding DSC2:1) c.536A>G (p.D179G) [70], 2) c.712_714delGAT [71] 3), c.1660C>T (p.Q554X), homozygous truncation mutation [72]. Two other homozygous mutations have been reported in the gene encoding DSG2: 1) (p.F531C) [73] and 2) c.1003A > G [74], with an involvement of both ventricles. Very recently another homozygous missense variant (c.245G>A, p.G82D) in Patatin Like Phospholipase Domain Containing 2 (PNPLA2), an enzyme involved in the hydrolysis of triglycerides in fatty-acids and diacylglycerol, has also been identified and associated with massive lipogenesis and fibrosis at the level of myocardium [75].

Although ACM genetic fundamentals have been thoroughly examined, the reasons underpinning low penetrance and variable expressivity [16] are still not properly understood. Genetic determinants, as compound or digenic heterozygosity, may play a role [76], as well as environmental factors. Rigato et al. also demonstrated that patients with multiple mutations showed a more severe phenotype compared to the single mutation carriers [77].

1.2.5 Diagnosis

The clinical diagnosis of ACM is still very complicated due to the spectrum of phenotypic expressions that the pathology shows, and this explains also because the incidence of the pathology is underestimated [19]. Analyzing the electrocardiogram (ECG) of ACM patients, abnormalities are visible, as the inverted T waves in the right precordial leads (v1-v3) and

ventricular arrhythmias. Many pathologies can be confused with ACM, as myocarditis, dilated cardiomyopathy, Brugada syndrome, coronary heart disease, pulmonary hypertension and intracardiac left to-right shunts.

Therefore in 1994 the International Task Force Criteria for the diagnosis of ACM have been proposed, in order to give guidelines for the diagnosis of the disease. The criteria were distinguished on a scoring system with "major" and "minor" criteria, classified in six categories. The criteria have been set up based on the clinical experience, family history, structural, functional and electrocardiographic abnormalities in patients with severe disease [78]. However, lack of sensitivity for identification of early-stage and minor form of ACM have been reported during the years. For this reason, in 2010, a revision of the guidelines has been proposed, in order to improve the diagnostic sensitivity (Table 2) [79]. In order to state ACM diagnosis, the presence of two major criteria, one major criteria with two minor criteria, or four minor criteria belonging to different categories are required. An ACM diagnosis is defined borderline if one major and one minor criterion or three minor criteria from different categories are satisfied. A possible diagnosis is obtained also by one major or two minor criteria from different categories [80].

The main techniques used for the investigation of ACM are electrocardiography, echocardiography, cardiac magnetic resonance (CMR), angiography and RV biopsy [79]. CMR is a non-invasive imaging method, which can give an indication of the morphology and the functionality of both ventricles, giving a quantitative assessment of ventricular volumes and ejection fractions and specifications of myocardial tissue. Of note, the observation of fatty infiltration in the RV only cannot be considered as sufficient diagnostic criterion since it also can be observed in other infiltrative diseases such as sarcoidosis, amyloidosis, congenital heart diseases and pulmonary hypertension [81, 82]. Other invasive techniques are also performed, including RV angiography and endomyocardial biopsy (EMB). The latter is less common and carry out only by specialized centers, due to the increased risks to sample the RV free wall or the affected areas identified by using 3-dimensional electroanatomic voltage mapping (EAM) [83]. EAM has recently been used for the diagnosis of suspicions cases of ACM, with unexplained ventricular arrythmias. This method is highly sensitive, able to recognize low-voltage regions which reflect fibro-fatty replacement of the myocardium [80], [84].

The discovery of mutations in specific genes involved in the pathogenesis of ACM has offered the possibility to increase the accuracy of the clinical diagnosis [17].The potential

clinical utility of genetic screening is based on the possibility 1) to obtain a diagnosis in the early stage of the disease, 2) confirm the diagnosis in a proband with a clinical suspicion of ACM, 3) distinguish true cases from phenocopies, 4) identify genetically-affected family members at a preclinical stage, and 5) stratify the risk of arrythmias and SCD [85]

However, the diagnosis of ACM remains still a challenge, and new tools need to be discovered. For instance, plakoglobin mislocalization from intercalated disc could represent a good candidate, though the main disadvantage is the fact that immunohistochemistry can be only performed on samples obtained with invasive procedures [86, 87]. Moreover, the positivity to this test could also be ascribable to other pathologies as sarcoidosis and giant cell myocarditis [88]. Sommariva et al. observe lower plasma level of miR-320 in ACM patients: This result is particularly interesting considering that the alterations in the level of this miR are not influenced by the physical activity of ACM patients compared to controls [89], leading to the conclusion that the expression of this biomarker is not linked to mechanical stretch and heart remodeling and suggesting its role as possible biomarker for the disease.

Table 2. Revised Task Force Criteria [79]

Major	Minor
I. Global or regional dysfunction and structural alterations*	
By 2D echo	**By 2D echo**
• Regional RV akinesia, dyskinesia, or aneurysm and 1 of the following (end diastole): ○ PLAX RVOT ≥ 32 mm (corrected for body size [PLAX/BSA] ≥ 19 mm/m²) ○ PSAX RVOT ≥ 36 mm (corrected for body size [PSAX/BSA] ≥ 21 mm/m²) ○ *or* fractional area change ≤ 33%	• Regional RV akinesia or dyskinesia *and* 1 of the following (end diastole): ○ PLAX RVOT ≥ 29 to <32 mm (corrected for body size [PLAX/BSA] ≥ 16 to <19 mm/m²) ○ PSAX RVOT ≥ 32 to <36 mm (corrected for body size [PSAX/BSA] ≥ 18 to <21 mm/m²) ○ *or* fractional area change > 33% to ≤40%
By MRI	**By MRI**
• Regional RV akinesia or dyskinesia or dyssynchronous RV contraction *and* 1 of the following: ○ Ratio of RV end-diastolic volume to BSA ≥ 110 mL/m² (male) or ≥100 mL/m² (female) ○ *or* RV ejection fraction ≤ 40%	• Regional RV akinesia or dyskinesia or dyssynchronous RV contraction *and* 1 of the following: ○ Ratio of RV end-diastolic volume to BSA ≥ 100 to <110 mL/m² (male) or ≥90 to <100 mL/m² (female) ○ *or* RV ejection fraction > 40% to ≤45%
By RV angiography	
• Regional RV akinesia, dyskinesia, or aneurysm	
II. Tissue characterization of wall	
• Residual myocytes < 60% by morphometric analysis (or <50% if estimated), with fibrous replacement of the RV free wall myocardium in ≥1 sample, with or without fatty replacement of tissue on endomyocardial biopsy	• Residual myocytes 60% to 75% by morphometric analysis (or 50% to 65% if estimated), with fibrous replacement of the RV free wall myocardium in ≥1 sample, with or without fatty replacement of tissue on endomyocardial biopsy
III. Repolarization abnormalities	
• Inverted T waves in right precordial leads (V_1, V_2, and V_3) or beyond in individuals > 14 years of age (in the absence of complete right bundle-branch block QRS ≥ 120 ms)	• Inverted T waves in leads V_1 and V_2 in individuals > 14 years of age (in the absence of complete right bundle-branch block) or in V_4, V_5, or V_6 • Inverted T waves in leads V_1, V_2, V_3, and V_4 in individuals > 14 years of age in the presence of complete right bundle-branch block
IV. Depolarization/conduction abnormalities	
• Epsilon wave (reproducible low-amplitude signals between end of QRS complex to onset of the T wave) in the right precordial leads (V_1 to V_3)	• Late potentials by SAECG in ≥1 of 3 parameters in the absence of a QRS duration of ≥110 ms on the standard ECG • Filtered QRS duration (fQRS) ≥114 ms • Duration of terminal QRS <40 µV (low-amplitude signal duration) ≥38 ms • Root-mean-square voltage of terminal 40 ms ≤ 20 µV • Terminal activation duration of QRS ≥ 55 ms measured from the nadir of the S wave to the end of the QRS, including R′, in V_1, V_2, or V_3, in the absence of complete right bundle-branch block
V. Arrhythmias	
• Nonsustained or sustained ventricular tachycardia of left bundle-branch morphology with superior axis (negative or indeterminate QRS in leads II, III, and aVF and positive in lead aVL)	• Nonsustained or sustained ventricular tachycardia of RV outflow configuration, left bundle-branch block morphology with inferior axis (positive QRS in leads II, III, and aVF and negative in lead aVL) or of unknown axis • >500 ventricular extrasystoles per 24 hours (Holter)
VI. Family history	
• ARVC/D confirmed in a first-degree relative who meets current Task Force criteria • ARVC/D confirmed pathologically at autopsy or surgery in a first-degree relative • Identification of a pathogenic mutation† categorized as associated or probably associated with ARVC/D in the patient under evaluation	• History of ARVC/D in a first-degree relative in whom it is not possible or practical to determine whether the family member meets current Task Force criteria • Premature sudden death (<35 years of age) due to suspected ARVC/D in a first-degree relative • ARVC/D confirmed pathologically or by current Task Force Criteria in second-degree relative

1.2.6 Treatment

Considering that the causal mechanisms of ACM are poorly understood, and the symptoms not well-defined, it is very difficult to define a standard therapeutic approach. The main goal is to prevent life-threatening arrhythmias and in particular the SCD [90]. Possible proposed interventions are changes in the lifestyle, reduction of strenuous physical exercise and anti-arrhythmic drugs administration. Indeed, it has been shown that combination of beta-blockers and amiodarone can suppress the non-sustained VT and it can reduce the frequency of sustained ventricular arrhythmias and the VT rate [79].

The surgical alternative is the implantation of a cardioverter defibrillator (ICD), a battery powered device placed under the skin that checks constantly the heart rate by thin wires connected directly to the heart. If an abnormal rhythm is detected, the device sends an electric shock to restore the normal heartbeat [91].

In patients at the final stage of the disease and with progressive heart failure, a heart transplantation is suggested [92] [93]. Healthy mutation carriers should undergo periodic cardiac follow-up with the aim of an early identification of warning symptoms.

1.2.7 Molecular pathways associated with ACM

Considering that a large number of already described mutations associated to ACM phenotype occur in genes responsible for mechanical connections, it has been speculated that alterations in the ID might be responsible for an alteration in the cell-adhesion [44] with a subsequent stretch-induced intracellular stress. This could lead firstly to lipotoxicity and secondly to CMs lipoapoptosis [94, 95]. However, the cellular mechanism of CMs degeneration has not being completely understood, yet. Several groups tried to propose a possible molecular pathway for the fatty accumulation observed in ACM patients, starting from the idea that mutations in desmosomal genes can lead to a re-localization of the PG from the membrane to the nucleus [96]. This translocation seems to suppress the canonical Wnt pathway, inducing a switch to adipogenesis [97].

The Wnt pathway consists of a family of highly conserved secreted glycoproteins, able to control several biological functions as cell proliferation, survival, differentiation and adult tissue homeostasis [98]. Specifically, the Wnt pathway regulates the accumulation of β-catenin, a protein also located in the adherens junction. When β-catenin is not bound to Wnt proteins, it is sequestered in the cytosol by a degradation complex, composed of four proteins: Casein Kinase 1 (CK1), Glycogen Synthase Kinase 3 (GSK3), Axin and Adenomatous Polyposis Coli (APC) [99]. At that stage, GSK3 phosphorylates β-cat that

does not accumulate in the cytoplasm, but it is degraded after the ubiquitination. While, when the Wnt pathway is active, Wnt ligands, as Wnt1 and Wnt3a bind Frizzled receptors (FZD), leading to the activation of phosphoprotein Disheveled (Dsh) and low-density lipoprotein-receptor-related protein, LRP5 o LRP6 co-receptors. This induces the inhibition of GSK3, preventing the phosphorylation of β-cat and allowing its translocation and accumulation at the nuclear level. In the nucleus β-cat binds TCF/LEF (T-cell factor/lymphoid enhancing factor) transcription factors, exerting a cellular response via transcriptional enhancer activity [99].

The Wnt pathway appears as an important switch regulator of myogenesis versus adipogenesis. Indeed, the canonical Wnt/β-cat signaling has been demonstrated to directly regulate the Peroxisome Proliferator Activated Receptor y (PPARy), the key activator of the adipocyte differentiation [100]. Activation of the Wnt/β-cat signaling enhances myogenesis but inhibits adipogenic transcriptional factors like CCAAT-enhancer-binding protein alpha (C/EBPα) and PPARγ, thus maintaining preadipocytes in an undifferentiated state. On the other hand, the suppression of Wnt signalling pathway results in the activation of PPARγ transcription, thus inducing the molecular switching to adipogenesis and proliferation of adipocytes [10, 99].

The fibro-fatty substitution in ACM might be mainly controlled by the altered Wnt pathway through the nuclear translocation of plakoglobin [10]. Indeed, plakoglobin shows approximately 85% sequence identity with β-cat [101], and this leads to the assumption that they can compete for a significant number of functions, such as the nuclear localization and the following binding to TCF/LEF transcription factors. However, the binding site and the effects of the two proteins are different: β-catenin binds the first 50 amino acids of the transcription factors, producing gene transcription, while plakoglobin weakly binds transcription factors from 51 up to 80 amino positions, [102]. The translocation of plakoglobin into the nucleus might occur when there is a compromised cell-cell adhesion due to an ACM mutation [15]. Indeed, previous studies demonstrated that inhibition of desmoplakin expression is sufficient to cause nuclear translocation of plakoglobin, leading to the inhibition of Wnt/β-cat pathway and promoting the switch to adipogenesis [70], [96].

Another interesting pathway which has been proposed as a possible mechanism involved in the fibro-fatty replacement is the Hippo pathway, an evolutionarily highly conserved signalling, composed of a group of serine/threonine kinases [103]. This pathway is involved in several processes, as the control of tissue growth in adults and the regulation of cell

proliferation and differentiation [104]. In mammals, the most common kinases are the mammalian sterile 20-related kinases, 1 and 2 (MST1 and MST2) and the Large tumor suppressor 1 and 2 kinases (LATS1/2). In addition, the Hippo pathway includes two factors: Yes-associated protein (YAP) and the transcriptional co-activators with a PDZ-binding motif (TAZ), and both of them are able to translocate into the nucleus, binding the TEA domain transcription factors family (TEAD family), regulating the transcription of several genes involved in the cell proliferation [104] [105]. Physiologically MST1/2 phosphorylate LATS1/2, allowing the repression of the activity of the two transcriptional coactivators, YAP and TAZ. The Hippo cascade can be started by the phosphorylation of MST1 and 2, mediated by TAO kinases (TAOK1/2/3) [106]: the phosphorylated, and thereby active MST1/2, is now able to phosphorylate SAV1 and MOB1A/B, two scaffold proteins, essential with MST1/2 for the phosphorylation of LATS1/2 [107]. LATS1/2, in the active form, can phosphorylate and inactivate YAP and TAZ [108]. For its importance, the activation of this pathway is regulated at multiple levels by upstream molecules, as KIBRA [109], RAFFs and Neurofibromin 2 (NF2) [110]. In a normal heart, inactive phosphorylated NF2 is localized at the ID, while in ACM patients non-phosphorylated active forms of NF2 are more common. In addition, reduced protein levels of phosphorylated Protein Kinase C-α (pPKC-α), a repressor of NF2, have been observed in ACM cases [110]. pPKC-α requires plakophilin2 as scaffold protein for its localization at the level of ID. An impaired junctional localization of pPKC-α has been seen in ACM patients with mutations in *PKP2,* providing a trigger for the activation of NF2. In ACM hearts, all these disfunctions lead to the activation of the Hippo pathway [111]. In addition YAP is also considered as a trigger for the suppression of Wnt pathway, since it interacts with β-catenin, leading to its sequestration and, therefore promoting a switch to the adipogenic cascade [111].

The Transforming Growth Factor beta (TGFβ) pathway has also been proposed as a possible mechanism for the loss of CMs observed in ACM [112]. TGFβ pathway is a complex signaling, involved in several cellular processes. In particular, it has been demonstrated to be responsible of the regulation of both apoptosis and necrosis of myocytes and this pathway can also influence the accumulation of fibrotic tissue and hypertrophy in the heart [100], [113]. TGFβ can interact with type I and type II receptors [101], while type III receptors can be considered as co-receptors for the binding with TGF, acting as regulator of the TGFβ pathway [102]. Basically, TGFβ can bind the type II receptor, also known as TGFBR2, able to phosphorylate the type receptor TGFBR1, and the signal is diffused after the phosphorylation of Smad2 or Smad3 receptors [103]. The complex composed of TGFBR1

and TGFβ moves into the nucleus, where it can bind co-activators as p300 and Cre-binding protein (CBP) or repressors like TGIF or Skil [104], regulating the transcriptional activity of several genes.

Li et al. show an upregulation of TGFβ pathway in CMs of mice with mutation in the *JUP* gene [112]. They notice an increase in the expression of phospho-Smad2, TGFβ1 and Plasminogen Activator Inhibitor type 1 (Pai1). The increased expression of these factors seems to be related to the progress of the disease in the mice, since in the early stage the change in the expression of these markers is not visible [112]. In mammals, three isoforms of TGFβ have been identified (TGFβ1, TGFβ2, TGFβ3) [106], and in Jup mutant mice only TGFβ1 increases its expression, while no difference has been noticed for the other two isoforms. This upregulation of TGFβ in Jup mutant mice, with an ablation of Jup gene in cardiomyocytes, seems to be due to an increased stress at the level of myocardium, due to an impaired coupling of cardiomyocytes. Notably, this possible mechanism has been referred only to Jup mutants and further studies are necessary to elucidate its possible involvement also in presence of mutations in other genes [112]

Recently the RhoA/MRTFA pathway has also been proposed as another possible molecular mechanism for the adipogenic accumulation in ACM patients [114]. RhoA belongs to the RAS family proteins, a GTPase family able to activate or inactive signaling molecules, as Rho kinases (ROCK), its downstream myosin phosphatase targeting protein (MYPT) and myosin light chain (MLC). The activity of this family protein is based on the binding with GTP or GDP: when these proteins are bound to the former, they are in an activated state, while they are inactive when bind the latter. It has been shown that RhoA is involved in the remodeling of the actin cytoskeleton in human CMs: more specifically RhoA is able to activate the myocardiac related transcription factor A/serum response transcription factor (MRTF/SRF) [114].

It has been demonstrated that RhoA/ROCK pathway could stimulate the switch to the adipogenic pathway. Mechanistically the reduced RhoA-GTPase activity and the remodeling of actin cytoskeleton, lead to an increase in G-actin level, which start to accumulate into cytoplasm, binding the MRTFA. Therefore, MRTFA cannot translocate into the nucleus and the transcription of myogenic genes is prevented, while the transcription of adipogenic genes, as PPARγ, is induced [114].

1.2.8 Mitochondrial ROS: possible new players in ACM?

Despite many molecular pathways has been described to be involved in ACM, the precise molecular mechanisms of the disease remain yet not fully understood [115]. Intriguingly, although evidence has been provided that antioxidants could reduce lipoapoptosis in ACM CMs obtained from iPSC (iPSC-CMs) [94], an in depth investigation of Reactive Oxygen Species (ROS) in ACM is still missing. ROS are highly reactive molecules serving as signaling molecules but capable of inducing pathological cellular response when present in excessive quantities. ROS can be generated by mitochondria during oxidative phosphorylation in the form of superoxide and hydrogen peroxide, and through the activation of different cellular enzymes including NADPH oxidase, xanthine oxidase and nitric oxide synthase (NOS) [116]. Cells possess mechanisms to protect themselves against excess of ROS, including enzyme systems (superoxide dismutase, catalase and glutathione peroxidase) and non-enzymatic ROS scavengers such as vitamins C and E, the ratio of reduced glutathione (GSH) to oxidized glutathione disulfide (GSSH) and the cytosolic ratio of NADH to NAD^+ [117], [118], [119]. Importantly, although the exact mechanisms are still unclear, it is accepted that arrhythmogenesis and oxidative stress are strictly correlated, possibly involving the function of main cardiac ion channels [120].

Recent studies report that mitochondrial oxygen consumption and ROS levels increase during adipogenesis [121] [122]. The treatment with mitochondrial antioxidants, as MitoCP and MitoTempo, is able to reduce lipid accumulation, as well as the protein levels of C/EBPα and proliferator activated receptor gamma 2 (PPARγ2) [123]. This shows that ROS are essential for the transcription of adipocyte differentiation proteins. Mitochondria can generate ROS at the level of Complex I and II within the matrix [124], while Complex III is able to generate superoxide either within the matrix and the intermembrane space [124]. Tormos et al. silence in Mesenchymal Stromal cells the expression of two subunits of Complex III, the Rieske iron sulfur protein (RISP) and ubiquinone binding protein (QPc), observing a reduction in the ROS production. In addition, they observe an attenuation in PPARγ mRNA and in the transcription of its target genes. Interestingly, in the presence of antimycin A, a selective inhibitor of Complex III, the transcription of PPARγ is blocked, indicating a connection in the activation of Complex III and the adipogenic cascade [123].

Several works show also that ROS should not only be considered as a consequence of differentiation, but as a promoting factor [125, 126] and that the treatment with ROS scavenger and antioxidant seems to be able to reduce the adipogenic phenotype.

Wang et. al have recently demonstrated that in human mesenchymal stromal cells an increase in intracellular ROS concentration is visible in the early-stage of adipocyte differentiation, and at the same time there is an overexpression of PPARy, [127]. Also, in this case, the treatment with the mitochondrial ROS scavenger MitoTempo seems to be able to reduce ROS as well as PPARy expression [127]. These evidences seem to be in line with previous works, where intracellular ROS levels led to adipocyte differentiation by regulating PPARy.

1.3 Cardiac mesenchymal stromal cells (CStCs)

1.3.1 Mesenchymal stromal cells: definition

Mesenchymal stem cells (MSCs) were isolated for the first time from bone marrow by Friedenstein and colleagues as non-hematopoietic bone marrow cells. They showed that the isolated population was multipotent, being able of originating bone and cartilage and reconstituting the bone marrow microenvironment [128]. MSCs are not only able to provide mechanical support to Hematopoietic Stem Cells (HSCs), sustaining their proliferation and differentiation, but also to differentiate in several mesodermal lineages [129]. MSCs are also currently generating interest as a potential therapeutic tool for several diseases, as muscular dystrophy [130] , systemic lupus erythematosus [131], heart failure [132], and bone disorders [133, 134]. One of the main advantages of using these cells in the disease treatment is because MSCs show low level of immunogenicity and this reduces a possible immune rejection [135].

The current definition of mesenchymal cells as stem cells was coined in 1991 by Caplan [136]. According to this definition, bone marrow non-hematopoietic cells could be considered as stem cells, since they are able to self-renew and to differentiate into several cell types. Recently the term “stem” has been criticized referred to non-hematopoietic bone marrow cells, considering their heterogenous nature and their replicative senescence [137], [138] . On the contrary, it is very well recognized that bone marrow hematopoietic cells are able to reconstitute hematopoiesis in lethally irradiated mice [139] and in patients with leukemia undergoing myelosuppressive therapies [140, 141].

The term Mesenchymal or Marrow Stromal Cells (MStCs) has been introduced to indicate the fibroblast-like cell populations with residual plasticity, that can be isolated from bone marrow. The definition of stromal cells has also been enlarged to all the fibroblast-like, plastic adherent cell populations that can be isolated from adult and fetal connective tissue of several organs as adipose tissue [142], skeletal muscle [143], liver [144] and heart [145].

In 2006, the Mesenchymal and Tissue Stem cell Committee of the International Society for Cellular Therapy (ISCT) [146] reported the following criteria that cells have to fulfill in order to be defined as MStCs:

- *Plastic adherence* in standard culture conditions;
- *Positivity to specific surface antigens* as CD105, CD73 and CD90 and lack of expression of typical hematopoietic markers as CD34, CD14, CD45, CD19 and HLA-DR;
- *Multipotent differentiation* in mesodermal tissues, as chondrocytes, osteocytes and adipocytes, under *in vitro* differentiating conditions.

1.3.2 Cardiac Mesenchymal Stromal Cells

In a normal adult heart, cardiomyocytes represent only the 30% of the total cell number, while the remaining 70% consist of non-cardiomyocytes cells, among which cardiac mesenchymal stromal cells (CStCs, i.e. cardiac fibroblasts) are the vast majority [147].

CStCs have a crucial role in multiple aspects of myocardial function and pathophysiology of the heart, including synthesis and deposition of extracellular matrix (ECM), cell-cell communication with cardiomyocytes and endothelial cells [148]. In addition, they are able to guarantee the normal 3D structure, function and biochemical features of the heart [149, 150]. CStCs have also a key role during pathological remodeling of the heart that occurs in response to pathological changes, such as hypertension, myocardial infarction and heart failure [151]. Indeed, it has already been demonstrated their ability to at least partially repair infarcted myocardium in rats [145], dogs [152] and more recently in humans [153].

In a study, Rossini et al. isolate an unselected population of CStCs, obtained from adult human auricles, comparing it with Bone Marrow Mesenchymal Cells (BMStCs), derived from the same patient. In the work, it is specifically analyzed whether CStCs could be more oriented towards the cardiovascular phenotype compared to BMStCs. The results demonstrate that, in spite of a remarkable similarity in the expression of specific mesenchymal-associated markers, notable differences at the molecular and functional level are observable. CStCs, seem to be less competent than BMStCs in producing adipocytes and osteocytes, but more oriented towards the cardiovascular phenotype and more prone to express cardiac markers [154].

In addition, CStCs actively contribute to the cardiac electrophysiology, involving direct gap-junctional coupling of fibroblasts and myocytes, which are essential in maintaining an

optimal electrical conduction in the heart [155]. Interestingly, CStCs can also affect electrophysiology passively, acting as obstacles to spread electrical excitation due to fibrosis deposition [156].

However, despite their already well-recognized role in the electromechanical dysfunction and fibrosis deposition in several cardiac pathologies leading to SCD [157, 158], the real role of CStCs in these diseases has not been completely described, yet.

1.3.3 Cardiac stromal cells as a model for the investigation of Arrhythmogenic Cardiomyopathy

Recently Sommariva and colleagues demonstrate, for the first time, that CStCs can play a role in the adipogenic substitution in the heart of human ACM patients [159]. CStCs are isolated from ventricular biopsies of ACM patients, then amplified and characterized. They demonstrate by gene expression analysis that CStCs derived from ventricular biopsies of ACM patients and healthy controls express desmosomal genes as *PKP2*, *JUP*, *DSG2* and *DSC2*.

After the exposure to the adipogenic medium, isolated ACM CStCs are able to accumulate more lipid droplets than NON ACM CStCs. This result is furthermore confirmed in this cellular model by the evaluation of the expression of adipogenic markers, through qRT-PCR and Western Blot analysis [159].

Importantly, slices of ACM explanted hearts are stained with antibodies against the mesenchymal surface markers CD29 and CD105 together with PLIN-1, a marker generally expressed in adipocytes. This ex-vivo analysis reveal lipid accumulation in cells co-expressing PLIN1 and CD29/CD105, demonstrating that the cells involved in the lipid accumulation have a mesenchymal origin.

Therefore, based on these evidences, it is arguably that CStCs might be a novel-non contractile cell type contributing to exaggerated adipocyte accumulation in ACM hearts. In addition, this model is also suitable as a tool for disease modeling and for drug screening. CStCs can be easily isolated from ventricular tissues and then amplified. The advantage to use this model to study ACM is the possibility to have a complete mature cell phenotype with whole genetic background of patients [159].

Other cell models are also used for the investigation of ACM as cardiomyocytes obtained after cardiomyogenic differentiation of Induced Pluripotent Stem Cells [160] [161]. One of the main advantages of this model is that their replicative potential is unlimited, and they are

also suitable for high-throughput screening, and iPSCs carry the same genetic background of patients, representing also a unique tool for personalized medicine approach. On the other hand, a limitation of this cardiomyocyte model is due to their immature, fetal-like phenotype, which does not allow to recapitulate completely the adult phenotype.

Of note, for what concerns *in vivo* models of ACM, most ACM-transgenic mice usually exhibit ventricular arrhythmias, conduction disturbances and massive presence of fibrous tissue [162], but fail to show adipocytes accumulation in the heart, or accumulate very low quantity of myocardial fat [96, 163-166].

Several animal models have been reported, as mice with mutations in desmosomal genes [167], [168], [96],[169],[170],[171] and transgenic zebrafish model [172],[173]. These models allow for a better understanding of the functionality of the whole heart, both from the morphological and electrophysiological point of view, but on the other hand they have as big limitation not to be of human origin.

1.4 The Acetyltransferase GCN5

Epigenetic mechanisms, as DNA methylation, histone modifications, ATP-dependent chromatin remodeling and microRNA-dependent mechanisms are critical for the physiological cellular life. Genetic material is organized into a complex structure, the chromatin, composed of DNA and five histone proteins (H1, H2A, H2B, H3 and H4), which can undergo to several modifications as acetylation, methylation, phosphorylation, ubiquitination, etc. [174]. These modifications on the histones can act at the chromatin level, altering spatially and temporally the gene expression, thus finely regulating the development of the organisms [175, 176]. These changes can be transient, in response to environmental stimuli for example, or they can also be inherited through mitosis and meiosis, leading to the creation of a new genetic transmissible variability [177]. Therefore, these processes can alter the physical accessibility of transcription factors and enzymes responsible for the control of gene expression.

Several studies have demonstrated that defects in histone modifications can be associated with many diseases as well as heart failure [178]. Histones have the function of assembling DNA, and at the same time to modulate the physical access of nuclear factors to DNA. Histone N-terminal tails protrude from histones and they may undergo several modifications, as methylation, acetylation, phosphorylation and ubiquitination that can occur on at least 30

sites for each nucleosome, the essential unit of the chromatin polymer, with a core composed of histone proteins [179].

One of the most extensively studied histone modifications is the acetylation, a dynamic process controlled by two families of enzymes: histone acetyltransferases (HATs) and histone deacetylases (HDACs). Acetylation involves the transfer of an acetyl functional group from one molecule to another, and it generally takes place on the amino group of lysine (K) residues within histone tails. The modification results in a reduction of positive charges at the level of histones tails, weakening their interaction with negatively charged phosphate groups of DNA and other histones, thus losing the canonical chromatin structure. In turn this new conformation leads to an increased accessibility of transcription factors to the genes, promoting high levels of gene transcription [180].

Considering their important role in the gene expression, great attention has been given to the isolation and characterization of histone acetyltransferases. The first studied histone-specific HAT enzyme was p55 isolated from Tetrahymena [181]. Interestingly p55 has been shown to be the homologue of the yeast general control nonderepressible 5 (GCN5), with the only difference that the yeast form has a terminal extension at the N-terminal.

It is common to identify five families of HATs [182]:

1. GNATs (GCN5-related N-acetyltransferases),
2. MYST (for 'MOZ, Ybf2/Sas3, Sas2 and Tip60')-related HATs,
3. CBP HATs (for p300/CREB binding protein);
4. General transcription factor HATs including the TFIID subunit TBP-associated factor-1 (TAF1),
5. Nuclear hormone-related HATs SRC1 and ACTR (SRC3)

The GNAT superfamily consists of the HATs GCN5, PCAF, Hat1, Elp3, Hpa2. In humans and mouse, it is possible to find, beside the normal gene encoding GCN5, a second gene encoding p300/ CBP-associated factor (PCAF). Because of their remarkable degree of homology both proteins represent a GCN5 acetyltransferase-subclass [183, 184].

In addition, it should be considered that GCN5 and PCAF are only two subunits of a large multi-protein complex, the SAGA (Spt-Ada-Gcn5 acetyltransferase) complex, a 2MDa multi-protein chromatin modifying complex. SAGA contains GCN5 as the catalytic HAT subunit and preferentially acetylates nucleosomal histones H3, H2B, and, to some degree, H4 [182-186].

In humans GCN5, also known as KAT2A, has been investigated *in vitro* and *in vivo* and its roles seems to be analogous to the yeast form. It has been shown, that hGCN5 exhibits a broad range of functions, as cell proliferation, differentiation, cell cycle, and DNA damage repair [187, 188].

1.4.1 GCN5 non-histone targets

Beside the important role of histone acetylation, GCN5 is also responsible for the acetylation of other non-histone targets, as hormone receptors, signal transducers or nuclear receptors. Moreover, acetylation of nonhistone proteins has been demonstrated to regulate protein function by altering stability, cellular localization and protein–protein interactions [189]. For instance, it has been shown that GCN5 can have a role in the regulation of proliferator-activated receptor gamma coactivator 1-alpha (PGC1-α) activity, a transcriptional factor highly expressed in the heart, and in the brown adipose tissue. The main role of PGC1-α is the regulation of genes involved in the mitochondrial biogenesis [190] and in the gluconeogenic pathways in fasted and diabetic states [191]. It has already been demonstrated that GCN5 is able to mediate the acetylation of PGC1-α on several residual of lysines [191], leading to an inactivation of PGC1-α activity. On the contrary, SIRT1, deacetylating PGC1-α is able to restore its functionality [192]. This switch from the active and non-active form of PGC1-α occurs when the NAD+/NADH increases, meaning that the cell is in energy deficiency. Therefore, it is clear GCN5 and SIRT1 have a pivotal role in the fasted state of the cell, finely regulating the gluconeogenic activity of PGC1-α [193].

Another important role of GCN5 is the acetylation of the Peroxisome proliferator-activated receptors (PPARs) [194], and in detail the transcriptional activation of the nuclear the receptor PPARγ [195].

As already described, one of the main hallmarks of ACM is the fibro-fatty accumulation and the mechanisms underlying this phenomenon have not been completely clarified yet. Adipogenesis is a very complex process controlled by an adipogenic transcriptional cascade, in which PPARγ serves as master regulator. PPARγ is a ligand-activated transcription factor, necessary and, at the same time, sufficient to perform the adipocyte differentiation [195]. In detail, PPARγ expression is activated by two transcription factors, belonging to the family of the transcription factors CCAAT/enhancer-binding proteins, C/EBPβ and C/EBPδ. Specifically, after the adipogenic stimulus, Polimerase II (Pol II) is recruited onto PPARγ promoter via C/EBPβ, to activate PPARγ gene expression. Once the cascade is activated, PPARγ is regulated through histone modifications, as H3lysines 9 (H3K9ac) and 27

(H3K27ac) acetylation at the PPARγ gene locus. These acetylations are performed by epigenetic enzymes as HATs/HDACs [195]. However, it is still unclear which are the exact enzymes responsible for the histone H3 acetylation involved in the regulation of PPARγ. A possible speculation regards the involvement of GCN5: the acetylation of the promoter region of PPARγ mediated by GCN5 might increase PPARγ expression [196].

In a recent study of 2014, Jin et al. demonstrate a possible involvement of GCN5 in the acetylation of H3 in an immortalized brown pre-adypocytes fibroblast line with a double knockout for GCN5/PCAF. It has been shown that, in absence of GCN5/PCAF, Pol II is recruited to the PPARγ promoter via C/ EBPβ, but Pol II elongation is inhibited, leading to inhibition of PPARγ transcription [195]. Indeed GCN5/PCAF KO cells exposed to an external adipogenic stimulus showed a reduction in adipogenic gene expression and an inhibition in lipid droplets accumulation. These results highlighted the possible involvement of GCN5/PCAF activity in the regulation of PPARγ gene.

Another study demonstrated that in preadipocytes GCN5/PCAF directly acetylates C/EBPβ which leads to an increased transcriptional activity of C/EBPβ and also a decrease in its interaction with an mSin3A/HDAC1-containing transcriptional corepressor complex. This would prove the assumption of GCN5 acting upstream of PPARγ [196].

2 Aims

The main goal of my PhD project has been the investigation of a possible correlation between the acetyltransferase GCN5 and the adipogenic phenotype associated with ACM pathology. To this aim, CStCs obtained from affected right ventricle of ACM patients have been used as cell model in the present study.

3 Material and Methods

3.1 Cardiac Stromal Cells

3.1.1 Ethical Approval

The present study is in compliance with the Declaration of Helsinki and was approved by "Centro Cardiologico Monzino IRCCS" (07/06/2012) and by "South Tyrol Azienda Sanitaria" (13/03/2014, N.1/2014) Ethics Committees. Written informed consent was obtained from all participants.

3.1.2 Isolation, culture and characterization of Cardiac Stromal Cells

Right ventricle samples were obtained from eight ACM patients undergoing catheter biopsies for diagnostic purposes at the Centro Cardiologico Monzino (Milano, Italy). Gender, age, clinical manifestations and type of mutation of each ACM patient involved in this study is summarized in Table 3. As control samples (NON ACM) seven endomyocardial fragments of free wall ventricles from explanted hearts of donors (accidental death), not suitable for organ transplantation, were used. Control samples were kindly provided by "Treviso Tissue Bank Foundation".

Table 3. **Clinical characteristics of ACM patients.**

ACM patient ID	Sex Age	Type / age of first manifestation	Dysfunction and structural alterations			Tissue characterization of wall	Repolarization ab.	Depolarization / conduction ab.	Arrhythmias	Family history
			Echo	CMR	AG					
ACM 1	M 44	Sustained VT / 42	negative	minor	n.a.	major	negative	negative	major	major
ACM 2	M 41	PVC / 32	major	n.a.	major	not conclusive	major	negative	minor	major
ACM 3	M 51	Sustained VT / 50	minor	minor	n.a	minor	negative	negative	major	negative
ACM 4	M 57	Polymorphic PVC / 56	negative	minor	n.a.	minor	negative	minor	minor	negative
ACM 5	F 38	ECG-inverted T waves / 37	negative	negative	n.a.	major	minor	negative	minor	major
ACM 6	M 64	PVC / 63	major	major	n.a.	not conclusive	major	major	minor	negative
ACM 7	M 41	PVC / 34	minor	minor	n.a.	major	minor	negative	minor	negative
ACM 8	M 49	PVC / 47	negative	minor	n.a.	not conclusive	major	major	major	negative

Abbreviations: **VT**: Ventricular Tachycardia, **PVC**: Premature Ventricular Contraction, **ECG**: Electrocardiography, **AG**: angiography, **CMR**: Cardiac Magnetic Resonance, **ab**: abnormalities, **n.a**: not available.

The isolation, first amplification and immunophenotyping of the CStCs was performed by our collaborators at Centro Cardiologico Monzino in Milano. Frozen aliquots of CStCs were then sent to the Institute for Biomedicine at Eurac Research, for further experiments.

In detail, ventricular samples of both ACM patients and NON ACM subjects were processed as previously described by Pilato et al. [197]. Briefly cardiac biopsies were washed in Phosphate-Buffered Saline (PBS, Lonza) and cut into 2-3 mm^3 pieces and incubated for 1.5 hours at 37°C under continuous agitation in a solution composed of Iscove's Modified Dulbecco's Medium (IMDM, Lonza) and 3 mg/ml collagenase NB-4 (Serva, Germany). The digested fragments were then centrifuged for 10 min at 400 x g at Room Temperature (RT), and the pellet was then re-suspended in basal medium (BM), composed of IMDM (Lonza), supplemented with 20% Foetal Bovine Serum (FBS, Hyclone, Italy), 10.000U/ml Penicillin, 10,000µg/ml Streptomycin (Pen/strep, Thermo Fisher Scientific) and 20mM L-Glutamine (L-Glu, Thermo Fisher Scientific), plated onto uncoated Petri dishes (Corning) and placed in a humified incubator gassed with 5% CO_2 at 37°C. The day after the enzymatic digestion, cells were washed twice in PBS, in order to remove debris and non-adherent cells, and fresh

medium supplemented with 10ng/mL basic fibroblast growth factor (bFGF), was added to the fragments. bFGF supplemented medium was refreshed every 24h for 3 days. After 5-7 days, fragments started to attach on the Petri dish and cells to spread on the surface of the dish. Once a confluency of 60% was reached, cells and the fragments were washed twice in PBS and Trypsin 0.05% was added for 5 minutes at 37°C. The enzymatic activity of Trypsin was stopped adding to the cells BM, and cells were collected and centrifuged for 5 min at 400 x g, while the fragments were replated into new Petri dishes for further amplification. Cells, after the centrifugation, were then plated into new Petri dishes for further amplification.

CStCs immunophenotyping was performed by flow cytometry. Cells were detached with 0.02% EDTA solution (Sigma-Aldrich) and stained with FITC/PE-conjugated antibodies for 10 minutes and analyzed using a FACSCalibur (Becton–Dickinson, Italy). The analysis was performed using the Cell-Quest Software. Only cells positive for the expression of the mesenchymal markers CD105, CD29, CD44 and negative for CD31 (platelet endothelial cell adhesion molecule), CD34 (hemopoietic and endothelial marker), CD45 (lymphocyte common antigen), CD14 (cluster of differentiation 14), and HLA-DR (human leukocyte antigen) were amplified for further experiments (Table 4).

Table 4. Immunophenotyping of CStCs.

Marker	ACM 1	ACM 2	ACM 3	ACM 4	ACM 5	ACM 6	ACM 7	ACM 8
CD105	91.37	96.71	99.62	84.93	99.22	93.46	96.32	95.66
CD29	90.51	96.79	99.35	96.27	99.62	98.46	95.26	95.57
CD44	94.84	96.83	99.47	85.87	98.32	98.84	94.67	95.61
CD31	1.92	0.00	0.00	5.14	0.00	0.10	2.66	4.85
CD34	0.00	0.00	0.00	0.48	0.04	0.02	4.89	3.10
CD45	0.00	0.00	0.16	1.25	0.00	0.04	1.88	0.10
CD14	0.00	0.00	0.00	2.35	0.00	0.02	1.58	4.47
HLA-DR	0.00	0.00	0.00	1.26	0.04	0.08	1.48	3.11

Aliquots of >1x10^6 CStCs were then frozen in a cryogenic solution composed of Foetal Bovine Serum (FBS, Hyclone, Italy) and 10% dimethyl sulfoxide (DMSO) and sent to our laboratory at Eurac Research in Bolzano for further amplification and experiments.

3.1.3 Amplification of Cardiac Stromal Cells

Cryovials containing the cell suspension, were put in a 37°C water bath until the cell suspension was almost completely thawed. The mixture of cells and cryogenic solution was then diluted in 2.5 mL of BM and centrifuged at 400 x g for 5 minutes. After supernatant removal, the cell pellet was resuspended in fresh 0.5 mL of BM and transferred into a 60mm

Petri dish (Corning). 3 more mL of BM were added to the dish, which was then placed in a 37°C incubator gassed with 5% CO_2. Medium was changed every 2 days. When approximatively 70-80% confluent, cells were detached and replated to promote their amplification. Specifically, the growth medium was carefully removed, and cells were washed twice with PBS in order to remove any residual of medium and serum, and incubated with 0.05% Trypsin-EDTA solution (Gibco) for 5 min at 37°C. Trypsin was then stopped, adding BM. Cells were then centrifuged for 5 minutes at 400 x g. The supernatant was removed, and the pellet re-suspended in 1 ml of BM. Cells were replated in 10mm Petri dishes (Corning) at a density of 7500 cells/cm^2.

3.1.4 Adipogenic differentiation

As previously described [94], intracellular lipid accumulation, as one of the main hallmarks of ACM, was enhanced in CStCs after the exposure to an adipogenic medium (AM) consisting of IMDM, supplemented with 10% FBS (FBS, Gibco), 0.5 mmol/L 3-isobutyl-1-methylxanthine (IBMX, Sigma- Aldrich), 0.1 mmol/L indomethacin (Sigma-Aldrich), 0.1 µmol/L hydrocortisone (Sigma-Aldrich), 10.000 U/ml Penicillin/Streptomycin (Thermo Fisher Scientific), 20 mM L-Glutamine (Thermo Fisher Scientific). The factors added to the medium had a specific role in the activation of the PPARγ pathway, the main responsible of the lipid accumulation [195]. More specifically, IBMX is a non-specific inhibitor of cAMP and cGMP phosphodiesterases: the increase in cAMP level activates PKA pathway, required for the transcriptional activation of PPARy and thus adipogenic gene expression [198]. Indomethacin stimulates adipogenesis [195], upregulating PPARγ, while hydrocortisone is responsible of high levels of lipogenic differentiation [199].

In the present project, CStCs were exposed for 7 days to the adipogenic medium. After 3 days from the beginning of the procedure, the medium was refreshed and left until the end of the treatment.

3.2 Western Blot

Western Blot (WB) is a well-established molecular technique used to evaluate the expression of specific proteins in cells and tissues. This procedure involves multiple steps: 1) preparation of cell lysate and protein extraction, 2) electrophoretic separation of proteins based on the molecular weight on a polyacrylamide gel matrix (SDS-PAGE), 3) transfer onto a membrane (nitrocellulose or polyvinylidene fluoride (PVDF)), 4) incubation with

primary antibodies, coupled with a signal-inducing secondary antibody, 5) detection of the signal.

3.2.1 Cell lysates and protein extraction

In order to perform WB analysis, CStCs protein lysates were prepared using RIPA lysis buffer, composed of 10 mM Tris-HCl pH 7.4, 150 mM NaCl, 1% Igepal CA630 (NP-40), 1% sodium deoxycholate (NaDoc), 0.1% SDS (Sodium Dodecyl Sulphate), 1% Glycerol. RIPA enables efficient cell lysis and protein solubilization, avoiding protein degradation and interference with protein immunoreactivity and biological activity [200]. In addition, phosphatase (PhosSTOP EASYpack, Roche) and protease inhibitors (Complete Tablets, Mini EASYpack, Roche) were added to the RIPA buffer, in order to prevent the digestion of the sample by activation of endogenous proteases.

Briefly, growth medium was accurately aspirated, and cells were washed twice with PBS, in order to eliminate any residual of FBS of the culture medium, that could alter the subsequent protein quantification. Then, 100 µl of RIPA buffer supplemented with protease inhibitors 10% and phosphatase inhibitors 7% were added directly to the plate and cells were detached using a cell scraper. The lysates were then sonicated for 10 seconds with ultrasonic waves at 10% power (SonoPlus, Bandelin), in order to lyse the membrane, allowing the release of the protein content. It is important to underline that all the procedures were carried out at 4°C to prevent protein degradation. If not processed immediately, the cell lysates were stored at -80°C.

3.2.2 Protein quantification

In order to quantify the amount of proteins in the cell lysate, the Pierce® BCA (BiCinchoninic Acid) Protein Assay Kit 8 (Thermo Scientific) was used. This kit is a two-component, high-precision, detergent-compatible assay reagent able to measure total protein concentration compared to a protein standard. The kit employs a redox reaction where the solution changes its colour according to the amount of proteins in the samples. The working solution is obtained mixing two reagents, A and B, in a ratio of 50:1. The reagent A contains BiCinchoninic Acid, NaOH and sodium tartrate 0.1M, while the reagent B contains 4% of copper sulphate ($CuSO_4$). The BCA Protein Assay is based on the reduction of Cu^{2+} to Cu^{1+} by the protein samples with the colorimetric detection of the cuprous cation (Cu^{1+}) by bicinchoninic acid. Then, two molecules of bicinchoninic acid form a complex with the molecule Cu^{1+}, developing the intense purple-colored reaction product. This complex exhibits a strong linear absorbance at 562 nm with increasing protein concentrations. A

series of dilutions of known concentration of bovine serum albumin (BSA) were prepared (2000 µg/µl, 1000 µg/µl, 750 µg/µl, 500 µg/µl, 250 µg/µl, 125 µg/µl, 25 µg/µl, 0 µg/µl) and used as standard curve.

Then, 25 µl of the solution prepared for each standard point were dispensed in the 96-well plate, while the protein lysate was diluted 1:10 in RIPA buffer, and then distributed in the same plate. At the end, 200 µl of working solution of BCA were added to each well and then the plate was incubated at 37°C for 20 minutes.

After the incubation, the absorbance at 562 nm was measured using a spectrophotometer (Victor X3, Perkin Elmer). The protein concentration of each unknown sample was obtained by the interpolation of the optical density (O.D.) of each unknown sample with the calibration curve.

3.2.3 SDS-PAGE

SDS-PAGE (sodium dodecyl sulfate (SDS) polyacrylamide gel electrophoresis (PAGE)) is a technique widely used in molecular biology to separate proteins according to their molecular weight by migration through a polyacrylamide gel under the application of an electric field. In detail, SDS is present both in the running buffer, and in the gel, since it is an anionic detergent, able not only to denature secondary and non–disulfide–linked tertiary structures, but also to apply a negative charge to each protein in proportion to its mass. In this way, thanks to the activity of SDS, no difference is present anymore in terms of shape and charge among protein, and this ensures that the separation is only based on the molecular weight.

Before starting the electrophoretic run, samples were prepared. Briefly, the sample preparation consisted of a mix composed of 15 µg of proteins in a final volume of 20 µl that contained 2 µl NuPAGE® Sample Reducing Agent (10X) and 5 µl NuPAGE® LDS Sample Buffer (4X) (both from Thermo Fisher Scientific). NuPAGE® LDS Sample Buffer (4X) is composed of 106 mM Tris-HCl ,141 mM Tris base, 2% LDS (Lithium Dodecyl Sulfate) at pH 8.4, 10% Glycerol (to enhance the sample density), 0.51 mM EDTA (calcium chelating agent), 0.22 mM SERVA® Blue G250 which marks the migration front line and 0.175 mM Phenol red as pH indicator. NuPAGE® Sample Reducing Agent (10X) contains also 500 mM of Dithiothreitol (DTT), used to break disulfide bonds and to maintain protein samples in a reduced state during the following electrophoresis step. Samples were denatured at 95°C and then loaded on a polyacrylamide gel. In this work, we used precast gels with a specific gradient of polyacrylamide concentration (NuPAGE® 4-12% Bis-Tris gels, Thermo Fisher

Scientific), able to separate proteins with a molecular weight ranging from 3.5 kDa up to 160 kDa. In addition, in order to determine the approximate molecular weight of the run proteins, a molecular weight size marker of known molecular weight (Precision Plus Protein™ Western C™ Standard Dual Colour, BioRad) was loaded. The electrophoretic separation was performed using the electrophoretic cell (XCell SureLock® Mini-Cell Electrophoresis Cell, Invitrogen), in presence of NuPAGE® MES SDS Running buffer (20X) (Thermo Fisher Scientific) diluted to 1X in Milli-Q water. In detail, MES Running buffer was composed of 50 mM MES, 50 mM Tris Base, 0.1% SDS, 1 mM EDTA, pH 7.3.

The gel ran for 10 minutes at 100V until samples entered in the running gel. Then the voltage was increased up to 150V for about 1.5 hours.

Basically, applying the electric field, negatively charged proteins started to migrate across the gel, moving from the negative electrode (the cathode) to the positive electrode (the anode). Depending on the size, proteins differently migrated in the gel: smaller proteins moved further down the gel, while larger ones moved slower.

3.2.4 Protein transfer

In order to detect the proteins of interest in the samples, it was necessary to transfer and immobilize proteins on a polyvinylidene difluoride (PVDF) or nitrocellulose membrane (Immuno-Blot® PVDF Membrane for Protein Blotting, Biorad; Immuno-Blot® Nitrocellulose Membrane for Protein Blotting, Biorad), by ´electroblotting´. The transfer of proteins from the gel is obtained through a flow of current from the cathode to the anode, thus the negatively charged proteins migrate towards the anode and during this path they stick on the membrane.

To facilitate the transfer, the so called ´wet-sandwich´ was assembled. Starting from the negative pole to the positive pole the sandwich was composed of, a sponge, a filter paper, the SDS gel, the membrane, a second filter paper and a final sponge. The sandwich was then inserted in the transfer cell (Mini Trans-Blot® Electrophoretic Transfer Cell, BioRad) with a Transfer Buffer Solution containing NuPAGE® Transfer Buffer (20X) at pH 7.2 (Thermo Fisher Scientific) diluted to 1X in Milli-Q water and 10% of methanol.

Electroblotting was performed by administering a constant amperage of 400 mA, for 2h at 4°C. Additionally, during the blotting procedure, the transfer buffer was cooled with an ice pack to avoid heating and consequent protein damage.

At the end of the transfer step, it was possible to evaluate the quality of the transfer procedure, visualizing the transferred proteins using a Ponceau solution. Ponceau is a sodium salt dye of red color, used for the rapid detection of protein bands on nitrocellulose membrane and PVDF membranes. The coloration is reversible, and the dye is washed away with simple PBS-0.1% Tween.

3.2.5 Antibodies incubation and detection

Once the transfer was ended, the membrane was incubated in a blocking solution, consisting of non-fat milk or BSA at 5% in phosphate- buffer saline plus 0.1% detergent Tween 20 (PBS-T) for at least 1 hour at RT in agitation. This step prevented the non-specific binding of the antibody to the membrane, saturating the membrane and reducing the unspecific interactions between the primary antibody and other proteins.

After the blocking step, the membrane was incubated overnight at 4°C in agitation in a solution containing the specific primary antibody for the detection of the protein of interest.

The protein analysis was performed using the antibodies listed in the Table 5.

Table 5. Primary antibodies used for the western blot analysis.

Protein	AB	Host	Company	Solution	Dilution
PPARy	Sc-7273	Mouse	Santa Cruz	BSA	WB 1:100
GCN5	Monoclonal, C26A10	Rabbit	Cell Signaling	Milk	WB 1:1000
GAPDH	Sc-32233	Mouse	Santa Cruz	Milk	WB 1:1000

The day after, the membrane was washed three times with PBS-T to remove all the residual of antibody and then incubated with an anti-mouse or anti-rabbit secondary antibody conjugated to HRP (horseradish peroxidase) and diluted 1:10000 in the same solution used for the primary antibody, for 1 hour at RT.

The detection of the target protein was performed adding the substrate for the enzyme HRP. The detection system is a solution of H_2O_2 (Hydrogen Peroxide) and luminol called ECL (Enhanced ChemiLuminescence) at ratio of 1:1 (Pierce™ ECL Western Blotting Substrate kit). The enzyme, due to the presence of H_2O_2, catalyses the oxidation of ECL, producing a detectable chemiluminescence signal.

The membrane was incubated with the detection solution for 5 minutes at RT in darkness and then the signal detected using the ChemiDoc™ Touch Imaging System (Bio-Rad). The

signal of the target protein was analyzed using the software Image Lab 5.2.1 analyser (BioRad), then normalized on the expression of Glyceraldehyde 3-phosphate dehydrogenase (GAPDH), a housekeeping protein, which should be stably expressed in the samples.

3.3 GCN5 knockdown

In this work the genetic knockdown of GCN5 was performed using small lentiviral particles (ORIGENE Catalog nr. RC207889L2V), containing short hairpin RNA (shRNA), able to transiently knock down *in vitro* the expression of GCN5. shRNA are directly synthesized in the cell, thanks to the activity of a DNA vector [201]. shRNA is composed of two complementary sequences of 19-22 base pair, linked to a short loop of 4-11 nucleotides similar to short harpins, able to integrate into the DNA. After the transcription, the shRNA sequences are translocated in the cytosol, and here the sequences are digested by an endogenous enzyme, Dicer, able to digest the shRNA in siRNA, that can bind target mRNA (in our case GCN5 sequence) and deliver it to a degradation complex [202].

Cells were plated at a density of 7500 cells/cm^2 on IbiTreat μ-Dish 35 mm dishes (IBIDI), that show the high optical quality necessary for confocal microscopy. These dishes were then used for LipidTox staining and the consequent confocal image acquisition. In parallel, cells were plated and transfected in 12-wells plates (Corning), in order to obtain protein lysates used to confirm the reduction in terms of GCN5 protein expression, after exposure to shRNA.

When the 80-90% of the confluency was reached, cells were transfected with the lentiviral particles. The number of viral particles needed for the transfection was calculated according to the desired multiplicity of infection (MOI), considered as the number of transducing lentiviral particles per cell. We performed a titration with different MOI concentration, 25 MOI, 50 MOI and 100 MOI to understand which concentration was the most suitable one to reach a high efficiency of transfection. The concentration adopted for our experiments was 100 MOI.

Three different conditions were analyzed:

- The shRNA particles able to silence GCN5 particles and expressing Green Fluorescent Protein (GFP);
- A scramble control which contained lentiviral particles with only the GFP, used as a positive control to prove that the infection worked properly;

- The negative control, where cells were only exposed to adipogenic medium;

In these two last conditions, Polybrene, 10mg/ml was added. Polybrene is a small, positively charged molecule that binds to cell surfaces, neutralizes surface charge, increases binding between pseudoviral capsid and the cellular membrane. Thus, it has been proved to greatly enhance transduction efficiency.

Briefly, culture medium was gently removed, and 100 MOI of shRNA particles diluted in adipogenic medium were added onto the cells. The small dishes were incubated at 37°C with 5% CO_2 and after 3 days the medium containing the lentiviral particles was removed and replaced with fresh adipogenic medium and incubated for other 4 days. At the end of the treatment, pictures of cells were taken with a fluorescence microscope (Zeiss, Vert.A1). Microphotographies in both phase contrast and green fluorescence were taken on the same field. Then the number of GFP-positive cells was counted and normalized on the total number of cells counted in the Brightfield pictures. This ratio gave us the possibility to calculate the efficiency of transfection.

Then the cells plated on IBIDI were washed three times with PBS and fixed with paraformaldehyde (PFA 4%) (Sigma-Aldrich), for 15 min at RT. PFA 4% was then removed and cells washed twice with PBS, to remove any residual of PFA. The cells plated in the 12-well plate were lysated in RIPA Buffer and then used for the Western Blot analysis.

3.3.1 LipidTox immunofluorescence assay

To evaluate the lipid accumulation in CStCs after GCN5 silencing, cells were stained with HCS LipidTOX™ Deep Red Neutral Lipid Stain (Thermo Fisher Scientific), a dye with an extremely high affinity for neutral lipid droplets and detectable by confocal and fluorescence microscopy. HCS Lipid Tox dye emits in the red region (650 nm) thus creating no spectrum overlapping problems with the GFP emission wavelength (510 nm)

After the 7 days of infection, the growth medium was gently removed, and cells were fixed with PFA 4%, as previously described. Cells were then incubated for 20 min at RT in darkness with HCS LipidTOX™ diluted 1:1000 in PBS. The solution was removed, and cells washed three times with PBS. Nuclei were counterstained with DAPI (Thermo Fisher Scientific) and the images were acquired with the confocal microscope (Leica Microsystem CMs GmBH Type: TCSSP8X), with a 40X oil immersion objective. The integrated intensity of the signal was quantified using ImageJ Software.

3.4 GCN5 Pharmacological inhibition

CStCs were either exposed for 7 days to adipogenic medium supplemented with MB-3 (Sigma-Aldrich) 200 μmol/L, a selective inhibitor of GCN5 activity [203], or to standard adipogenic medium, as control. Before starting our experiments, we evaluated whether the treatment with MB-3, could affect the cell viability.

3.4.1 Cell viability

Cell viability was assessed after the exposure to GCN5 inhibitor, MB-3. Cells were plated as reported above and after 7 days in presence or not of MB-3, cells were trypsinized, as already described. 10 μl of cells suspension were diluted in 10 μl of Trypan Blue stain 0.4% and counted using the cell counter (Countess, Invitrogen).

3.4.2 Bodipy assay

In order to evaluate the lipid accumulation after the adipogenic treatment, cells were fixed as previously described and stained with BODIPY® 493/503 (Thermo Fisher Scientific), a green-fluorescent dye, with a nonpolar structure and long-wavelength absorption. This dye also shows hydrophobic proprieties and it is able to bind the cytoplasmatic lipid droplets.

CStCs were plated as already described before, onto IbiTreat μ-Dish 35 mm (IBIDI) dishes and after the adipogenic treatment in presence or not of MB-3, cells were fixed as previously described. Cells were then incubated for 20 min at RT in darkness with BODIPY® 493/503 0.5 μM diluted in PBS. Nuclei were counterstained with DAPI (ThermoFisher) and the images were acquired with the confocal microscopy (Leica Microsystem CMs GmBH Type: TCSSP8X) with a 40X oil immersion objective. Lipid droplets stained with Bodipy, emitted green light and the integrated intensity of the signal was quantified using ImageJ Software.

3.5 Transmission Electron Microscopy sample collection

Transmission Electron Microscopy (TEM) analysis was performed on ACM CStCs in basal condition and after the 7-day exposure to adipogenic medium in presence or not of the specific GCN5 inhibitor, MB-3.

In detail, after the treatment, cells were detached with 0.05% Trypsin-EDTA solution as described in the previous paragraph. After the centrifugation step, the supernatant was removed and the pellet resuspended in Karnovsky fixative, composed of 4% paraformaldehyde and 5% glutaraldehyde. The samples were then sent to the group of Prof. Costanza Lagrasta at the University of Parma (Department of Medicine and Surgery) where

they were washed several times with 0.1 M phosphate buffer (pH 7.2), post-fixed in 1% osmium tetroxide (OsO_4) for 90 minutes at RT and dehydrated by increasing concentration of alcohol. Then, cells were washed with propylene oxide and embedded in epoxy resin. Sections of 0.5 μm thickness were stained with methylene blue and safranin, able to stain, respectively, nuclei and the cytoplasm. This staining allowed to morphologically select the field of interest. Subsequently, ultrathin 60-80 nm thick sections were collected on a 300-mesh copper grid and, after the staining with uranyl acetate to label proteins and nuclei acids, and lead citrate able to stain the membrane and the glycogen accumulation, they were qualitatively examined under a transmission electron microscope (Philips EM 208S, Fei Electron Optics BV, Eindhoven, Netherlands). All chemicals were purchased by Sigma Aldrich, St. Louis, MO. High power micrographs collected at X5600 magnification were employed to evaluate the volume fraction occupied by lipid droplets. All morphometric data were blindly collected.

3.6 Transcriptome analysis

3.6.1 Sample collection

In collaboration with the NGS Facility of the Department of Cellular, Computational and Integrative Biology – CIBIO, University of Trento, the analysis of the whole transcriptome of ACM CStCs, cultured for 7 days AM in presence or not of MB-3 was performed. Cells were cultured as previously described and the cell pellet resuspended in TRIzol reagent, a complete, ready-to-use reagent used for the isolation of high-quality total RNA. This monophasic solution of phenol and guanidine isothiocyanate is designed to inactivate immediately endogenous ribonuclease (RNase) and to ensure the purification of intact RNA.

Total RNA was extracted by using the Direct-zol RNA Kit (Zymo Research). All centrifugation steps were performed at 12.000 x g at RT. The RNA extraction protocol was based on centrifugation with spin columns. An equal volume of ethanol was added to the cell suspension and then added to a Zymo-Spin™ IIC Column in a Collection Tube and centrifuged for 30 seconds. The column was then transferred in a new collection tube and washed with RNA Wash Buffer (provided by the kit). In order to avoid DNA contamination, samples were treated with 80 μL of DNAse I reaction Mix, containing DNase 1 (6U/μl) and DNA Digestion Buffer (provided by the kit). Consequently, Direct-zol™ RNA PreWash was added to the column and centrifuged. The column was then cleaned with RNA Wash Buffer and centrifuged for 2 minutes in order to remove all the wash buffer. In the end, to the column

DNase/RNase-Free Water was added to elute the RNA of the samples. The concentration of eluted RNA was detected using a NanoDrop 1000 (Thermo Scientific), and the ratio 260/280 and 260/230 was checked (the first ratio should be > 1.8, while the second one ranging from 0.40 up to 2.01).

To check the quality of isolated total RNA and mRNA integrity and purity, the Experion RNA StdSens Analysis Kit (Bio- Rad) was used. The customized Experion RNA chip offers an optimized microchannel architecture within an ergonomic caddy for exceptional RNA separation. Each RNA StdSens chip holds up to 12 samples which are run on an Experion electrophoresis station. Only 1 μL of each sample is required. Within each chip, a series of microchannels connects the sample wells to a separation channel and buffer wells. A set of electrodes in the electrophoresis station applies a voltage across the microchannels, causing charged molecules in the samples to migrate into and through the separation based on their size and charge. The assay procedure was performed by carefully following each step as described in the protocol.

Experion software is able to plot the fluorescence intensity as a function of migration time, generating an electropherogram for each sample (Fig.2). The software also converts the electropherogram data into densitometric bands, which appear in a virtual gel, as shown in Fig.3. Each lane of the virtual gel corresponds to a different sample, and all samples from a chip are shown in a single gel view. Experion software also constructs RNA quality indicator (RQI) which gives a quantitative indication of the integrity of the sample. All samples that reported a concentration ≥ 100ng/ul and RQI value ≥ 9) were sent to the NGS Facility, at the University of Trento, where further analyses were performed.

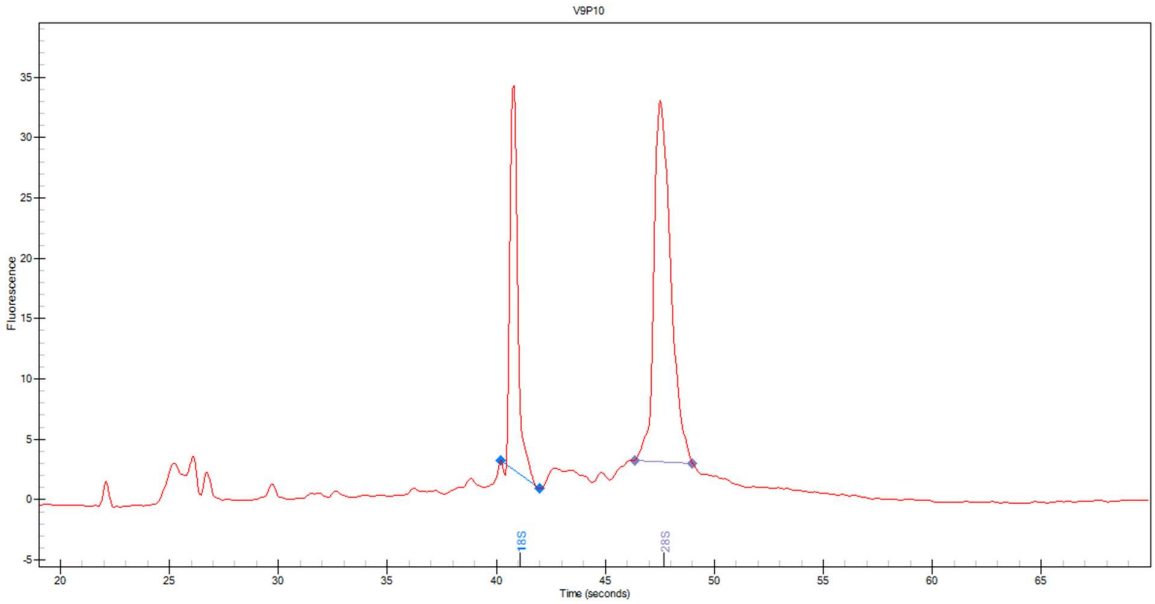

Figure 2. Example of an electropherogram generated by an Experion RNA HighSens analysis of total RNA from eukaryotic cells. The 18S and 28S rRNA peaks are automatically identified by Experion software.

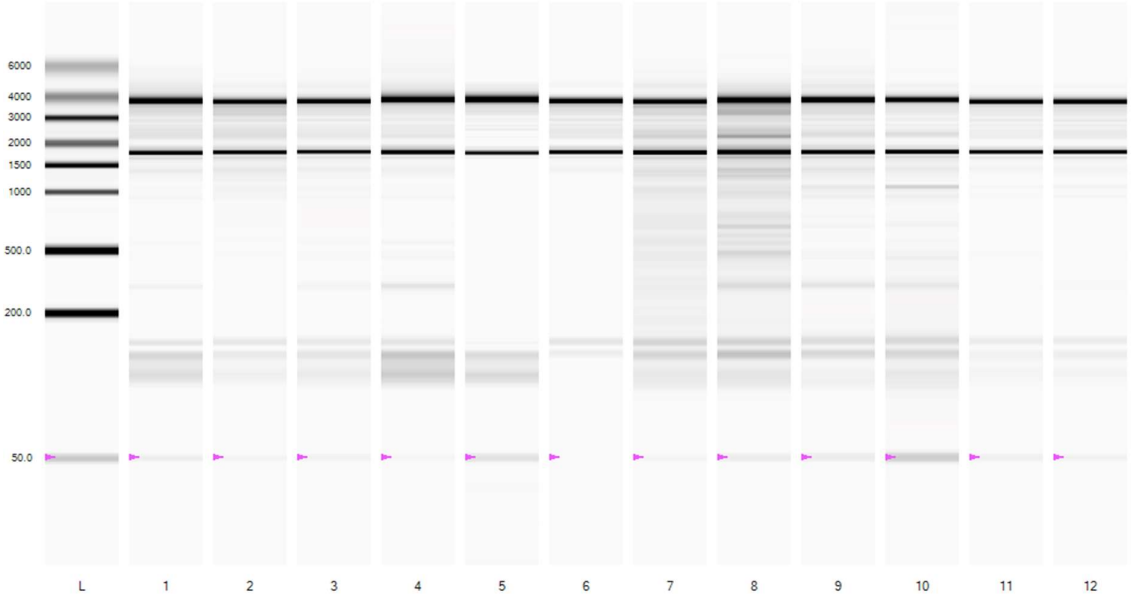

Figure 3. Virtual gel generated by Experion RNA StdSens analysis of total RNA from eukaryotic cells. The image reports the separations of the RNA ladder (L) and 12 samples on a single chip.

The sequencing and the bioinformatic analysis were performed at the NGS Facility, at the University of Trento. The concentrations of the samples were checked again using the Qubit RNA. 500 ng of RNA for each sample were used for the preparations of the libraries, using the QuantSeq 3' mRNA-Seq Library Prep FWD (Lexogen). Samples were sequenced using

the platform HiSeq2500, following the protocol SR1000. The results of the sequencing were collected in fastq files, using the software CASAVA, FastQC (Version 0.11.3). Then the reference genome was aligned to the Homo Sapiens assembly GRCh38 using STAR with recommended options and thresholds (version 2.5) [204]. HTSeq-count was used to generate raw gene counts (version 0.9.). Counts normalization to Trimmed Mean of M-values (TMM) for visualization methods was performed by edgeR package (v.3.24.3) [205] [206]. The differential expression analysis was performed using DESeq2 package (v.1.22.2) [207], and for significance testing, the Wald test was used. Genes were considered differentially expressed with adjusted p-value <0.05 and a log2 fold change greater than 1 or smaller than -1. For statistical analyses, the adjusted p-values were generated via the Benjamini-Hochberg procedure. Functional annotation on differentially expressed genes was carried out through enrich web tool [208] [209]. Results were then collapsed, filtered (max top 5 terms for each category) and represented as barplots using R/biocondoctur environments (pppubr package).

3.7 Reactive Oxygen Species evaluation

In order to assess the concentration of mitochondrial Reactive Oxygen Species (ROS) in NON ACM CStCs and ACM CStCs in adipogenic conditions, Mitochondrial Superoxide Indicator, MitoSOX™ Red (Thermo Fisher Scientific) was used. The growth medium was gently removed, and the cells were washed twice with HBSS (Gibco), previously pre-warmed at 37°C, in order to completely remove any residual medium. Then cells were incubated with MitoSox 5 μM diluted in HBSS at 37°C for 10 min. The solution was gently removed, and cells fixed with PFA 4% as previously described. The nuclei were counterstained with DAPI and the images were acquired with the confocal microscope (Leica Microsystem CMs GmBH Type: TCSSP8X) and the integrated intensity of the signal was quantified using ImageJ Software.

In addition, we tried to reduce the amount of mitochondrial ROS using a specific mitochondrial scavenger, known as MitoTempo. Cells were plated as previously described and, once the 80% confluency was reached, they were exposed to MitoTempo (500 nM) in presence of adipogenic medium for 7 days. The medium was then removed, cells washed twice and fixed with PFA 4% and the labeled with MitoSox, as previously described.

3.8 Respiratory activity in mitochondria of NON-ACM CStCs vs ACM CStCs

Given the already described relationship between lipogenesis and mitochondrial activity [126] cells were tested for their oxygen consumption. Mitochondrial oxidative phosphorylation (OXPHOS) was measured in ACM CStCs and NON ACM CStCs by means of high-resolution respirometry (Oxygraph-2K, OROBOROS INSTRUMENTS, Innsbruck, Austria).

The Oxygraph-2k (O2k, OROBOROS INSTRUMENTS, Innsbruck, Austria) is an instrument composed of two independent chambers that can be tightly closed and contain oxygen sensors. The chambers are electronically connected to the manufacturer's software DatLab, which allows to have a real-time read out of the concentration of oxygen in each of the two chambers. The temperature in the chambers is a crucial parameter for the measurements and it needs to be maintained constant between 25°C and 37°C. Homogenous oxygen distribution in the medium is ensured by constant stirring at 750 rpm.

The mitochondrial activity was measured in a specific medium, MiR05 (mitochondrial respiration medium), containing 0.5 mM ethylene glycol tetra-acetic acid (EGTA), 3 mM $MgCl_2$,$6H_2O$, 60mM Lactobionic Acid, 20 mM Taurine, 10 mM KH2PO4, 20 mM HEPES, 110 mM D-sucrose, 1 g/l essentially fatty acid-free bovine serum albumin. The SUIT (substrate uncoupler inhibitor titration) protocol (SUIT-011, BioBlast), was used to perform the experiments (Fig. 4). This protocol allowed us to evaluate the maximal OXPHOS capacity of the cells, through the administration of substrates and inhibitors able to study specific coupling/control states. Precisely NADH linked substrates (N) and succinate linked substrates (S) were used, thus promoting the reduction of NADH and $FADH_2$.

After the stabilization of baseline respiratory rates, cells were permeabilized with Digitonin (10 μg·10^6 cells), in order to allow the substrates, which were added later in the protocol, to enter the cells. Then the Leak respiration was taken into consideration, known as the state in which there is only an oxygen consumption, without the phosphorylation of ADP into ATP. In this state it was possible to get an idea of the oxygen used to maintain the mitochondrial membrane potential. (LEAK, leak-state respiration). Then the OXPHOS was evaluated through the administration of malate (1mM), glutamate (10 mM) and ADP (1.25 mM), while succinate (10 mM), added later, allowed the flux of the electrons through the reduction of $FADH_2$ (OXPHOS state). Next, the maximal electron transfer (ET) system capacity was evaluated after titration of carbonyl cyanide m-chlorophenyl hydrazone, an uncloupler

(CCCP, steps 0.05uM). Rotenone (Rot), a compound that inhibits oxidation of malate and it is required by complex I, was added. Thereby, complex I was blocked.

Finally, the injection of antimycin A (Ama, 5 mM) led to the assessment of the residual oxygen consumption (ROX state). Antimycin A is an antibiotic produced by Streptomyces spp., able to inhibit complex III.

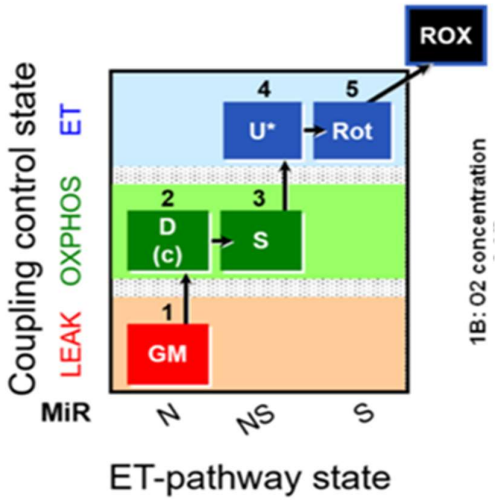

Figure 4. SUIT protocol used for the analysis of the NON-ACM CStCs and ACM CStCs after the exposure to the adipogenic medium.

3.9 Immunoistochemistry ACM hearts

Autoptic hearts were collected and processed at the Department of Medicine and Surgery at the University of Parma. Samples were fixed in 10% neutral buffered formalin for one week, and the solution was refreshed after the first three days. Multiple biopsies from the cardiac walls were collected from the heart and then embedded in paraffin. Embedded samples were cut in sections of 3 microns and then stained using haematoxylin-eosin. These sections were used for a preliminary evaluation of the tissues. After this first step, 4-microns sections were prepared for the staining with the GCN5 antibody (GCN5L2 (C26A10) Rabbit mAb #3305). The number of GCN5 positive cells was calculated analyzing 8 images acquired with a 40X objective and, in detail, counting the total number of cells of interest (spindle cells and cardiomyocytes) and the number of positive cells for GCN5. The percentage was obtained dividing the number of positive cells to GCN5 over the total number of counted cells and multiplying it by 100.

3.10 Statistical analysis

The samples used for the experiment were obtained at least from 7 controls and 8 ACM patients. Cells obtained from the same patient but in a subsequent amplification step were considered as biological replicates. In the case the same passage number for the same biological sample was used for the experiment, the values were averaged, and the obtained value used for further statistical analysis.

The statistical analysis was performed only for the experiments in which at least three independent measurements were collected.

The data of Western Blot analysis and respirometry experiments are reported as mean ± sem (standard error of the mean) and significance was assessed by non-parametric Mann-Whitney test. For more than two groups a non-parametric Kruskal-Wallis was used followed by appropriate post-hoc multiple comparison test. To account for the hierarchical structure of the experiments, we fit random intercept models (mixed or multilevel models). A multilevel model needs to specify fixed (e.g. group treatments) and random effects (e.g. number of fields in a slide). The model then recognizes the existence of data hierarchies, and separately takes into account variances at each level in the hierarchy, resulting in a more powerful data analysis approach. Details on the specific test used are reported in the figure legends. Under each figure a table is reported, reporting the Beta value, which represents an estimated effect of the treatment, corresponding to the increase/decrease of the measure of interest. A p-value < 0.05 was considered statistically significant. Analyses were performed using GraphPad Prism software 8.2.0. N.; random intercept models were fitted using the "mixed" command in Stata 14 (StataCorp. 2015. Stata Statistical Software: Release 14. College Station, TX: StataCorp LP.).

4 Results

4.1 Culture of NON ACM and ACM CStCs in basal amplification medium

NON ACM and ACM Cardiac Stromal Cells (CStCs) were amplified in complete basal amplification medium (BM), as reported in Materials and Methods. No morphological difference under the microscope was observed between NON ACM and ACM CStCs during the amplification steps: both NON ACM and ACM CStCs showed a fibroblast-like morphology (Fig.5). Cells were expanded for a maximum of 10 amplification steps (passage 10), before growth arrest occurred due to replicative senescence.

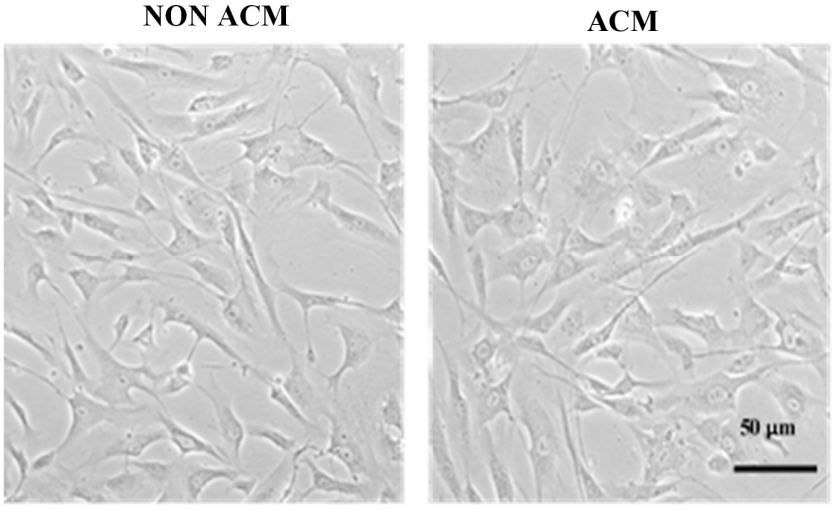

Figure 5. Morphological comparison between NON ACM CStCs and ACM CStCs. Representative phase contrast images of NON ACM and ACM CStCs cultured in BM. *Original magnification 10X.*

4.2 Evaluation of GCN5 protein expression in NON ACM and ACM CStCs in basal condition

In our study, we hypothesized a possible role of GCN5 in the adipogenic accumulation associated with ACM pathology. Firstly, we wanted to evaluate whether there was a difference in the protein expression level of GCN5 in NON ACM CStCs compared to ACM CStCs cultured in BM. A statistically significant higher expression of GCN5 in ACM CStCs was observable by Western Blot analysis (Fig.6).

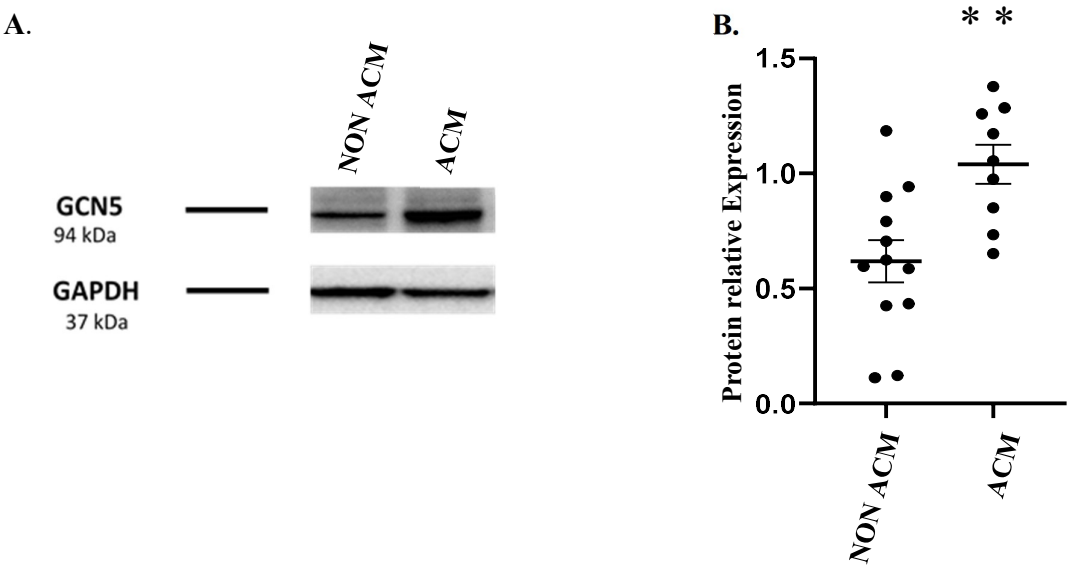

Figure 6. GCN5 protein expression in NONACM CStCs and ACM CStCs in basal condition. **A.** Representative bands. **B.** Densitometric analysis showing GCN5 protein expression in BM. (NON ACM=12; ACM=9. Mann-Whitney test: ** p <0.0043 vs NON ACM CStCs).

4.3 GCN5 gene knockdown

Considering the upregulation of GCN5 protein expression in ACM CStCs compared to controls, we prompted to investigate the possible role of GCN5 in ACM-associated lipid accumulation by knocking down its expression. Therefore, ACM CStCs were cultured in adipogenic medium (AM) to trigger intracellular lipid droplet formation [159] and subjected to GCN5 knockdown by infection with lentiviral particles for the delivery of shRNAs against GCN5. Specifically, three conditions were assessed: 1) ACM CStCs in adipogenic medium with the lentiviral particles coding for both shGCN5 and Green Fluorescent Protein (GFP); 2) ACM CStCs exposed to adipogenic medium in presence of lentiviral particles coding for scramble shRNA and with a C-terminal monomeric GFP; 3) ACM CStCs in adipogenic medium.

After 7 days of treatment, the efficiency of the transfection was evaluated by counting the number of infected, GFP-positive cells, over the total number of cells. Approximatively, the 80% of cells resulted positive for the GFP (Fig.7 A), proving a good infection efficiency. Western Blot analysis confirmed that GCN5 expression was reduced approximatively by 70% (Fig.7 B) in CStCs exposed to shGCN5. Importantly, GCN5 knockdown was associated with a significant decrease (negative beta) of CStCs intracellular lipid accumulation ($p=4.6x10^{-10}$), while there was no evidence of a significant difference when using the scramble vector (p=0.360). (Fig.7C; 7D).

A.

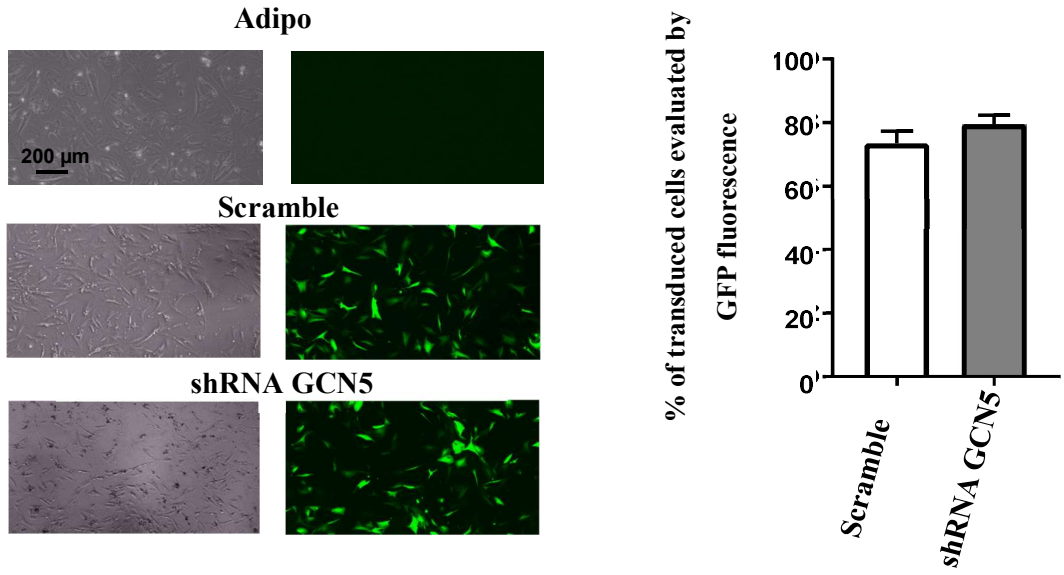
Adipo
200 µm
Scramble
shRNA GCN5
% of transduced cells evaluated by GFP fluorescence
100
80
60
40
20
0
Scramble
shRNA GCN5

B.

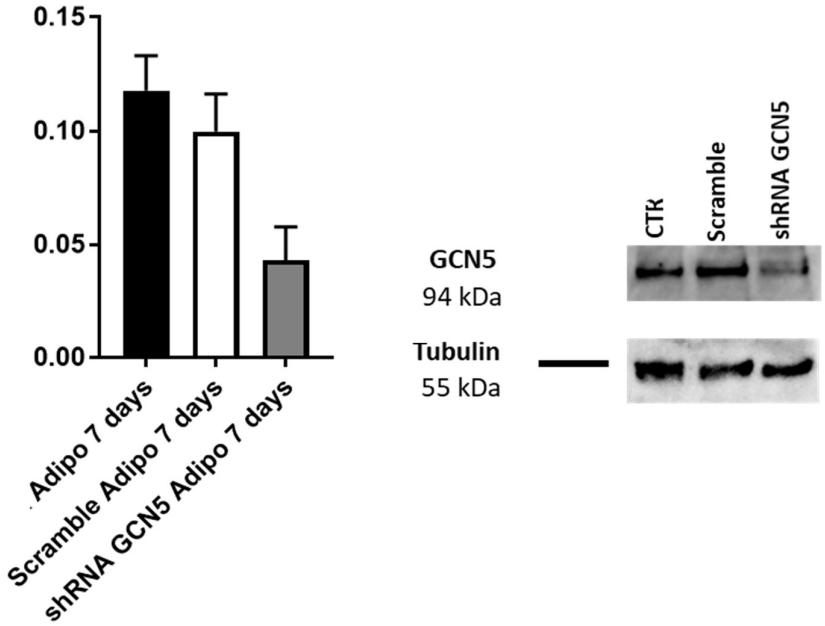
0.15
0.10
0.05
0.00
Adipo 7 days
Scramble Adipo 7 days
shRNA GCN5 Adipo 7 days
CTR
Scramble
shRNA GCN5
GCN5
94 kDa
Tubulin
55 kDa

C.

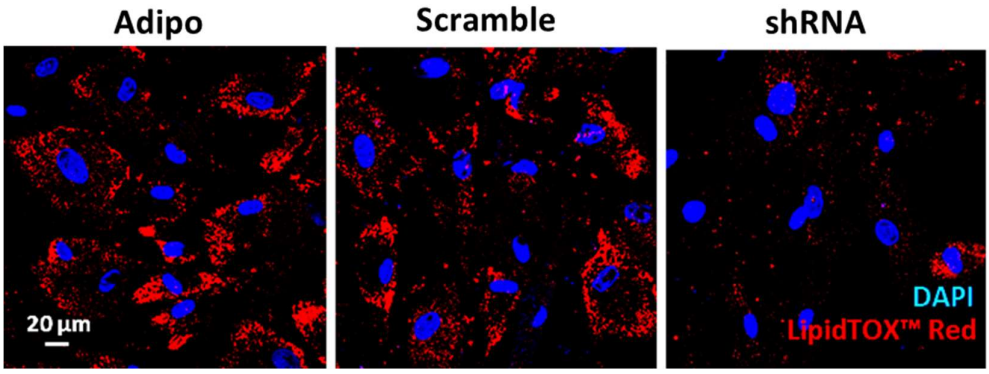

D.

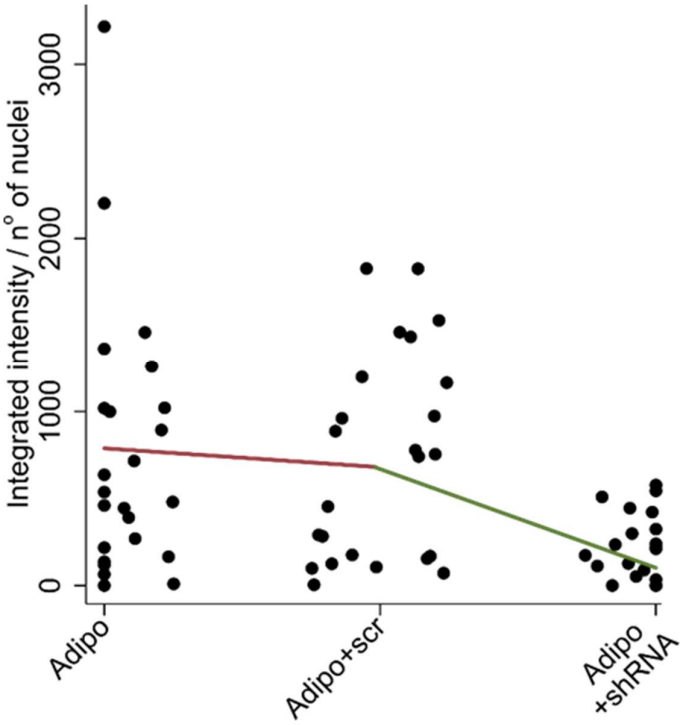

Outcome: Intensity	Beta	95% Confidence Interval	P value
Adipo + scramble vs Adipo	-99.2	-311.7; 113.20	0.360
Adipo + shRNA GCN5 vs Adipo	-675.6	-888; -463.1	$4.6x10^{-10}$

Figure 7. Evaluation of GCN5 knockdown in terms of GCN5 protein expression and rescue of the lipid accumulation. A. Representative images of the percentage of infected cells after gene knockdown. Bar graph displaying the percentage of infected cells (Wilcoxon test, ns). **B**. Western blot and densitometric analysis, showing GCN5 protein expression in ACM CStCs after gene knockdown. (ACM=3. Kruskall-Wallis test, ns). **C.** Representative confocal images of lipid accumulation in GCN5-knocked down cells, showing lipid droplets in red (HCS LipidTOX™ Deep Red Neutral Lipid Stain) and nuclei in blue (DAPI). *Original Magnification 40X*. **D**. Scatter plots of integrated intensity and table of descriptive statistics of lipid accumulation after GCN5 knockdown in ACM patients. Comparisons were made using the adipogenic treatment as reference category. Results are based on 3 independent patients, with 8 observations available for each treatment group.

4.4 Pharmacological inhibition of GCN5

After testing the effect of GCN5 knockdown by RNA interference, we wanted to confirm the effect of GCN5 pharmacological inhibition on intracellular lipid accumulation. To this aim, ACM CStCs were cultured for 7 days in adipogenic medium or adipogenic medium supplemented with MB-3 (200 μM), a specific inhibitor of GCN5 activity [203]

After the treatment with MB-3, cells showed a tendency to bundle organization (Fig.8 A). However, cell viability was not influenced by the MB-3 exposure (Fig.8 B).

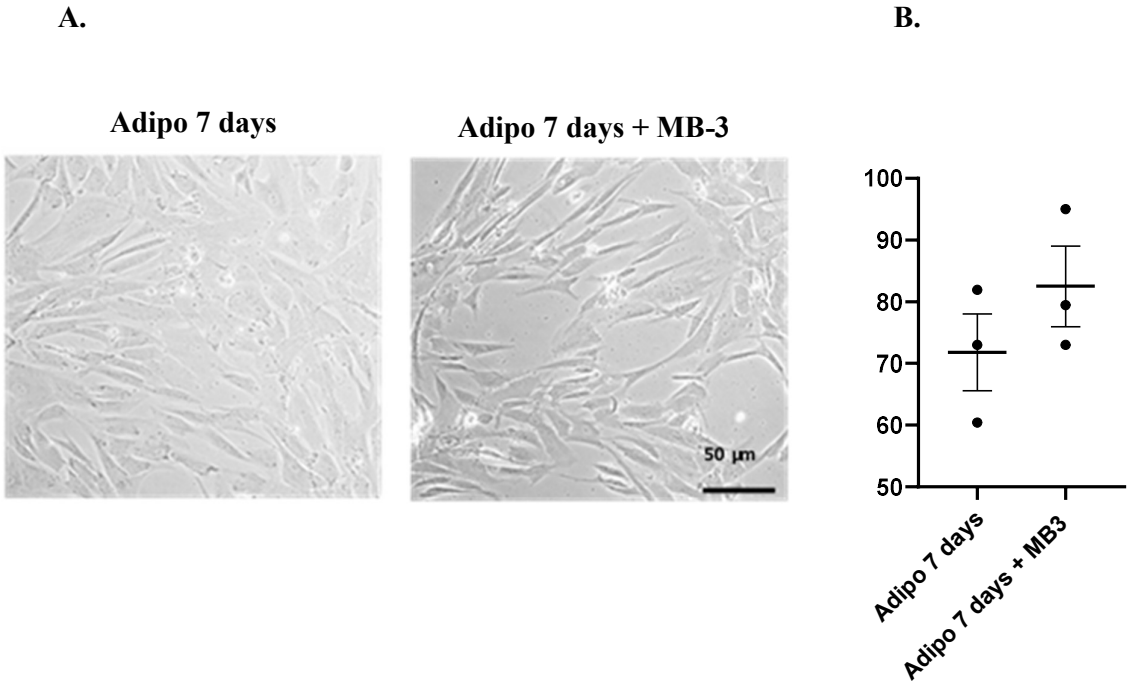

Figure 8. Evaluation of cell viability of ACM CStCs after the treatment with MB-3. A. Representative images of ACM CStCs after the exposure to 7-days adipogenic treatment either in the absence (left) and in the presence (right) of 200μM MB-3. *Original magnification 10X.* **B.** Dot plots representing the percentage of live cells after the exposure to the adipogenic treatment in presence or not of MB-3. (ACM=3, Wilcoxon test, ns).

4.5 Evaluation of lipid accumulation after MB-3 treatment

ACM CStCs in adipogenic medium exhibited evident lipid droplet accumulation. The treatment with MB-3 induced a significant ($p=5.5x10^{-17}$) decrease (negative beta) of lipid accumulation in these cells (Fig. 9).

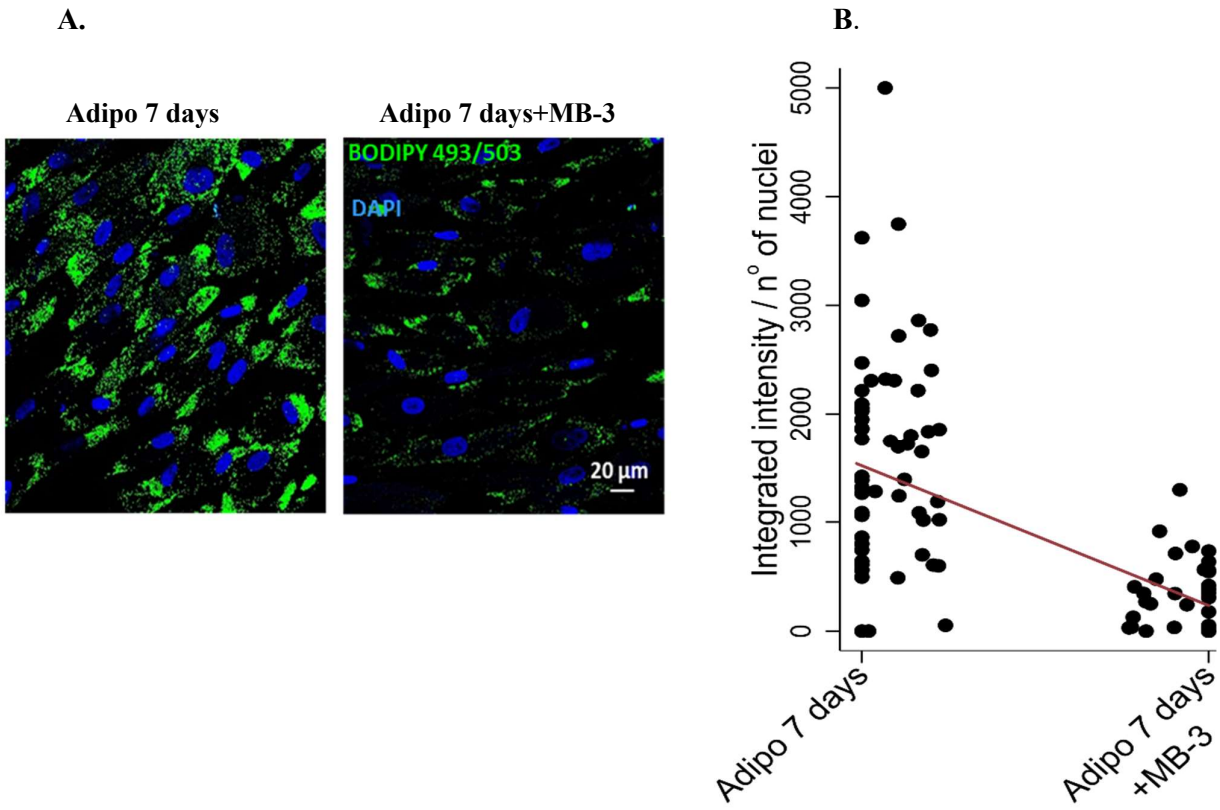

Outcome: Intensity	Beta	95% Confidence Interval	P value
Adipo 7 days vs Adipo 7 days + MB3	-1059.9	-1308.0; -811. 8	$5.5x10^{-17}$

Figure 9. Lipid accumulation in ACM CStCs after the exposure to the adipogenic medium and in presence of MB-3. A. Representative images of lipid accumulation droplets, in green (BODIPY 493/503), in ACM CStCs after the exposure to adipogenic medium without or with the treatment with MB-3. Nuclei are counterstained with DAPI (blue). *Original Magnification 40X*. **B.** Scatter plot and table of descriptive statistics of Bodipy fluorescence normalized on the total number of nuclei per field in ACM CStCs either in the absence or in the presence of MB-3. Results are based on 4 independent patients, with 7-15 observations available for each treatment group.

4.6 Evaluation of lipid droplets using the Transmission Electron Microscope (TEM)

An independent evaluation of intracellular lipid accumulation in basal medium and in the presence or absence of MB-3 was also performed by TEM analysis in collaboration with the Department of Medicine and Surgery of the University of Parma. As shown in Fig.10, TEM analysis confirmed an increase (positive beta) in lipid accumulation in ACM CStCs in AM compared to the ones in BM ($p=1.5x10^{-9}$) (Fig.10 A,B), while the exposure to MB-3 determined a statistically significant reduction (negative beta) of intracellular lipid accumulation ($p=0.002$) (Fig.10 C) , evaluated as the ratio between the area occupied by lipid droplets and the total area of the analyzed cells. (Fig.10 D).

A.

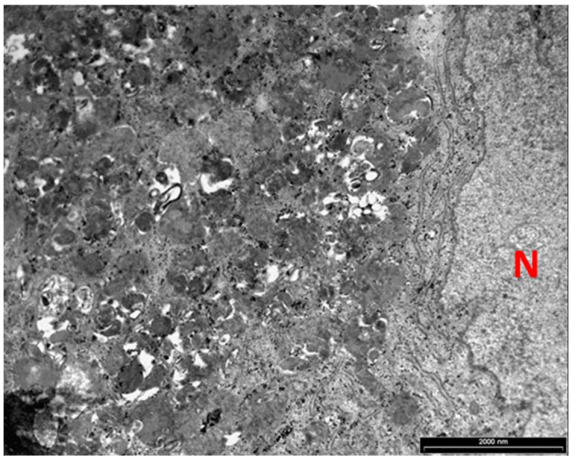

B.

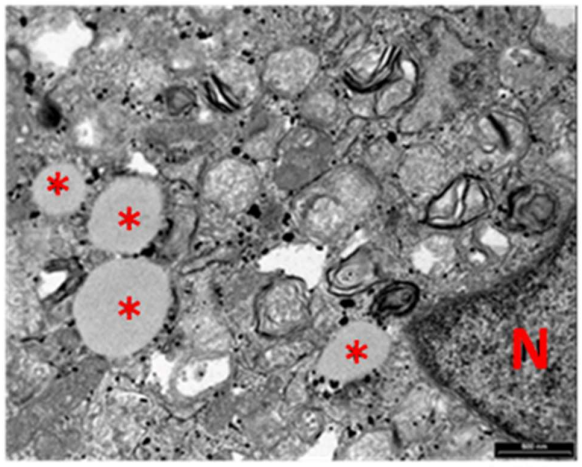

C.

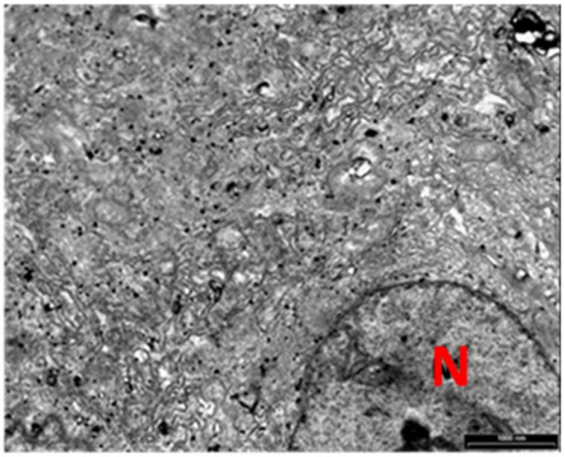

D.

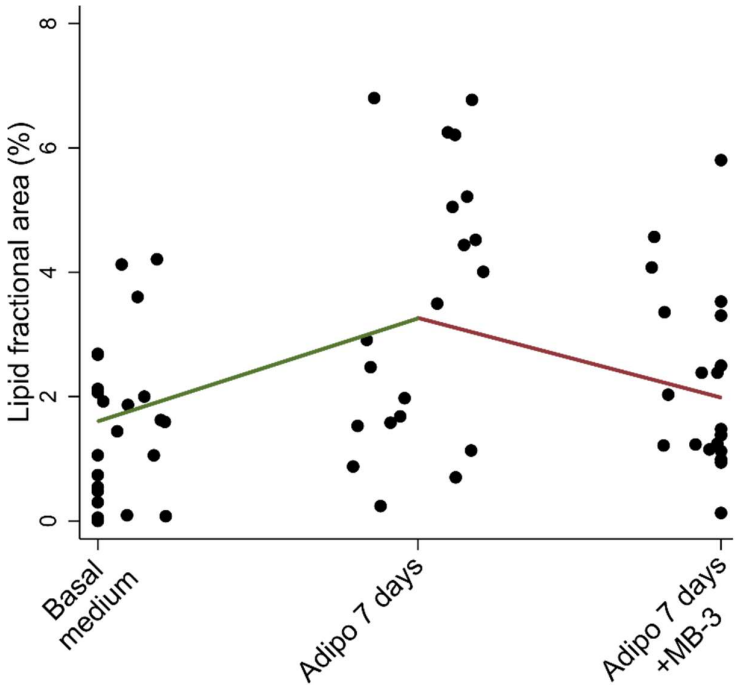

Outcome: Intensity	Beta	95% Confidence Interval	P value
Basal medium vs Adipo 7 days	1.7	1.0;2.4	$1.5x10^{-9}$
Adipo 7 days vs Adipo 7 days + MB3	-1.2	-1,9; -0.4	0.002

Figure 10. Lipid accumulation in ACM CStCs in BM, AM and after the treatment with MB-3. A. Representative images of lipid accumulation in ACM CStCs in BM (*original magnification 8900*); **B.** after the exposure to AM (*original magnification 18000*) and **C.** in presence of MB-3 (*original magnification 11000*). Red asterisks indicate lipid droplets, while the "N" indicates cell nuclei. **D**. Scatter plots and table of descriptive statistics of lipid fractional areas under the two different conditions tested in ACM patients. Results are based on 3 independent patients, with 5-9 observations available for each treatment group.

The results reported so far indicate that GCN5 inhibition (either by expression reduction or by pharmacological inhibition) led to reduced intracellular lipid accumulation in ACM CStCs samples.

4.7 Evaluation of upregulated and downregulated processes in ACM CStCs after GCN5 pharmacological inhibition

In order to evaluate the molecular pathways upregulated and downregulated after the exposure of ACM CStCs to the adipogenic treatment in presence/absence of MB-3, we performed a transcriptome analysis. The library preparation and the sequencing were performed at the NGS facility, University of Trento.

Starting from the list of the differentially expressed genes, reported in Appendix 1, listed in ascending order of expression based on the log2foldchange value, we used two bioinformatic tools in order to identify their biological functions trying to identify possible pathways specifically modulated by MB-3 in ACM CStCs cultured in adipogenic medium. Since a large collection of diverse gene set libraries is publicly available, we organized our analyses/results in two main categories: a first set of databases, that we called "Pathways and Ontologies", that is able to give an ontological description of the pathways involved, and the second one called "Transcription", which gives an indication about the possible factors able to regulate our gene lists. In particular we used the bioformatics tool "Enrichr" to access the data, subsequently processed in R/Bioconductor environment. Considering the high number of differentially expressed genes, it was possible to distinguish between upregulated and downregulated pathways. The reported graphs represent the enrichment of the biological terms based on the Combined score, a combination of the logarithm of the p-value computed using the Fisher's exact test and the rank score computed using a modification to Fisher's exact test in which we compute a z-score for deviation from an expected rank.

Among the upregulated processes in ACM CStCs exposed to adipogenic medium and MB-3, we found particularly interesting the following ones:

- oxidoreductase activity, acting on the aldehyde or oxo group of donors, NAD or NADP as acceptor; oxidoreductase activity, acting on NAD(P)H, quinone or similar compound as acceptor (Fig.11);
- aldo-keto reductase (NADP) activity, and more in detail the downregulated genes ALDH2, NQO1, AKR1C1, AKR1C3, AKR1B1, AKR1C2 (Fig.11);
- NADPH, NAD, NAP, NADH processes, with the NQO1 gene (Fig.11).

On the contrary, the most interesting downregulated processes were:

- extracellular matrix organization process, and more specifically the downregulated gene ADAM12 (Fig.13);
- Beta1 integrin cell surface interactions process, and the genes COL1A1, COL3A1, COL1A2, COL5A1, COL4A1, COL4A4, COL11A1, COL4A3, COL5A2 (Fig.13);
- Integrin-linked kinase signaling, collagen biosynthesis and modifying enzymes, assembly of collagen fibrils and other multimeric structure, collagen formation, with the downregulated genes COL1A1, COL3A1, COL4A3, COL4A1, COL4A4, COL4A2 (Fig.13).

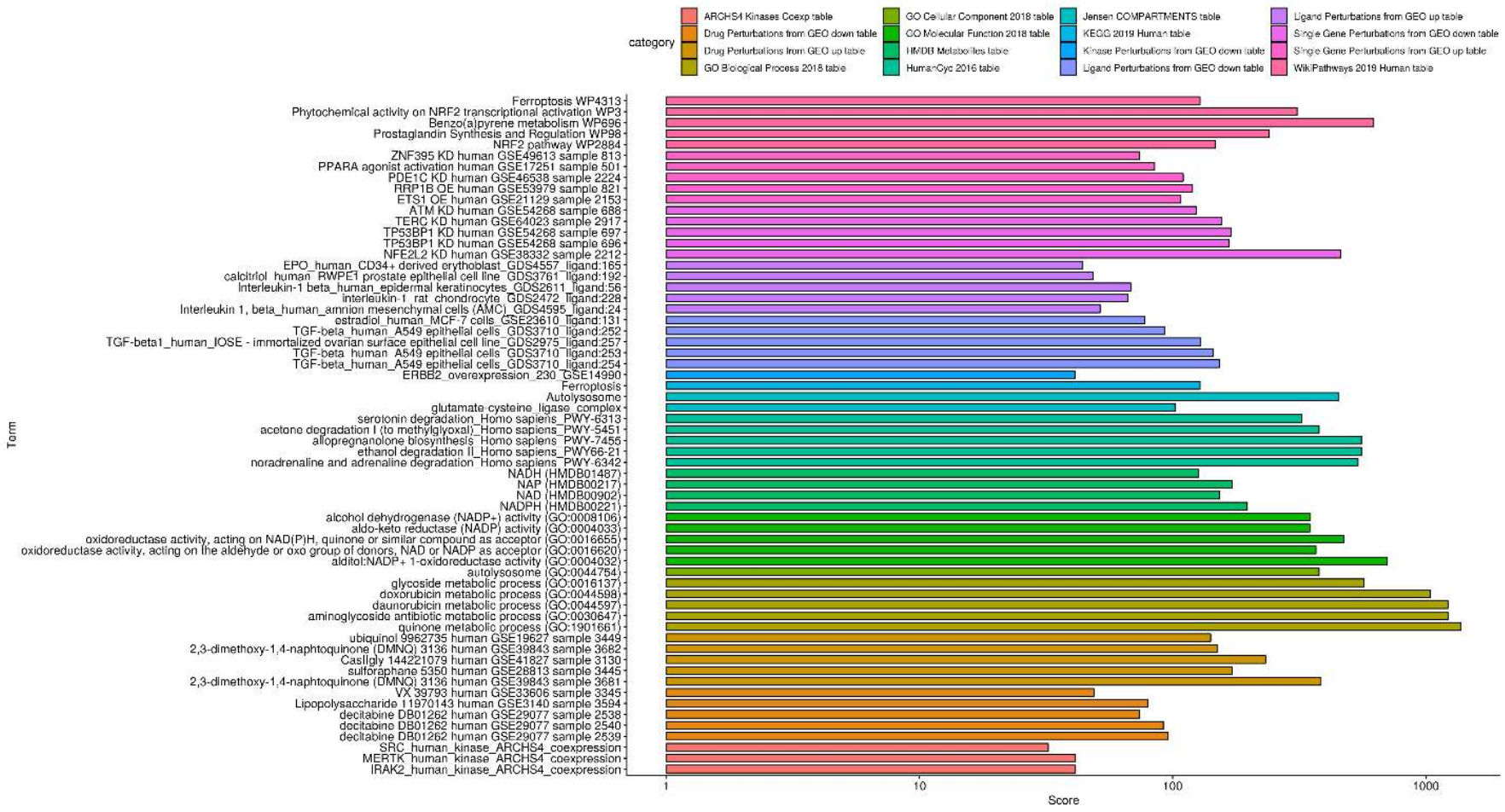

Figure 11. List of the processes resulting upregulated in ACM CStCs exposed to MB-3. The processes were identified using as bioinformatic tools the ´Pathways and ontologies´ databases.

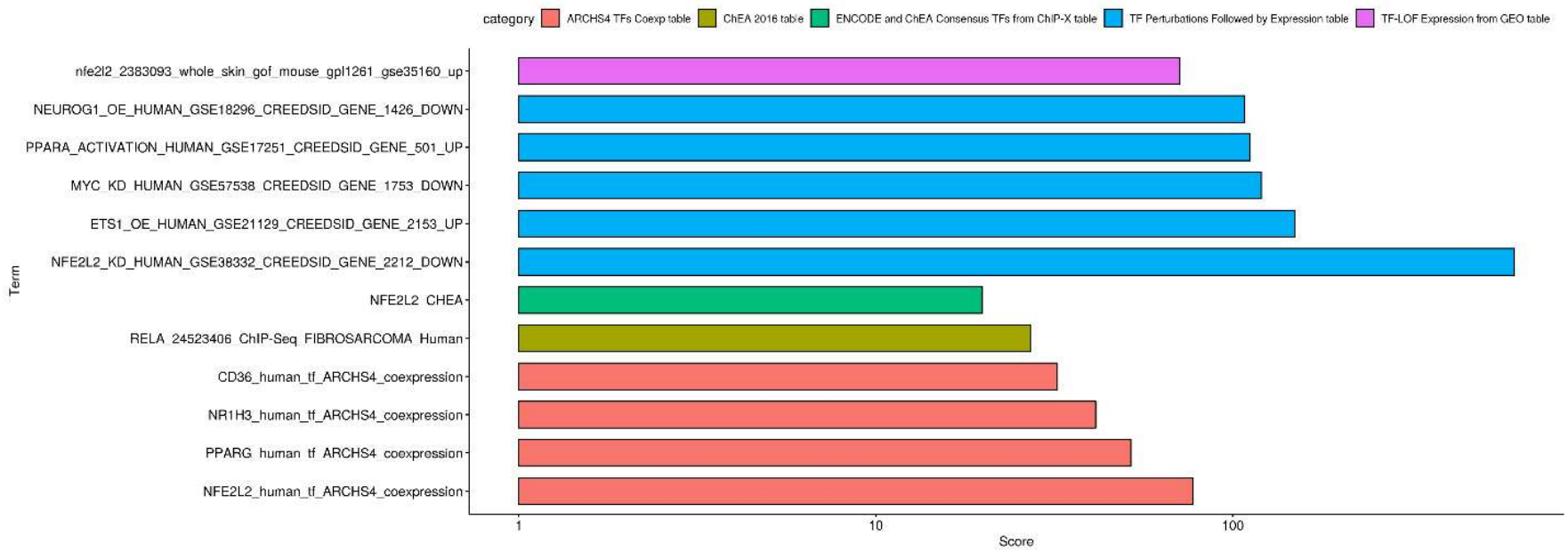

Figure 12. List of the processes resulting upregulated in ACM CStCs exposed to MB-3. The processes were identified using as bioinformatic tools the ´Transcription' databases

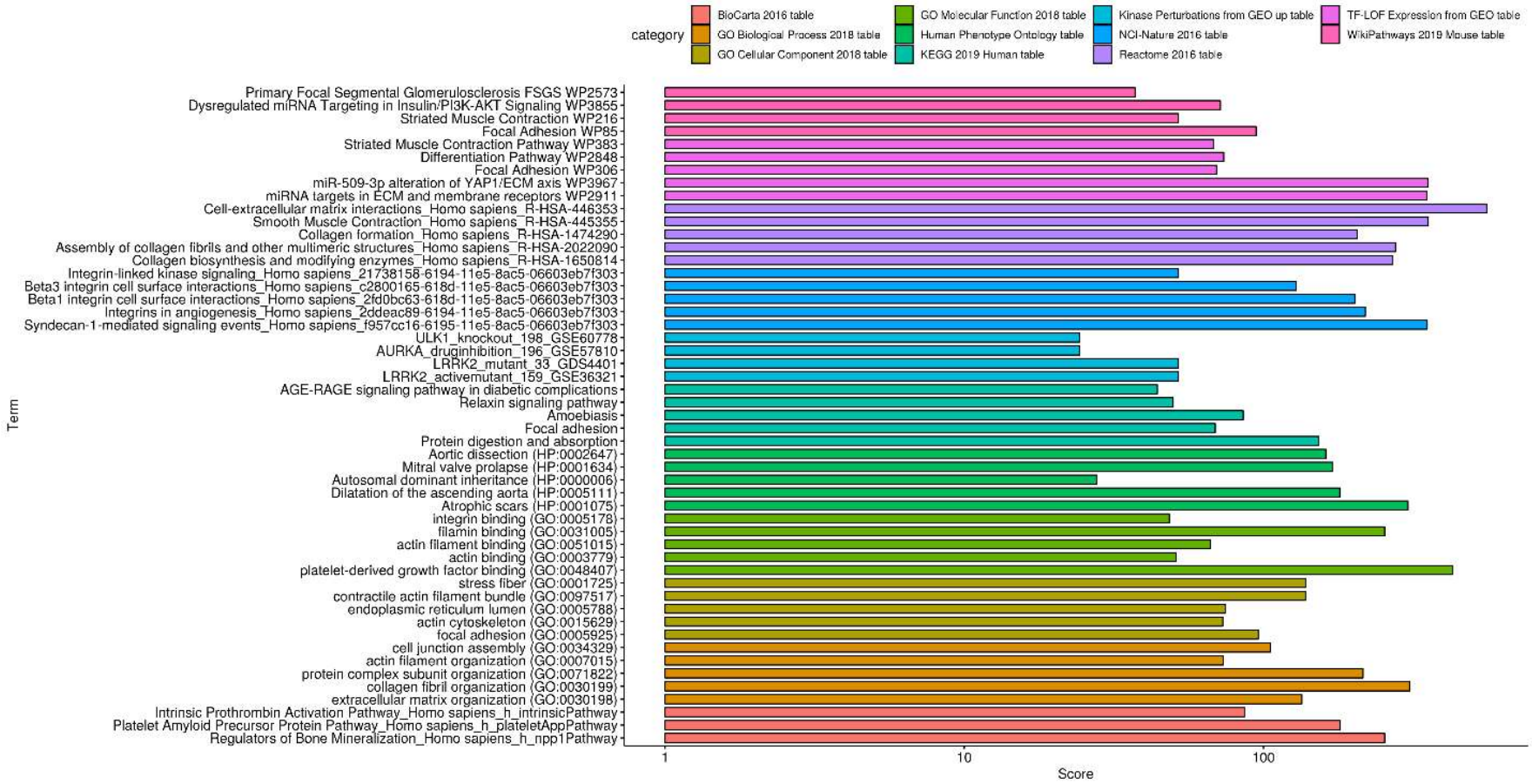

Figure 13. List of the processes resulting downregulated in in ACM CStCs exposed to MB-3. The processes were identified based on the 'Pathways and ontologies' databases.

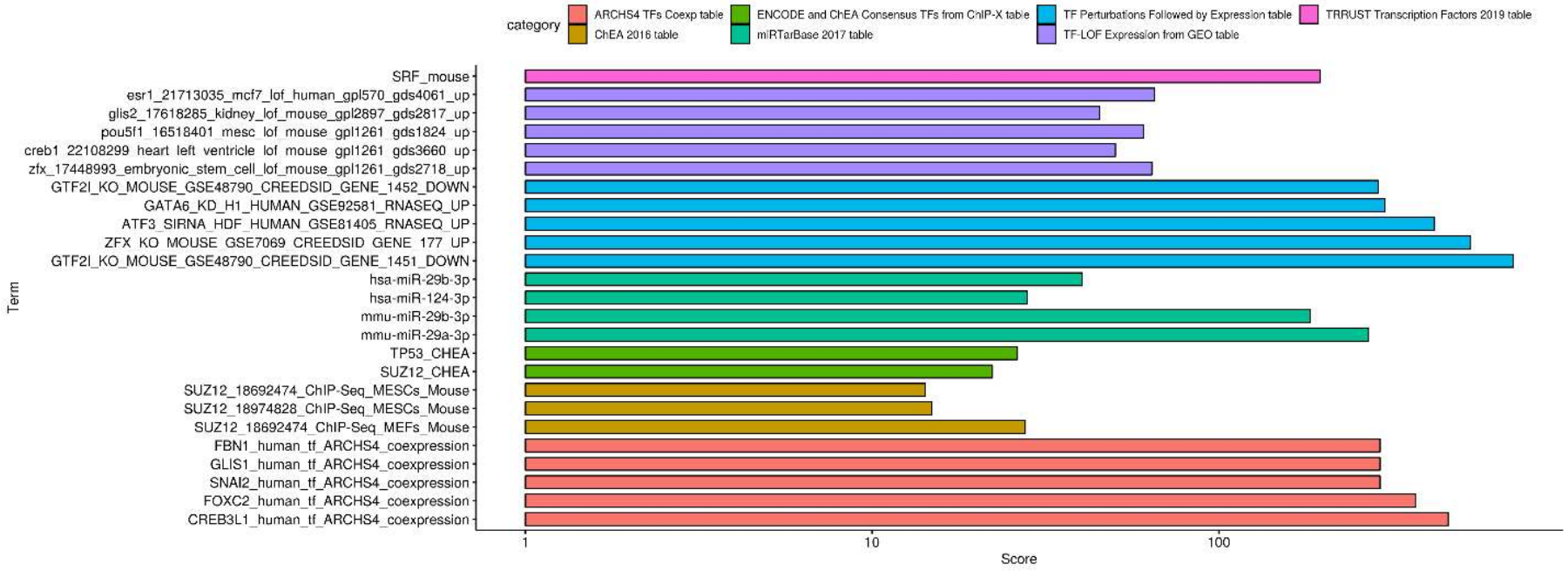

Figure 14. List of the processes downregulated in in ACM CStCs exposed to MB-3. The processes were identified using as bioinformatic tools the ´Transcription´ database.

4.8 Evaluation of respirometry activity in NON ACM CStCs vs ACM CStCs in adipogenic conditions

Transcriptome results revealed an upregulation in NAD and redox balance related processes after the treatment with MB-3. For this reason, we started to deeply investigate the oxygen consumption, namely the respiratory capacity, in ACM CStCs and NON ACM CStCs by means of high-resolution respirometry (Oxygraph-2K, OROBOROS INSTRUMENTS, Innsbruck, Austria). As described in Materials and Methods, this protocol allowed the evaluation of several respiration states.

As shown in Fig.15 B, at the beginning of the respirometry protocol, we measured the routine respiration, and we did not observe any difference between NON ACM and ACM CStCs. Also during the LEAK state (3MG), no difference in the oxygen consumption was displayed. After the addition of ADP (4D), the mitochondrial OXPHOS capacity seemed to be slightly increased in ACM CStCs compared to NON ACM CStCs. The administration of Cytochrome C enabled us to test the integrity of the outer mitochondrial membrane: an increase in oxygen consumption rate after Cytochrome C would have indicated a damaged outer mitochondrial membrane [210]. However, in this experiment, there was no increase in oxygen consumption rate after the addition of Cytochrome C in both samples (5c), allowing us to speculate that mitochondria were well- preserved.

Interestingly, the maximum mitochondrial respiratory capacity (OXPHOS, 6S), observed after the addition of succinate (S), was higher in ACM cells than in NON ACM cells. In other words, a higher respirometry activity was displayed in ACM CStCs compared to NON ACM CStCs (Fig.15).

A.

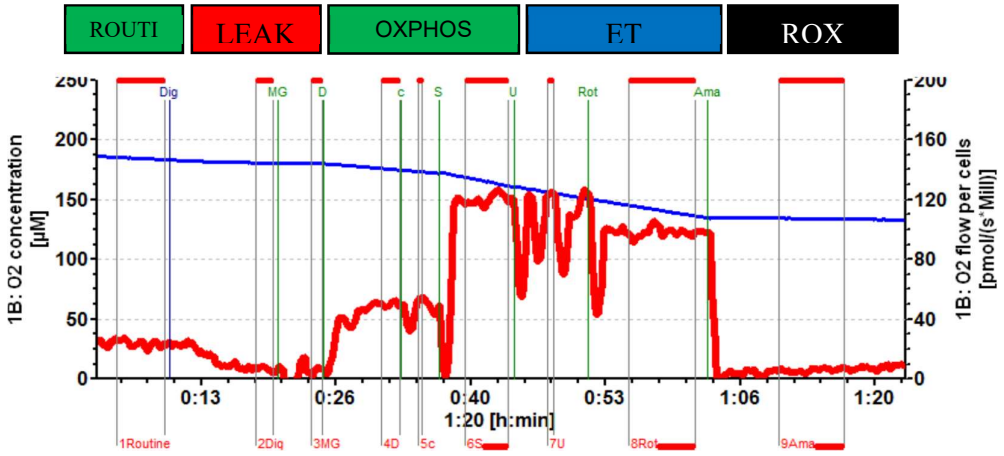

B.

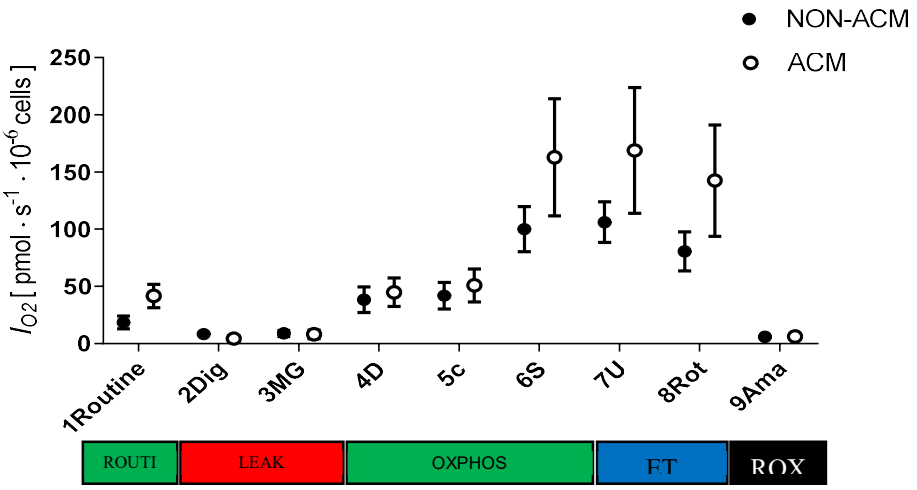

Figure 15. **Evaluation of the mitochondrial respiratory capacity in NON-ACM CStCs and ACM CStCs. A**. Representative trace of the respiration in cardiac stromal cells. **B**. The graph represents the different respiratory states of NON ACM CStCs and ACM CStCs after 7 days in adipogenic medium. (NON ACM CStC=2, ACM CStC=4). Abbreviations: **Dig:** Digitonin, **MG**: Malate + Glutamate, **D**: ADP, **C**: Cytocrome C, **S**: Succinate, **U**: Uncoupler (FCCP), **Rot**: Rotenone, **Ama**: Antimycin A.

4.9 Evaluation of mitochondrial Reactive Oxygen Species (ROS) in ACM CStCs

The upregulation of the redox balance related processes revealed by the transcriptome analysis and the fact that an increase has been described of the intracellular Reactive Oxygen Species (ROS) accumulation during the first stages of adipocyte differentiation [127] prompted us to evaluate the concentration of mitochondrial ROS in NON ACM CStCs vs ACM CStCs after 7 days of adipogenic treatment. Cells were stained with MitoSox Red dye, able to selectively bind the mitochondrial ROS. Images were acquired with confocal microscope and then used to quantify the fluorescence of the dye. The quantification of MitoSox signal showed an increase (positive beta) of mitochondrial ROS in ACM CStCs samples compared to NON ACM (p=0.051) (Fig.16).

A. **B.**

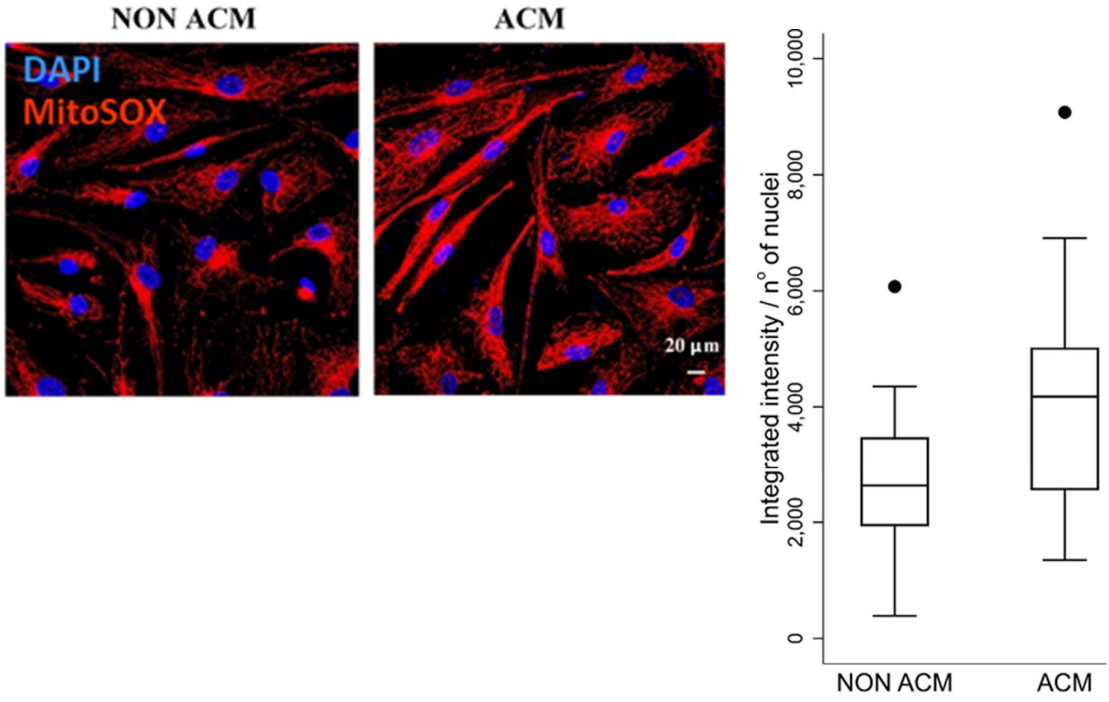

Outcome: Intensity	Beta	95% Confidence Interval	P value
ACM vs NON ACM Adipo 7 days	1665.1	-7.4; 3337.6	0.051

Figure 16. Mitochondrial ROS accumulation in NON ACM CStCs and ACM CStC. A. Representative images of ROS accumulation in NON ACM CStC and ACM CStC stained with MitoSox Red, able to bind the mitochondrial ROS, and with DAPI (blue) staining the nuclei. Images were taken after the exposure to adipogenic medium for 7 days. *Original Magnification 40X* **B**. Box plot and table of descriptive statistics of integrated ROS intensity. Results are based on 4 independent ACM patients, with 7-9 observations available for each treatment group, and 5 independent NON ACM subjects, with 3-9 observations available for each treatment group.

4.10 Evaluation of lipid accumulation after the exposure to the mitochondrial ROS scavenger MitoTempo

Taking into account the already reported connection between ROS accumulation and lipid accumulation [127], we treated our samples of ACM CStCs with the mitochondrial ROS scavenger, MitoTempo, in the presence of adipogenic medium. We observed a decrease (negative beta) in the lipid accumulation in ACM CStCs after the treatment with MitoTempo ($p=4.4x10^{-6}$) (Fig.17), showing for the first time that the treatment with a specific scavenger for mitochondrial ROS can affect intracellular lipogenesis

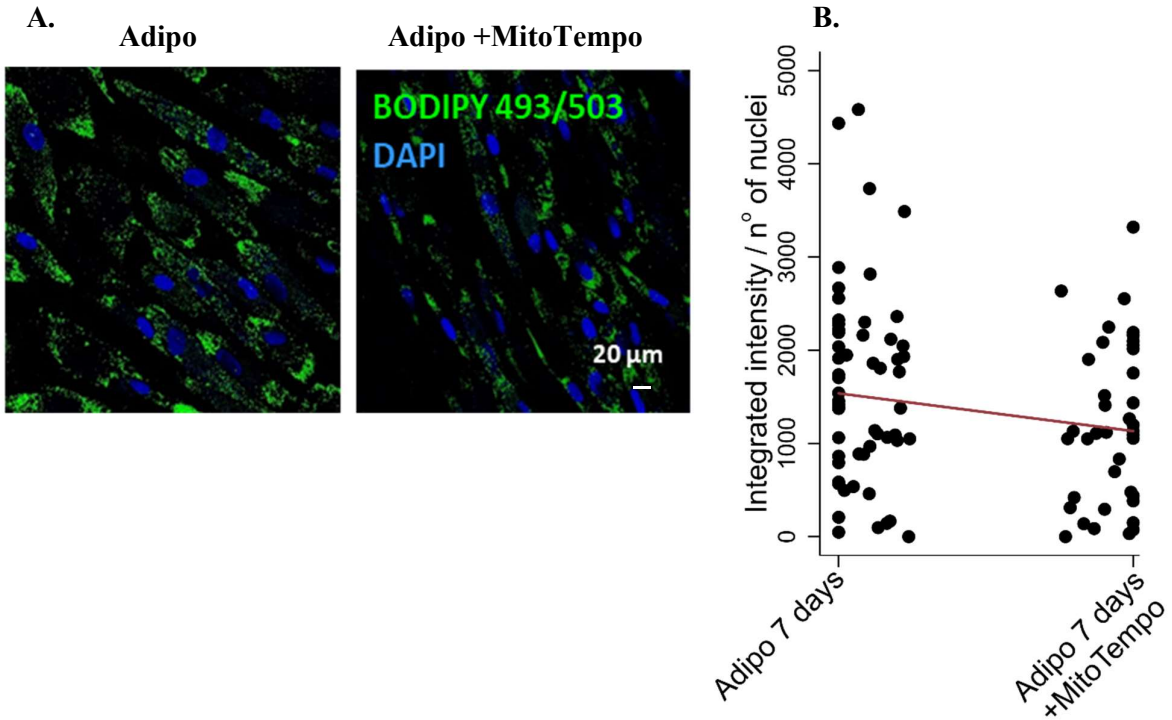

Outcome: Intensity	Beta	95% Confidence Interval	P value
ACM 7 days vs ACM 7 days + MitoTempo	-548.8	-783.0; -314.6	$4.4x10^{-6}$

Figure 17. Lipid accumulation in ACM CStCs after the treatment with MitoTempo. A. Representative images of lipid accumulation in ACM CStCs after the exposure to the adipogenic medium for 7 days in absence or in presence of MitoTempo. Intracellular lipids are stained with BODIPY 493/503 (green). Nuclei stained with DAPI show blue fluorescence. *Original Magnification 40X* **B**. Scatter plot of integrated intensity and table of descriptive statistics of lipid accumulation in ACM patients before and after treatment with MitoTempo. Results are based on 4 independent patients, with 7-15 observations available for each treatment group.

4.11 Evaluation of ROS after the treatment with MB-3

In order to confirm the possible link between ROS accumulation and adipogenesis, we tested whether the treatment with MB-3 could lead to a reduction in terms of mitochondrial ROS concentration. We exposed ACM CStCs to the adipogenic medium in presence or absence of MB-3 and, after the end of the treatment, we stained the cells with the MitoSox dye, able to selectively target mitochondria where it is oxidized by local superoxide.

Of note, the intensity of the MitoSox-associated fluorescence signal was significantly (negative beta; $p=3.0x10^{-8}$) reduced under MB-3 treatment, thus suggesting that GCN5 inhibition could reduce intracellular lipid accumulation by acting on mitochondrial ROS pathways (Fig.18).

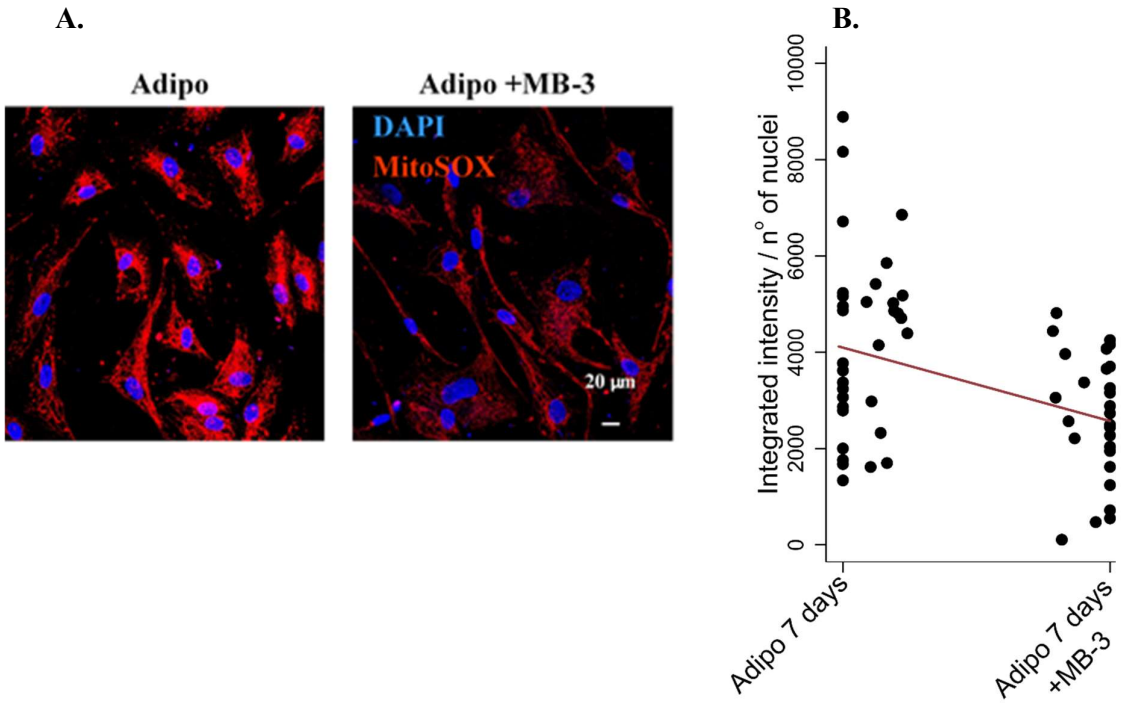

Outcome: intensity	Beta	95% Confidence Interval	P value
ACM 7 days vs ACM 7 days+MB-3	-1.394.0	-1887.1; -900.9	$3.0x10^{-8}$

Figure 18. ROS accumulation in ACM CStCs after the treatment with MB-3. A. Representative images of ROS accumulation in ACM CStCs stained with MitoSox, labelling mitochondrial ROS and DAPI staining nuclei, after the exposure to the adipogenic medium for 7 days in absence or in presence of MB-3. *Original Magnification 40X* **B**. Scatter plot and table of descriptive statistics of integrated ROS intensity in ACM patients before and after treatment with MB-3. Results are based on 4 independent patients, with 8-9 observations available for each treatment group.

4.12 Immunohistochemistry on human ACM hearts

Another important evaluation of GCN5 expression has been performed on human autoptic tissues at the Department of Medicine and Surgery of the University of Parma. Specifically, 3 autoptic tissues obtained from people diagnosed of ACM post-mortem, 1 sample of scars of myocardial infarction and 1 sample belonging to the heart of a person died not for cardiac problems, were used for the analysis.

The presence of GCN5 positive cells with a spindle morphology, typical of fibroblast cells, was observed only in ACM samples and, in detail, the calculated positivity was at about 5-15 % for the first sample, 30-40% for the second sample, and 20-30% for the third one, while no positive GCN5-positive cells were observed in myocardial infarction scar tissue and in the healthy heart (Fig.19).

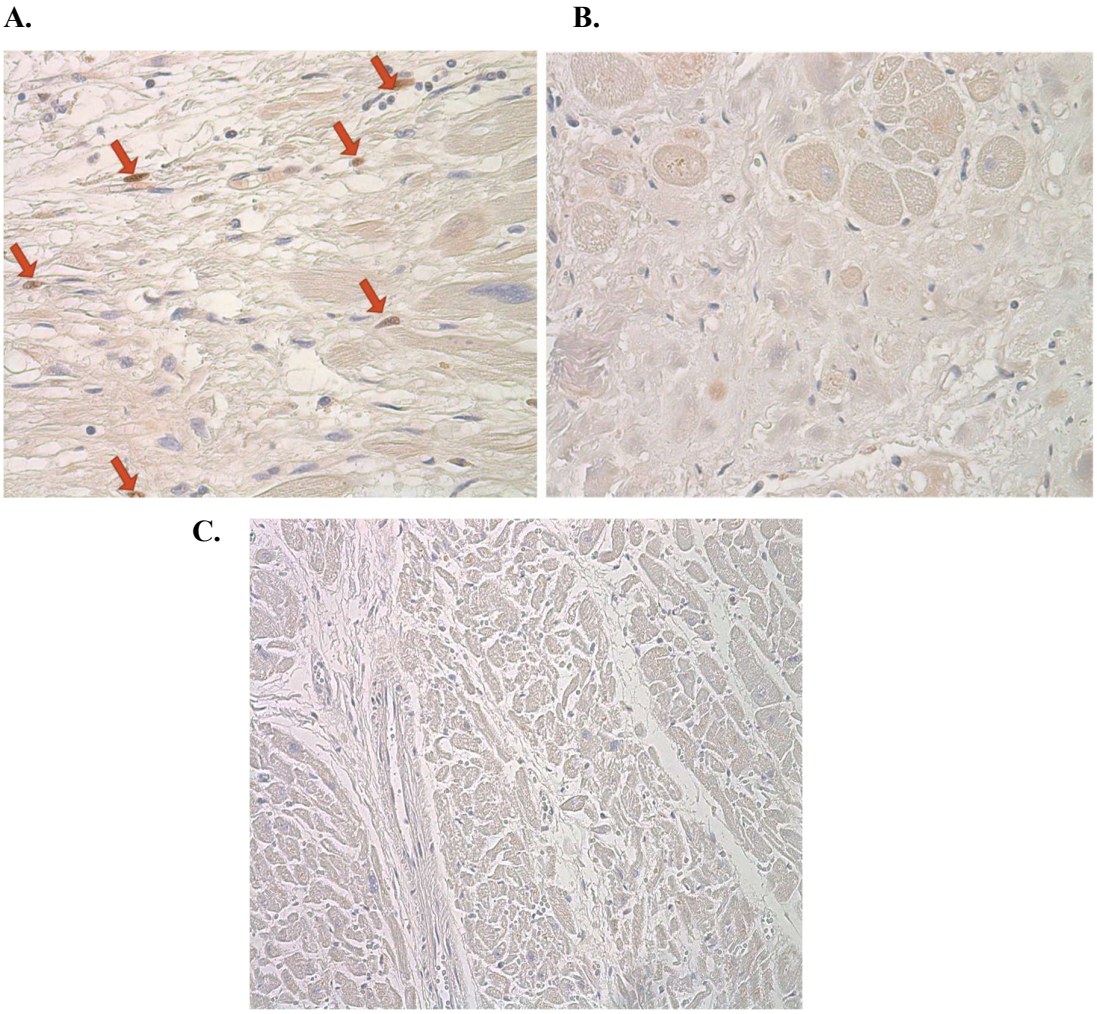

Figure 19. Representative images of ACM immunoistochemiytry for the evaluation of GCN5 expression in human tissue sections. **A**. ACM , **B**. Myocardial infacrtion scar and **C**. control heart. In the panel A. spindle cells GCN5 positive are indicated by the presence of red arrows.

5 Discussion

Arrhythmogenic Cardiomyopathy (ACM) is a rare genetic disorder with an incidence of about 1:5000 people [211], classically described as inherited in an autosomal dominant mode with low penetrance and variable expressivity [12, 31, 32]. In the early stages of the disease, manifestations are variable and often subtle: they include palpitations and syncope due to ventricular arrhythmias, microscopic fibro-fatty replacement of cardiac myocytes (CMs) and electrocardiographic abnormalities [90]. Macroscopic fibro-adiposis is the characteristic hallmark of the disease at late stages [212]. Therefore, ACM has a double pathologic phenotype: arrhythmias and fibro-fatty substitution leading to ventricular dysfunction.

No etiologic therapy is currently available for ACM patients. As for the arrhythmic issue, symptomatic treatments include, at present, the administration of antiarrhythmic drugs [213], the implantation of a cardioverter device [214] and the ablation of the arrhythmia substrate [215]. To date, no conventional therapies exist for fibro-fatty degeneration except heart transplantation in patients with end-stage heart failure [212].
Although arrhythmic events still represent the major issue for ACM patients, we still lack a comprehensive understanding of the molecular determinants of heart tissue degeneration that, in worst cases, can lead to heart transplantations in patients subjected to arrhythmia treatments by means of anti-arrhythmic drugs and/or sub-cutaneous implanted defibrillator. The involvement of the Wnt/β-catenin pathway in ACM has been demonstrated by different authors. Intriguingly, although unable to rescue desmosomal structure, the modulation of the Wnt pathway has been proven to be a successful approach to reduce intracellular lipid droplet accumulation as demonstrated by Caspi and colleagues [101], that treat ACM-iPSC-CMs with an inhibitor of the GSK-3β kinase. GSK-3β is a key player of the Wnt pathway, being part of the destruction complex that dephosphorylate β-catenin in the absence of Wnt ligands [115]. Of note, GSK-3β kinase is able to reverse disease phenotypes in a zebrafish model of ACM [216] and prevent cardiac dysfunction in two murine models of ACM [217]. Garcia-Gras and co-workers also suggest that Plakoglobin (PG) could translocate from the non-functional desmosomes into the nucleus, where it inhibits the Wnt/βcatenin pathway, promoting the switch from the activation of proliferation to adipogenic pathways [10, 96].

Though several evidences have been reported to support Wnt pathway as responsible of the ACM adipogenic phenotype [96, 115, 218], it has not been accepted as the only possible mechanism. Evidence also exists that the Wnt pathway could be affected by the activation of the Hippo pathway: Yes-associated protein (YAP), one of the main regulator of the Hippo

pathway, is considered as the trigger for the suppression of Wnt pathway, since it interacts with β-catenin, leading to its sequestration and, therefore promoting a switch to the adipogenic cascade [111]. Additionally, other studies suggest the involvement of other pathways, as the TGFβ pathway [112] and the RhoA/MRTFA pathway [114].

Recently, PPARy activation has been demonstrated to be crucial for modelling the disease using iPSC-CMs [94] and human primary cardiac stromal cells (CStCs) [159]. Intriguingly, the activation of PPARγ is known to induce the inhibition of canonical Wnt/β-catenin signaling in several tissues [219], thus suggesting the importance of these two pathways' s cross-talk also in the onset and progression of ACM. Kim et al. demonstrate that in patient-specific mutant PKP2-iPSCs-CMs, after the exposure to two adipogenic media, it is possible to observe the typical ACM phenotype. More specifically, the exposure to a 3 factor (3F) adipogenic medium, composed of insulin, dexamethasone and 3-isobutyl-1-methilxanthine (IBMX) is linked to an increased activation of PPARα, the main transcriptional regulator of fatty acid metabolism in adult cardiomyocytes [220], and to a mild activation of PPARγ pathway [94]. On the contrary, the addition of rosiglitazone and indomethacin to the 3F medium cause an overactivation of PPARγ pathway, resulting in extended lipogenesis and apoptosis [94]. Interestingly, the treatment with only rosiglitazone and indomethacin, in absence of the three other adipogenic factors, is not able to induce lipogenesis although producing an increased activation of PPARγ. These results suggest that the activation of both PPARγ and PPARα is requested for the recreation *in vitro* of the ACM phenotype [94]. In the same work, the authors also highlight the potential role of redox signaling in ACM, showing that the reduction of Reactive Oxygen Species (ROS) concentration in PKP2-iPSCs-CMs, using a specific ROS scavenger, is able to decrease the apoptosis in this cell model [94].

In several studies it has already been reported a link between adipogenesis and the acetyltransferase, GCN5 [195, 196]. GCN5 has a broad range of functions, as cell proliferation, differentiation, cell cycle, DNA repair [187, 195] and it is able to acetylate both histones [182, 184] and non-histonic substrates as PGC1-α, master regulator of mitochondrial biogenesis [191]. In general, HATs family, to which GCN5 belongs to, has already been demonstrated to be involved in the regulation of white adipocyte differentiation, increasing the transcription of some target genes [221, 222] The involvement of HATs has also been shown in the activation of CBP (CREB Binding Protein) and its homologue p300: HATs are able to bind these factors, enhancing adipogenesis [223]. The inhibition of both CBP and p300 is also able to silence the expression of adipogenic genes,

including PPARy [224]. *In vivo* model, as Crebbp+/-mice show reduced white adipose tissue mass, suggesting that CBP has a pivotal role in adipogenesis [225]. Jin et al. also demonstrate the inhibition of PPARγ transcription in an immortalized line of brown pre-adipocytes with a double knockout for GCN5 and its homologous PCAF [195]. In accordance with these findings, Wang et al. report that, in absence of GCN5/PCAF, Pol II is still recruit to the PPARγ promoter via CCAAT-enhancer-binding protein β (C/EBPβ), but Pol II elongation is inhibited, leading to the inhibition of PPARγ transcription. Indeed, GCN5/PCAF KO cells exposed to an external adipogenic stimulus show a reduction in adipogenic genes expression, as PPARγ, and a decrease in lipid droplets accumulation [195]. It has also been shown by Wiper-Bergeon that, when C/EBP proteins are acetylated at K98/101/102 by GCN5, the transcriptional potential of these co-factors is strongly increased, while the affinity with their corepressor complex is decreased [196]. In this specific study, the balance between the transcriptional role and the repression activity of this co-factor family is regulated by the presence of glucocorticoids and in 3T3 L1 pre-adipocytes and NIH 3T3 fibroblasts, C/EBP family regulation seem able to control the differentiation process of mature adipocytes [196]. Therefore, Wiper-Bergon et al. describe GCN5 as an important factor for the differentiation of embryonic preadipocytes [196].

In our model we observe an increased protein expression level of GCN5 in ACM CStCs compared to NON ACM CStCs. This observation prompt us to investigate if exaggerated lipid accumulation observed in ACM CStCs exposed to adipogenic medium [159] could be decreased by treatments aimed at reducing GCN5 expression or activity. More specifically, we obtain a consistent reduction of GCN5 expression in ACM CStCs by delivering GCN5-targeting short hairpin RNAs (shRNAs) through lentiviral particles. shGCN5-ACM-CStCs show a significantly reduced intracellular lipid accumulation compared to the scrambled control. In addition, a strong reduction in terms of lipid accumulation (quantified both by BODIPY staining and Transmission Electron Microscope analysis) is also observed when ACM CStCs are exposed to the adipogenic medium in the presence of MB-3, a selective GCN5 inhibitor.

Importantly, the immunohistochemistry on tissues obtained from people diagnosed post mortem of ACM, reveal the presence of spindle cells positive for GCN5 expression, while scar myocardial infarction tissues and heart sections from control individuals result negative for GCN5 expression.

To the aim of clarify the mechanisms of action by which GCN5 inhibition leads to a reduced intracellular lipid accumulation in ACM CStCs, we perform the analysis of the poly-(A)+ transcriptome of ACM CStCs exposed to adipogenic medium in presence or not of MB-3. MB-3 administration significantly modulates different processes, among which we find particularly interesting those related to extracellular matrix organization and redox metabolism.

More specifically, processes linked to extracellular matrix organization result to be downregulated in ACM CStCs exposed to adipogenic medium in the presence of MB-3. It has already been described that during adipogenesis an extracellular matrix remodeling occurs, due to the switch from a fibronectin stromal matrix typical of early adipocytes to a typical basement membrane of adult adipocytes [226, 227]. Particularly interesting for future validation studies seems the downmodulation of ADAM12 after MB-3 treatment. ADAM12 is a protein belonging to the ADAMs adhesion proteins and metalloproteases family, and there are two human forms derived from alternative splicing: 1) ADAM12-L, the long-transmembrane form and ADAM12-S, the shorter one, lacking the transmembrane cytoplasmatic domain [228]. It has already been reported an enhanced adipogenesis in a transgenic-mouse model for the overexpression of ADAM12 [229] and the role of ADAM12 has also been showed in the adipogenic differentiation of mesenchymal cells [230]. Kawaguchi et al. demonstrate that ADAM12 mRNA levels are particularly high when fibroblasts are in a pre-adipocyte state, though the expression of this protein is visible in almost all the stage of the adipogenic differentiation [231]. In addition, they observe that ADAM12 is able to impact several processes not only related to the re-arrangement of ECM in fibroblastic pre-adipocytes, but also to the actin cytoskeleton, and cell adhesion.

The re-organization of the adipose tissue is supported by collagen and elastic fibers: the network is composed of fibronectin and laminin which interacts with collagen fibers [232], providing the attachment for the integrins anchored to the adipocyte membranes [233]. Intriguingly, the MB-3 treatment downmodulates processes related to β1 integrin and to collagen biosynthesis, organization, formation and assembly. In particular, the downmodulation of genes coding for proteins of collagen family. Collagens are the most common structural proteins of ECM and they are generally divided in fibrillar (collagens I-III, V and XI) and non-fibrillar [233]. Previous studies show that preadipocyte cell lines, during differentiation, increase the expression on the cell surface of type I–VI collagens compared to undifferentiated cells [234].

Taken together these results seem to indicate that MB-3 is able to reduce fibrotic- related processes. Our observation requires in depth validation: the demonstration that MB-3 is also able to restore fibrotic pathways could open new perspectives for the treatment of both the fibrotic and the fatty substitution in ACM hearts.

Additionally, compared to cells exposed only to the adipogenic medium, the treatment with MB-3 seems to upregulate the processes linked to NAD related genes and, more in general, the processes related to the redox balance. In particular, the upregulation of the expression of Quinone reductase (NQO1) and Aldehyde dehydrogenase 2 (ALDH2) is observable in CStCs exposed to MB-3. NQO1 is a flavoprotein, containing the cofactor FAD, important to ensure NQO1´s stability and functionality [97]. NQO1 can be considered as a sensitive indicator of the redox state of cells and its expression has been described to increase after the increment in the (ROS) production in 3T3-L1 preadipocytes. Ross et al. show that NQO1 might be activated against oxidative stress when the redox balance is altered and the expression of detox enzymes, as SOD, are low [97].

ALDH2 plays an important protective role at mitochondrial level in several diseases, which also include the cardiovascular ones [235-237]. The main function of ALDH2 is linked to the detoxification of endogenous and exogenous aldehydes, able to protect the cell and to ensure its survival [235]. It has been shown that the upregulation of this gene might be able to have a good impact on myocardial fibrosis after myocardial infarction, since ALDH2 activity leads to a reduced expression of collagens protein and α-smooth muscle actin (α-SMA) [238-240]. Yuhan et al. show that the exposure to transforming growth factor β (TGFβ1) is able not only to induce the activation of the cardiac fibroblast in myofibroblasts, but also to activate Smad2 and Smad3 which are phosphorylated, activating the TGFβ pathway, and inhibiting ALDH2. The inhibition of Smad2 and Smad3 leads to a restore of ALDH2 activity and to a reduction in the rate of differentiation of human cardiac fibroblasts and collagen production [241].

In addition, several isoforms of genes belonging to the Aldo-Keto Reductases (AKRs) result to be upregulated in ACM CStCs compared to cells treated with MB-3. These enzymes mainly use as cofactors pyridine nucleotides and they generally catalyze oxidation-reduction reactions, as reduction of glucocorticoids and glucose [242]. In detail, AKRs are able to catalyze the reduction of aldehydes and ketones, and they used as cofactor NADPH.

Thus, transcriptome results seem to indicate that MB-3 could exert its anti-lipogenic action by acting on intracellular redox balance.

We firstly sustain this hypothesis by demonstrating that the mitochondrial ROS content in CStCs from ACM patients is higher compared to control CStCs. Additionally, when we treat the CStCs with the GCN5 inhibitor we observe a strong reduction in mitochondrial ROS levels, suggesting a possible link with GCN5 upregulation and mitochondrial oxidative stress in ACM CStCs. In agreement, and in line with previous reports showing that mitochondrial antioxidants are able to reduce lipid accumulation, together with the expression levels C/EBPα and proliferator activated receptor gamma PPARγ2 [123, 127], we also observe a reduction in the adipogenic accumulation of ACM CStCs after the treatment with the mitochondrial ROS scavenger MitoTempo, confirming that also in our model ROS are associated with intracellular lipid accumulation.

In agreement with our findings, recent studies have reported that mitochondrial oxygen consumption and ROS levels increase during adipogenesis [121, 122]. In Mesenchymal Stromal cells (MSCs) the inhibition of complexes of the respiratory chain involved in the ROS production could lead not only to a reduction of ROS concentration, but also to an attenuation in PPARγ mRNA levels and its target genes transcription. Wang et. al confirm that in MSCs an increase in intracellular ROS concentration is visible in the early-stage of adipocyte differentiation, and, at the same time, an overexpression of the transcription factor PPARy [127]. Intriguingly, the intracellular energetic balance is strictly connected with HATs' activity; indeed, Guapel et al. demonstrate in yeast that the siRNA knockdown of GCN5 leads to an increased accumulation of ROS, including superoxide, and cell death, while the treatment with antioxidants, as N-acetylcysteine (NAC) seem able to reduce these two mechanisms [243].

More experiments are required to elucidate if the increased mitochondrial ROS abundance observed in ACM CStCs is due to an increased ROS production or to a decreased detoxification capability.

Interestingly, it is already known that one of the main sources of ROS production is the electron transport system (ETS) of mitochondria: an alteration in the function of mitochondria could be responsible of an increased mitochondrial production, contributing to the onset of several disease as cardiomyopathies, diabetes and neurodegenerative disorders [244] Considering the evidences obtained in our results of the altered pathways related to the metabolic processes and the increased ROS concentration in ACM CStCs, we more deeply investigate the mitochondrial activity of our cells, evaluating their oxidative phosphorylation (OXPHOS) capacity. We observe an increase in the OXPHOS of ACM

CStCs compared to NON ACM CStCs after 7 days in adipogenic medium. In line, Ducluzeau et al. observe in 3T3-L1 mouse adipocytes an increase in the oxygen consumption and in the membrane potential [245]. They also link this increase in the respiration to an increased ROS production after 6 days of adipogenic stimulation, while this concentration seems to decrease at day 9 when an enhanced expression of antioxidant enzymes is observed [245]. This study seems to confirm our results regarding the increased oxygen consumption after adipogenic treatment.

Finally, it should also be considered that the primary phenotypic manifestation of ACM is the occurrence of arrhythmias [85]. In our study we do not perform experiments aimed to evaluate this specific phenotypical aspect, but we find particularly interesting the link between ROS and arrythmia. It has already been reported that lipid peroxidation, a common product of oxidative stress, can be associated with arrhythmic events [246], while the treatment with antioxidants, as omega-3 polyunsaturated fatty acids, could moderate the arrhythmic phenotype [247]. Interestingly, it is well recognized that the electroanatomical substrate of arrhythmia development depends on the cross-talk between cardiac myocytes and fibroblasts [248], but no further studies have been conducted in order to better characterize this aspect in ACM. The evaluation of a possible link between the increased ROS concentration in CStCs and the possible consequences on the communication with CMs, would be of particular interest.

6 Conclusions

In this study GCN5 has been proposed for the first time as a possible player in the higher accumulation of intracellular lipids observed in primary cardiac stromal cells isolated from ACM patients. Our results show that both the specific pharmacological inhibition and the RNA interference gene knockdown of GCN5 are able to reduce lipid accumulation in ACM CStCs exposed to an adipogenic trigger. Preliminary evidence obtained by transcriptome analysis performed on ACM CStCs seems to indicate that the treatment with the specific GCN5 inhibitor MB-3 has a significant effect on processes related to oxidative stress, already known for playing a role in adipogenesis [127]. We have confirmed the link between GCN5 and cellular redox balance by demonstrating that MB-3 treatment significantly reduces mitochondrial ROS abundance, which appears increased in ACM CStCs compared to control CStCS. In agreement with this hypothesis, the treatment of ACM CStCs with the mitochondrial ROS scavenger MitoTempo significantly reduces intracellular lipid accumulation. However, it is conceivable that the adipogenic reduction observed upon MB-3 treatment does not depend only on its apparent mitochondrial anti-oxidant effects. Other promising mechanisms of action that requires future in-depth investigation includes the alteration of processes related to the extracellular matrix remodeling, also described to be regulated during adipocyte differentiation [249].

In conclusion, the work performed in this thesis contributes to the elucidation of the molecular mechanisms underlying fatty accumulation in ACM and could potentially open new perspectives for ACM treatment. In fact, even though GCN5 is an acetyltransferase with pleiotropic cellular effects and, therefore, it cannot be considered as a proper pharmacological target, the investigation of its downstream effectors that we started to investigate with the transcriptome analysis could potentially bring to the identification of novel and more specific molecular determinants of the disease and more specific pharmacological interventions for the future.

All these new evidences on a possible role of GCN5 on ACM adipogenesis need to be confirmed by further experiments. First of all, it would be interesting to evaluate whether the overexpression of GCN5 in NON ACM CStCs is able to lead to a similar lipid accumulation, as observed in ACM CStCs. Secondly, all the modulated processes in presence of MB-3 need to be validated, in order to better elucidate the pathways and the specific players which could be used as a pharmacological target in order to reduce lipid accumulation.

RESEARCH PERIOD ABROAD

UNIVERSITY OF SURREY

SCHOOL OF BIOSCIENCES AND MEDICINE

Dr. Patrizia Camelliti

Dr. Alessandra Rossini

Co-culture of Induced Pluripotent Stem Cells derived Cardiomyocytes and Cardiac fibroblasts to study Arrhythmogenic Cardiomyopathy

7 Co-culture of Induced Pluripotent Stem Cells derived Cardiomyocytes and Cardiac fibroblasts to study Arrhythmogenic Cardiomyopathy

7.1 Aim

During my last year of PhD, I had the chance to spend a three-months period at the University of Surrey, in the laboratory of Dr Patrizia Camelliti. This exchange program has been supported by a Short-Term Fellowship, funded by EMBO. The aim of this project has been focused on the set up of a bi-dimensional model with Induced Pluripotent Stem Cells derived Cardiomyocytes (iPSC-CMs) of Arrhythmogenic Cardiomyopathy (ACM) patient and healthy control with human cardiac fibroblasts (CStCs) commercially available, evaluating the electrophysiological properties of this model.

7.2 Introduction

ACM has been considered, for a long time, a cardiomyocyte-specific disease, since this cell type express desmosomes, essential for cell-cell adhesion and, as already shown, generally mutated in the context of ACM. Evidence has been provided that direct transdifferentiation of cardiac myocytes into adipocytes occurs in ACM hearts [250]. Of note, iPSC-CMs have been demonstrated to at least partly recapitulate the phenotype of the disease *in vitro*, showing intracellular lipid accumulation and altered functional properties. In this context, a very recent study from the group of Moretti [114] shows that iPSC-CMs from a patient with *PKP2* mutation spontaneously convert into adipocytes when exposed to mechanical stress, demonstrating that mechanosensing plays a critical role in determining CMs identity. Intriguingly, the arrhythmogenic predisposition can be lethal even in the absence of macroscopic fibro-fatty substitution. Although a link between desmosomal proteins and arrhythmias has been shown by Cerrone and Delmar [251] demonstrating that decreased expression of plakophilin2 leads to a decrease in sodium current (I_{Na}) amplitude, the mechanisms of arrhythmia generation especially in the initial phase of the disease are yet poorly understood.

Recently another possible cell type has been proposed to be involved in ACM onset. As already described in the thesis (paragraph 1.3.3) Sommariva et al. [159] show that also non-contractile cardiac mesenchymal stromal cells (CStCs) can convert into adipocytes in ACM patients, suggesting that this cell model can also be a valid option for the *in vitro* investigation of ACM. Given the known role of activated fibroblasts [252], namely myofibroblasts, both in fibrosis and in abnormal electrical coupling with CMs [253] , it is conceivable to believe that fibroblasts and/or myofibroblasts play an important role not only

in the adipogenic, but also in the arrhythmogenic and fibrotic phenotypes associated with ACM disease.

Of interest, although it is well recognized that the electro-anatomical substrate of arrhythmia development depends on the cross-talk between cardiac myocytes and fibroblasts [248], there is a substantial lack of study investigating this interaction in the context of the ACM. The communication between cardiomyocytes and fibroblasts is based both on the effects of diffusible signaling factors released in the extracellular environment, but it is also based on the activity of junctional structures. Indeed, junctional coupling of myocytes and fibroblasts is able to modulate calcium fluxes which can also contribute to incidence of arrhythmias in fibrotic heart tissue [254].

Starting from these considerations, in order to better elucidate these mechanisms in the context of ACM, the project I performed during my stay at Surrey University was focused on two principal aims:

- Set-up a two-dimensional monolayer co-culture system of iPSC-CMs from ACM patient and control sample with commercially available primary CStCs;
- Investigate the electrophysiology of the cell monolayer composed both of iPSC-CMs and primary CStCs using advanced optical mapping.

7.3 Methods and experimental plan

7.3.1 iPSC amplification

iPSCs, reprogrammed at the Institute for Biomedicine, EURAC from Peripheral Blood Mononuclear Cells (PBMCs) of one ACM sample and one control sample, were sent at the University of Surrey to perform experiments.

Frozen iPSCs vials with >1 x 10^6 cells were thawed in the water bath at 37°C, until the cell suspension was almost completely thawed. The mixture of cells and cryogenic solution, composed of foetal bovine serum (FBS, Gibco) and 10% Dimethyl sulfoxide (DMSO, Sigma), was then diluted in 3 mL of StemMACS™ iPS-Brew XF (Miltenyi), a xeno-free media formulated and optimized for the amplification of iPSCs and their maintenance in a pluripotent state under feeder-free conditions. Cells were then centrifuged at 300 x g for 5 minutes, and the supernatant was removed, and the cell pellet was resuspended in fresh 0.5 mL of StemMACS™ iPS-Brew XF added with 10 µM Y-27632, able to improve the recovery of the cells. Cells were then plated in pre-coated plates with a coating of Matrigel®

(Corning), a basement membrane matrix, able to help the attachment and the expansion of cells. Plates were then placed in a 37°C incubator gassed with 5% CO_2. Medium was changed every day. After 4-5 days in culture, when iPSCs reached a confluence of 70-80%, cells were washed twice with phosphate buffer saline (PBS) and detached using Tryple reagent (Thermo Fisher Scientific), a recombinant cell-dissociation enzyme mix without animal-derived components. After the detachment, cells were centrifuged at 300 x g for 5 minutes and resuspended in the culture medium supplemented with 10 μM Y-27632 and 94.500 were plated in a new Matrigel coated plate. The medium was refreshed every day.

7.3.2 Cardiomyocyte differentiation

Once cells were 70% confluent, iPSCs underwent the cardiomyogenic differentiation, using the PSC Cardiomyocyte Differentiation Kit (Thermo Fisher Scienific). This is a complete ready-to-use and xeno-free system kit for the efficient differentiation of human iPSCs in cardiomyocytes. This differentiation kit has been formulated based on the protocol proposed by Burridge et al. [255]. The formulation is based on the modulation of the Wnt signaling pathway, and it consisted of the exposure of iPSCs to three different media. First, iPSCs were cultured for two days in Medium A, able to stimulate the Wnt pathway, replaced after two days with the Medium B, formulated to repress the Wnt pathway. After other two days, cells were exposed to the Maintenance medium, which maintained cells in a differentiated state until cardiomyocytes start beating. Spontaneously contracting cardiomyocytes started to appear after 8-10 days and they could be maintained in culture for 30-40 days before starting with further characterization experiments.

7.3.3 Dissociation and purification of beating cardiomyocytes

On the 25th day of differentiation, the beating monolayer of cardiomyocytes was dissociated in order to obtain single-cell population of cardiomyocytes. The efficiency of enrichment was 80-90%.

Firstly, the detachment of the beating monolayer was performed using an enzymatic optimized kit, the Multi Tissue Dissociation Kit 3 provided by Miltenyi Biotec. In detail, the beating monolayer was incubated for 10 min at 37°C with the Enzyme T, diluted 1:10 in the Buffer X. After gently pipetting, the enzymatic activity of the Enzime T was stopped by adding basal medium with a higher concentration of FBS (20%) and composed of KO-DMEM, 1 mM NEAAs, 1% Penicillin/Streptomycin, 20 mM L-Glutamine, 0.1 mM β-mercaptoethanol. CMs were dissociated to single-cell and passed into a MACS SmartStrainers (70 μm-filter) and the flow-through centrifuged for 5 min at 200 x g. After

the detachment, cardiomyocytes were enriched using the PSC-Derived Cardiomyocyte Isolation Kit provided by Miltenyi Biotec, following a protocol based on the depletion of non-cardiomyocyte contaminants by magnetic labeling of cells with microbeads. Specifically, the dissociated cells were resuspended in a Buffer, composed of PBS, 0.5% BSA and 2mM EDTA, and incubated for 5 min with Non-Cardiomyocyte Depletion Cocktail (Miltenyi Biotec) at 4°C. Cells were centrifuged for 5 min at 200 x g and the obtained pellet was resuspended in the same buffer previously described and incubated with Anti-Biotin microbeads. After 10 min of cold incubation and the adjustment of the volume to 500 ul, the cell suspension was ready for the magnetic separation using the LS Column with the appropriate MACS Separator (Miltenyi Biotec). The columns were placed in the magnetic field of the separator and rinsed with the same Buffer in which cells were resuspended. The cell suspension was applied onto the column and the flow-through collected in a tube: only cells without the microbeads labeling (cardiomyocytes) were collected in the tube, while the non-cardiomyocytes remained entrapped in the magnetic column. After the enrichment, CMs were plated in basal medium composed of KO-DMEM (ThermoFisher), 2% defined FBS (Hyclone Defined), 1 mM NEAAs (Thermo), 1% Penicillin/Streptomycin (Thermo), 20 mM L-Glutamine (Thermo), 0.1 mM β-mercaptoethanol (Thermo), on Matrigel-coated dishes for further experiments.

7.3.4 Amplification of human cardiac fibroblasts

Human ventricular cardiac stromal cells, CStCs, were purchased ScienCell Research Laboratories. They are isolated from human adult ventricle of subjects presenting non cardiac pathologies (https://www.sciencellonline.com/products-services/primary-cells/human/cell-types/fibroblasts/human-cardiac-fibroblasts-juvenile-ventricular.html).

CStCs are cryopreserved at passage 1 and delivered frozen; each vial contains >5 x 10^5 cells in 1 ml volume of medium. Cells were thawed, centrifuged at 100 x g for 5 minutes and resuspended in Fibroblast Medium-2 (FM-2). Once cells reached the confluence of 70%, they were ready to be split: after washing with PBS, 2 ml of Trypsin (Gibco) were added to the cells at 37°C for 3 minutes and 30 seconds. After the first incubation with Trypsin, most of the cells appeared still attached and only some of them floated. Floating cells were collected in a tube that containing 5 ml of FBS to inactivate Trypsin. The dish with the remining cells was then put back in the incubator for 1 more minute of Trypsin incubation and after this second incubation cells appeared rounded. 5 ml of Trypsin Neutralizing solution (TNS) were added to the cells to stop the activity of Trypsin. After pipetting up and down gently, detached cells were added to the previous collected ones and centrifuged at

100 x g for 5 minutes. The supernatant was removed, the pellet resuspended in 1 ml of medium and cells plated into flasks with other 6 ml of medium. Considering that our final aim was to culture CMs and CStCs together, we tried to expose CStCs to the basal medium, used to keep in culture CMs. We observed that CStCs normally grew in this different medium, therefore we were able to use this milieu for our co-culture model.

7.3.5 Co-culture model set up

After the purification step, 94.500 CMs were plated on 35 mm glass bottom dishes with a 14 mm glass coverslip diameter, coated with 25 ug/ml of Fibronectin (Sigma) diluted in PBS. CMs were cultured in basal medium supplemented with 10 μM Y-27632. The day after the dissociation, the medium was replaced with fresh medium.

After 5 days in culture, when CMs formed a complete monolayer, fibroblasts were added in a ratio CStCs:CMs of 2:1 in basal medium. This ratio was used was selected to mimic the physiological conditions, considering that there are more fibroblasts than myocytes in the heart.

Some dishes were also exposed to the adipogenic medium, used as an external trigger to induce the lipid accumulation, trying to reproduce *in vitro* the adipogenic phenotype observable *in vivo*. The adipogenic medium [94] was composed of basal medium, 2% FBS supplemented with Insulin 50 μg/ml, Desametazone 0,5 μM, IBMX, 3-Isobutyl-1-methylxanthine, 0,25 mM, Indometacin 200 μM and Rosiglitazone 5 μM (all these reagents are distributed by Sigma Aldrich).

Three experimental groups were designed:

- Control iPSC-CMs + healthy cardiac fibroblasts, both cultured in basal medium,
- ACM iPSC-CMs + healthy cardiac fibroblasts, both cultured in basal medium,
- ACM iPSC-CMs + healthy cardiac fibroblasts, both cultured in adipogenic medium, used as an external trigger to exacerbate the lipid accumulation in ACM iPSC-CMs as previously described.

Monolayers of ACM iPSC-CMs and control iPSC-CMs were used as experimental reference for each group.

7.3.6 Optical mapping measurements

After 48h in co-culture, iPSC-CMs electrophysiology was investigated using advanced optical mapping. Cultures were stained with the voltage sensitive dye FluoVolt 1x for 25 min at 37°C and maintained in culture medium supplemented with 10 μM blebbistatin (a myosin inhibitor), to prevent contraction. Mapping was performed on an upright macroscope

(Olympus MVX10) equipped with a high-performance high-speed EMCCD camera (Evolve™512, Photometrics) [256]. Recordings were collected at 530 frames per second from a 512x512 pixel region, during electrical stimulation at two different pacing rates 0.66 Hz and 1 Hz. The action potential duration (APD) was evaluated spatially, over 5-7 different recorded regions, and temporally, over five consecutive action potentials per recording, averaged for each dish.

Optical signals were analyzed using custom analysis program OPTIQ (Cairn Research, UK). APD at 50% (APD50), 75 % (APD75) and 90% (APD90) were calculated as the interval from the initial activation to 50%, 75% and 90% repolarization, respectively.

7.4 Results

Firstly, we compared the APD50, APD75 and APD90 in NON ACM and ACM iPSC-CMs homocellular monolayers, cultured in basal medium and paced at two different frequencies (0.66 Hz, 1 Hz) (Fig.20).

A.

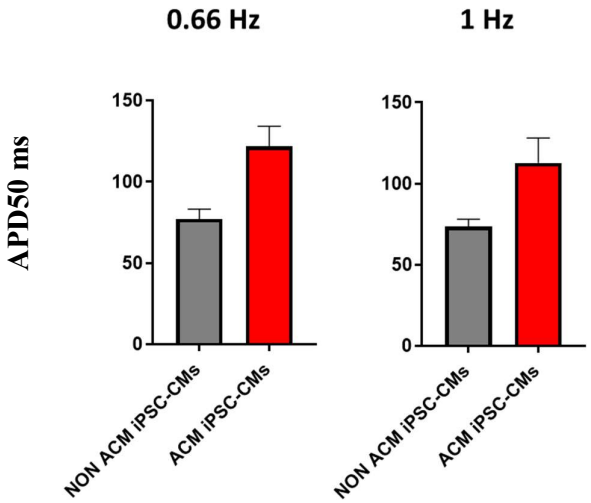

B.

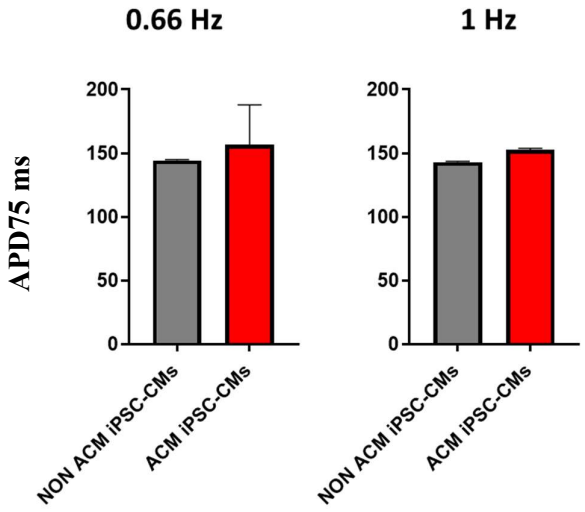

C.

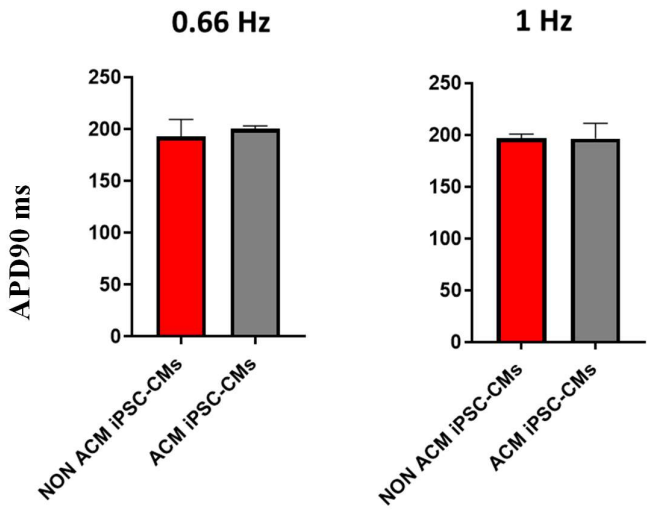

Figure 20. APD50, APD75, APD90 of NON ACM iPSC-CMs compared to ACM iPSC-CMs monolayer in basal medium at the two different frequencies (0.66 Hz, 1 Hz). A. APD50 variation **B**. APD75 variation **C**. APD90 variation at the two frequencies. (N=2 NON ACM, N=2 ACM).

It is possible to observe that, when pacing CMs monolayers at both frequencies no strong difference was observable between NON ACM and ACM iPSC-CMs in the variation of APD75 and APD90 values, while an increase in the APD50 values was observable in ACM iPSC-CMs monolayer at 0.66 Hz and 1 Hz compared to the NON ACM iPSC-CMs.

More interestingly is the comparison between the APD50, APD75 and APD90 values after adding CStCs to NON ACM and ACM iPSCs-CMs monolayer. In the graphs below we compared the APD50 (Fig.21 A), APD75 (Fig.21 B) and APD90 (Fig.21 2C) at the two pacing frequencies in the two models.

A.

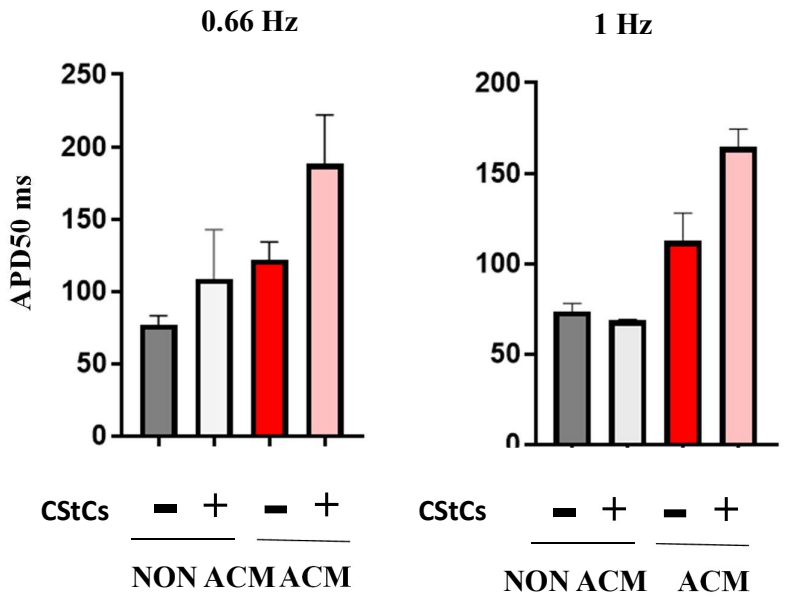
0.66 Hz
1 Hz
APD50 ms
250
200
150
100
50
0
CStCs
- + - +
NON ACM ACM
200
150
100
50
0
CStCs
- + - +
NON ACM ACM

B.

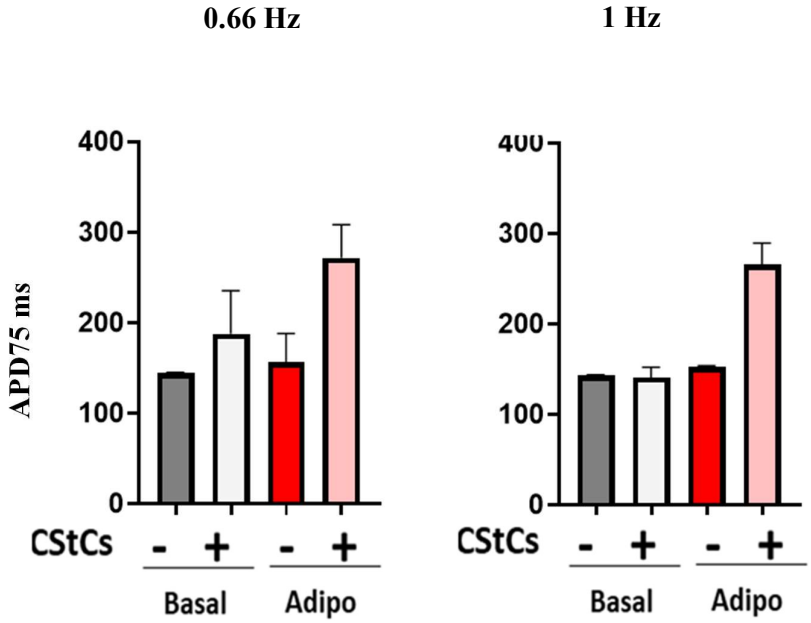
0.66 Hz
1 Hz
APD75 ms
400
300
200
100
0
CStCs
- + - +
Basal Adipo
400
300
200
100
0
CStCs
- + - +
Basal Adipo

C.

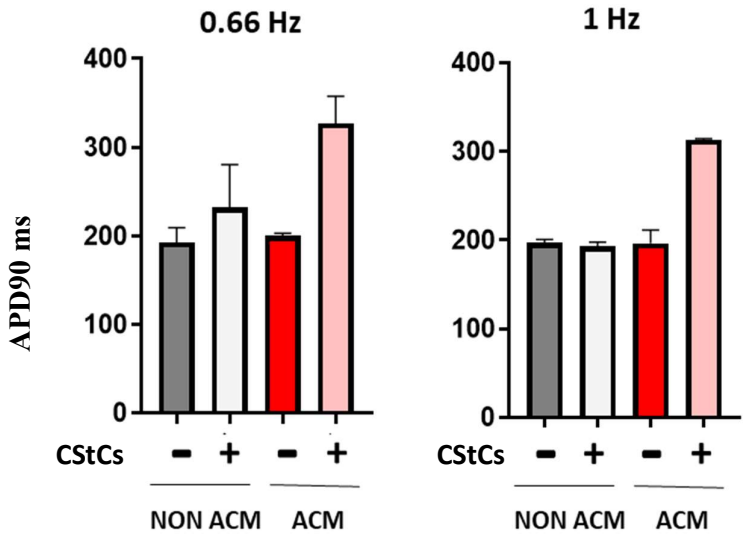

Figure 21. APD50, APD75, APD90 of NON ACM iPSC-CMs and NON ACM iPSC-CMs + CStCs compared to ACM iPSC-CMs and ACM iPSC-CMs + CStCs in basal medium at the two different frequencies (0.66 Hz, 1 Hz). A. APD50 variation. **B**. APD75 variation. **C**. APD90 variation. (N=2 NON ACM, N=2 ACM)**.**

In the case of NON ACM samples, there was no significant increase in the three APD values in presence of CStCs. In contrast, the presence of CStCs seemed to increase the APD values only in the ACM co-culture model at all the three APD taken into consideration, pacing cells with the two frequencies. This observation seems particularly relevant, as an APD prolongation is known to be potentially pro-arrhythmic [257, 258].

We also evaluated the changes in the APD values of ACM samples after the exposure to the adipogenic medium. We compared the APD50 (Fig.22 A), the APD75 (Fig.22 B), and APD90 (Fig.22 C) of ACM iPSC-CMs in presence or not of fibroblasts either basal medium or after the adipogenic treatment.

A.

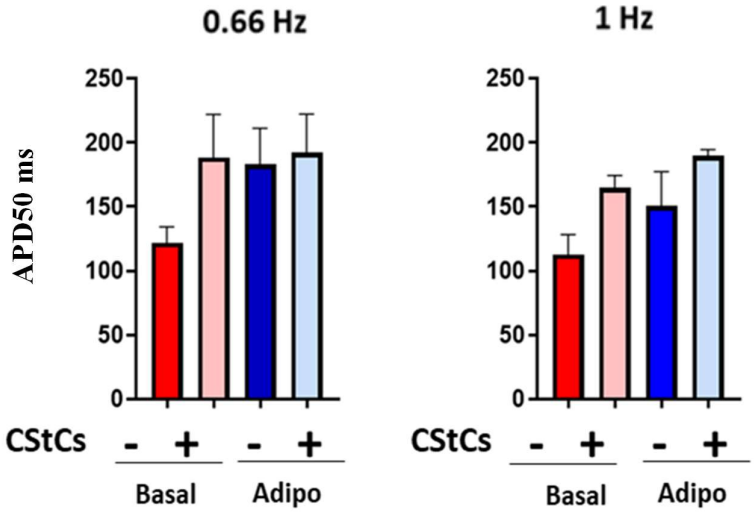
0.66 Hz
1 Hz
APD50 ms
250
200
150
100
50
0
CStCs
-
+
-
+
Basal
Adipo

B.

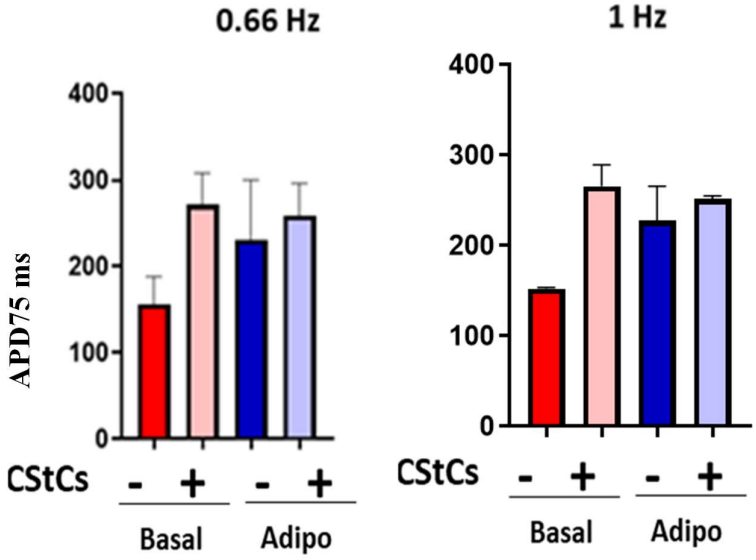
0.66 Hz
1 Hz
APD75 ms
400
300
200
100
0
CStCs
-
+
-
+
Basal
Adipo

C.

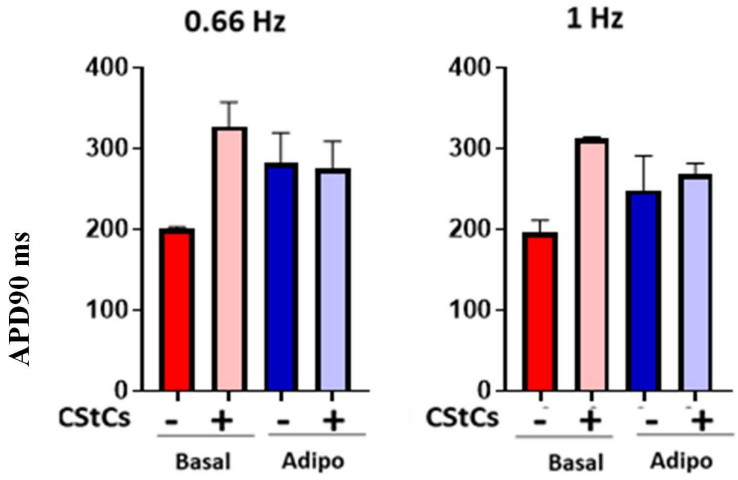

Figure 22. APD50, APD75, APD90 of ACM iPSC-CMs and ACM iPSC-CMs+ CStCs in basal medium and in presence of adipogenic medium at the two different frequencies (0.66 Hz, 1 Hz). A. APD50 variation **B**. APD75 variation **C**. APD90 variation**.** (N=2 NON ACM, N=2 ACM).

Comparing the APD values of monolayers of ACM iPSC-CMs in basal medium with the ones in adipogenic medium, an increase in all the three APD values at the two frequencies was observable, while the addition of CStCs seemed to be able to induce an increase only in basal condition. Indeed, the presence of fibroblasts in adipogenic medium did not induce a further increase. A possible speculation could be that the presence of fibroblasts already leads to a strong increase in the APD in basal condition and, therefore, the adipogenic external trigger did not affect this electrophysiological parameter.

7.5 Conclusions

In the 3 months I spent in the lab Dr Patrizia Camelliti, at the University of Surrey, I was able to create an *in vitro* model, based on the co-culture of iPSC-CMs and fibroblasts. This model has been used to perform experiments aimed at understanding the cross-talk between these two cell types in the ACM pathology. Of note, the results reported here have been collected in the limited amount of time covered by the EMBO fellowship. Therefore, they should be intended as preliminary results, needing to be validated by further experiments.

The preliminary results I have obtained show that the addition of healthy fibroblasts to a monolayer of iPSC-CMs seems to induce an increase in the APD50, APD75 and APD90 values only in case of ACM iPSC-CMs, while this effect is not visible with NON ACM iPSC-CM monolayers. This result is particularly interesting, considering that the longer APD has been associated with increased risk of arrhythmias [259, 260]. In addition, we would also like to re-create the model, using iPSC-CMs and cardiac fibroblasts both obtained from ACM patients, in order to clarify the cross-talk between these two cell models in the context of the pathology.

It would also be interesting to evaluate the conduction velocity of the spontaneous action potentials of the heterocellular co-culture of iPSC-CMs and CStCs. Delayed myocardial conduction velocity has, in fact, been described as one of the major causes of the establishment of re-entry circuits, which, in turns, are known to increase the risk of cardiac arrhythmias [261] . Optical mapping data can be used to generate local conduction vectors, that can be used either for the quantifying of the conduction of a specific area and for having an indication of the direction of activation [262] .

8 Bibliography

1. Al-Khatib SM, Stevenson WG, Ackerman MJ, Bryant WJ, Callans DJ, Curtis AB, Deal BJ, Dickfeld T, Field ME, Fonarow GC *et al*: **2017 AHA/ACC/HRS Guideline for Management of Patients With Ventricular Arrhythmias and the Prevention of Sudden Cardiac Death**. *Circulation* 2018, **138**(13):e272-e391.
2. Hayashi M, Shimizu W, Albert CM: **The spectrum of epidemiology underlying sudden cardiac death**. *Circ Res* 2015, **116**(12):1887-1906.
3. Srinivasan NT, Schilling RJ: **Sudden Cardiac Death and Arrhythmias**. *Arrhythm Electrophysiol Rev* 2018, **7**(2):111-117.
4. Lund LH, Edwards LB, Kucheryavaya AY, Benden C, Dipchand AI, Goldfarb S, Levvey BJ, Meiser B, Rossano JW, Yusen RD *et al*: **The Registry of the International Society for Heart and Lung Transplantation: Thirty-second Official Adult Heart Transplantation Report--2015; Focus Theme: Early Graft Failure**. *J Heart Lung Transplant* 2015, **34**(10):1244-1254.
5. Elliott P, Andersson B, Arbustini E, Bilinska Z, Cecchi F, Charron P, Dubourg O, Kuhl U, Maisch B, McKenna WJ *et al*: **Classification of the cardiomyopathies: a position statement from the European Society Of Cardiology Working Group on Myocardial and Pericardial Diseases**. *Eur Heart J* 2008, **29**(2):270-276.
6. **De L'Auscultation Mediate; ou Traite du Diagnostic des Maladies des Poumons et du Coeur, fonde principalement sur ce Nouveau Moyen d'Exploration**. *Edinburgh medical and surgical journal* 1822, **18**(72):447-474.
7. Maron BJ, Towbin JA, Thiene G, Antzelevitch C, Corrado D, Arnett D, Moss AJ, Seidman CE, Young JB: **Contemporary definitions and classification of the cardiomyopathies: an American Heart Association Scientific Statement from the Council on Clinical Cardiology, Heart Failure and Transplantation Committee; Quality of Care and Outcomes Research and Functional Genomics and Translational Biology Interdisciplinary Working Groups; and Council on Epidemiology and Prevention**. *Circulation* 2006, **113**(14):1807-1816.
8. Corrado D, Fontaine G, Marcus FI, McKenna WJ, Nava A, Thiene G, Wichter T: **Arrhythmogenic right ventricular dysplasia/cardiomyopathy: need for an international registry. European Society of Cardiology and the Scientific Council on Cardiomyopathies of the World Heart Federation**. *J Cardiovasc Electrophysiol* 2000, **11**(7):827-832.
9. Thiene G, Nava A, Corrado D, Rossi L, Pennelli N: **Right ventricular cardiomyopathy and sudden death in young people**. *N Engl J Med* 1988, **318**(3):129-133.
10. Lombardi R, Marian AJ: **Molecular genetics and pathogenesis of arrhythmogenic right ventricular cardiomyopathy: a disease of cardiac stem cells**. *Pediatr Cardiol* 2011, **32**(3):360-365.
11. Thiene G: **The research venture in arrhythmogenic right ventricular cardiomyopathy: a paradigm of translational medicine**. *Eur Heart J* 2015, **36**(14):837-846.
12. Marcus FI, Fontaine GH, Guiraudon G, Frank R, Laurenceau JL, Malergue C, Grosgogeat Y: **Right ventricular dysplasia: a report of 24 adult cases**. *Circulation* 1982, **65**(2):384-398.
13. Richardson P, McKenna W, Bristow M, Maisch B, Mautner B, O'Connell J, Olsen E, Thiene G, Goodwin J, Gyarfas I *et al*: **Report of the 1995 World Health Organization/International Society and Federation of Cardiology Task Force on the Definition and Classification of cardiomyopathies**. *Circulation* 1996, **93**(5):841-842.

14. Havranek S, Palecek T, Kuchynka P, Vitkova I: **[Arrhythmogenic left ventricular cardiomyopathy]**. *Vnitrni lekarstvi*, **62**(9):728-735.
15. Asimaki A, Protonotarios A, James CA, Chelko SP, Tichnell C, Murray B, Tsatsopoulou A, Anastasakis A, te Riele A, Kleber AG *et al*: **Characterizing the Molecular Pathology of Arrhythmogenic Cardiomyopathy in Patient Buccal Mucosa Cells**. *Circ Arrhythm Electrophysiol* 2016, **9**(2):e003688.
16. Basso C, Bauce B, Corrado D, Thiene G: **Pathophysiology of arrhythmogenic cardiomyopathy**. *Nat Rev Cardiol* 2011, **9**(4):223-233.
17. Corrado D, Thiene G: **Arrhythmogenic right ventricular cardiomyopathy/dysplasia: clinical impact of molecular genetic studies**. *Circulation* 2006, **113**(13):1634-1637.
18. Basavarajaiah S, Shah A, Sharma S: **Sudden cardiac death in young athletes**. *Heart* 2007, **93**(3):287-289.
19. Pinamonti B, Brun F, Mestroni L, Sinagra G: **Arrhythmogenic right ventricular cardiomyopathy: From genetics to diagnostic and therapeutic challenges**. *World J Cardiol* 2014, **6**(12):1234-1244.
20. Corrado D, Michieli P, Basso C, Schiavon M, Thiene G: **How to screen athletes for cardiovascular diseases**. *Cardiol Clin* 2007, **25**(3):391-397, v-vi.
21. Wasfy MM, Hutter AM, Weiner RB: **Sudden Cardiac Death in Athletes**. *Methodist DeBakey cardiovascular journal* 2016, **12**(2):76-80.
22. van Tintelen JP, Hofstra RM, Wiesfeld AC, van den Berg MP, Hauer RN, Jongbloed JD: **Molecular genetics of arrhythmogenic right ventricular cardiomyopathy: emerging horizon?** *Curr Opin Cardiol* 2007, **22**(3):185-192.
23. Frigo G, Bauce B, Basso C, Nava A: **Late-onset arrhythmogenic right ventricular cardiomyopathy**. *J Cardiovasc Med (Hagerstown)* 2006, **7**(1):74-76.
24. Nava A, Bauce B, Basso C, Muriago M, Rampazzo A, Villanova C, Daliento L, Buja G, Corrado D, Danieli GA *et al*: **Clinical profile and long-term follow-up of 37 families with arrhythmogenic right ventricular cardiomyopathy**. *J Am Coll Cardiol* 2000, **36**(7):2226-2233.
25. Hamid MS, Norman M, Quraishi A, Firoozi S, Thaman R, Gimeno JR, Sachdev B, Rowland E, Elliott PM, McKenna WJ: **Prospective evaluation of relatives for familial arrhythmogenic right ventricular cardiomyopathy/dysplasia reveals a need to broaden diagnostic criteria**. *J Am Coll Cardiol* 2002, **40**(8):1445-1450.
26. Sen-Chowdhry S, Syrris P, McKenna WJ: **Genetics of right ventricular cardiomyopathy**. *J Cardiovasc Electrophysiol* 2005, **16**(8):927-935.
27. Corrado D, Thiene G, Nava A, Rossi L, Pennelli N: **Sudden death in young competitive athletes: clinicopathologic correlations in 22 cases**. *Am J Med* 1990, **89**(5):588-596.
28. Basso C, Thiene G: **Adipositas cordis, fatty infiltration of the right ventricle, and arrhythmogenic right ventricular cardiomyopathy. Just a matter of fat?** *Cardiovasc Pathol* 2005, **14**(1):37-41.
29. Calabrese F, Basso C, Carturan E, Valente M, Thiene G: **Arrhythmogenic right ventricular cardiomyopathy/dysplasia: is there a role for viruses?** *Cardiovasc Pathol* 2006, **15**(1):11-17.
30. Basso C, Thiene G, Corrado D, Angelini A, Nava A, Valente M: **Arrhythmogenic right ventricular cardiomyopathy. Dysplasia, dystrophy, or myocarditis?** *Circulation* 1996, **94**(5):983-991.
31. Nava A, Thiene G, Canciani B, Scognamiglio R, Daliento L, Buja G, Martini B, Stritoni P, Fasoli G: **Familial occurrence of right ventricular dysplasia: a study involving nine families**. *J Am Coll Cardiol* 1988, **12**(5):1222-1228.

32. Awad MM, Calkins H, Judge DP: **Mechanisms of disease: molecular genetics of arrhythmogenic right ventricular dysplasia/cardiomyopathy**. *Nat Clin Pract Cardiovasc Med* 2008, **5**(5):258-267.
33. Akdis D, Brunckhorst C, Duru F, Saguner AM: **Arrhythmogenic Cardiomyopathy: Electrical and Structural Phenotypes**. *Arrhythm Electrophysiol Rev* 2016, **5**(2):90-101.
34. Rampazzo A: **Genetic bases of arrhythmogenic right ventricular Cardiomyopathy**. *Heart Int* 2006, **2**(1):17.
35. Delmar M, McKenna WJ: **The cardiac desmosome and arrhythmogenic cardiomyopathies: from gene to disease**. *Circ Res* 2010, **107**(6):700-714.
36. McGrath JA: **Inherited disorders of desmosomes**. *Australas J Dermatol* 2005, **46**(4):221-229.
37. McKoy G, Protonotarios N, Crosby A, Tsatsopoulou A, Anastasakis A, Coonar A, Norman M, Baboonian C, Jeffery S, McKenna WJ: **Identification of a deletion in plakoglobin in arrhythmogenic right ventricular cardiomyopathy with palmoplantar keratoderma and woolly hair (Naxos disease)**. *Lancet* 2000, **355**(9221):2119-2124.
38. Gerull B, Heuser A, Wichter T, Paul M, Basson CT, McDermott DA, Lerman BB, Markowitz SM, Ellinor PT, MacRae CA *et al*: **Mutations in the desmosomal protein plakophilin-2 are common in arrhythmogenic right ventricular cardiomyopathy**. *Nat Genet* 2004, **36**(11):1162-1164.
39. Pilichou K, Nava A, Basso C, Beffagna G, Bauce B, Lorenzon A, Frigo G, Vettori A, Valente M, Towbin J *et al*: **Mutations in desmoglein-2 gene are associated with arrhythmogenic right ventricular cardiomyopathy**. *Circulation* 2006, **113**(9):1171-1179.
40. Syrris P, Ward D, Evans A, Asimaki A, Gandjbakhch E, Sen-Chowdhry S, McKenna WJ: **Arrhythmogenic right ventricular dysplasia/cardiomyopathy associated with mutations in the desmosomal gene desmocollin-2**. *Am J Hum Genet* 2006, **79**(5):978-984.
41. van Tintelen JP, Entius MM, Bhuiyan ZA, Jongbloed R, Wiesfeld AC, Wilde AA, van der Smagt J, Boven LG, Mannens MM, van Langen IM *et al*: **Plakophilin-2 mutations are the major determinant of familial arrhythmogenic right ventricular dysplasia/cardiomyopathy**. *Circulation* 2006, **113**(13):1650-1658.
42. Smith EA, Fuchs E: **Defining the interactions between intermediate filaments and desmosomes**. *J Cell Biol* 1998, **141**(5):1229-1241.
43. Koch PJ, Franke WW: **Desmosomal cadherins: another growing multigene family of adhesion molecules**. *Curr Opin Cell Biol* 1994, **6**(5):682-687.
44. Basso C, Czarnowska E, Della Barbera M, Bauce B, Beffagna G, Wlodarska EK, Pilichou K, Ramondo A, Lorenzon A, Wozniek O *et al*: **Ultrastructural evidence of intercalated disc remodelling in arrhythmogenic right ventricular cardiomyopathy: an electron microscopy investigation on endomyocardial biopsies**. *Eur Heart J* 2006, **27**(15):1847-1854.
45. Franke WW, Borrmann CM, Grund C, Pieperhoff S: **The area composita of adhering junctions connecting heart muscle cells of vertebrates. I. Molecular definition in intercalated disks of cardiomyocytes by immunoelectron microscopy of desmosomal proteins**. *Eur J Cell Biol* 2006, **85**(2):69-82.
46. Meng W, Takeichi M: **Adherens junction: molecular architecture and regulation**. *Cold Spring Harb Perspect Biol* 2009, **1**(6):a002899.
47. Harmon RM, Green KJ: **Structural and functional diversity of desmosomes**. *Cell Commun Adhes* 2013, **20**(6):171-187.

48. Nielsen MS, Axelsen LN, Sorgen PL, Verma V, Delmar M, Holstein-Rathlou NH: **Gap junctions**. *Compr Physiol* 2012, **2**(3):1981-2035.
49. Revel JP, Karnovsky MJ: **Hexagonal array of subunits in intercellular junctions of the mouse heart and liver**. *J Cell Biol* 1967, **33**(3):C7-c12.
50. Sohl G, Willecke K: **Gap junctions and the connexin protein family**. *Cardiovasc Res* 2004, **62**(2):228-232.
51. Leo-Macias A, Agullo-Pascual E, Delmar M: **The cardiac connexome: Non-canonical functions of connexin43 and their role in cardiac arrhythmias**. *Semin Cell Dev Biol* 2016, **50**:13-21.
52. Agullo-Pascual E, Reid DA, Keegan S, Sidhu M, Fenyo D, Rothenberg E, Delmar M: **Super-resolution fluorescence microscopy of the cardiac connexome reveals plakophilin-2 inside the connexin43 plaque**. *Cardiovasc Res* 2013, **100**(2):231-240.
53. van Hengel J, Calore M, Bauce B, Dazzo E, Mazzotti E, De Bortoli M, Lorenzon A, Li Mura IE, Beffagna G, Rigato I *et al*: **Mutations in the area composita protein alphaT-catenin are associated with arrhythmogenic right ventricular cardiomyopathy**. *Eur Heart J* 2013, **34**(3):201-210.
54. Mayosi BM, Fish M, Shaboodien G, Mastantuono E, Kraus S, Wieland T, Kotta MC, Chin A, Laing N, Ntusi NB *et al*: **Identification of Cadherin 2 (CDH2) Mutations in Arrhythmogenic Right Ventricular Cardiomyopathy**. *Circ Cardiovasc Genet* 2017, **10**(2).
55. Te Riele AS, Agullo-Pascual E, James CA, Leo-Macias A, Cerrone M, Zhang M, Lin X, Lin B, Sobreira NL, Amat-Alarcon N *et al*: **Multilevel analyses of SCN5A mutations in arrhythmogenic right ventricular dysplasia/cardiomyopathy suggest non-canonical mechanisms for disease pathogenesis**. *Cardiovasc Res* 2017, **113**(1):102-111.
56. De Bortoli M, Postma AV, Poloni G, Calore M, Minervini G, Mazzotti E, Rigato I, Ebert M, Lorenzon A, Vazza G *et al*: **Whole-Exome Sequencing Identifies Pathogenic Variants in TJP1 Gene Associated With Arrhythmogenic Cardiomyopathy**. *Circ Genom Precis Med* 2018, **11**(10):e002123.
57. Merner ND, Hodgkinson KA, Haywood AF, Connors S, French VM, Drenckhahn JD, Kupprion C, Ramadanova K, Thierfelder L, McKenna W *et al*: **Arrhythmogenic right ventricular cardiomyopathy type 5 is a fully penetrant, lethal arrhythmic disorder caused by a missense mutation in the TMEM43 gene**. *Am J Hum Genet* 2008, **82**(4):809-821.
58. Beffagna G, Occhi G, Nava A, Vitiello L, Ditadi A, Basso C, Bauce B, Carraro G, Thiene G, Towbin JA *et al*: **Regulatory mutations in transforming growth factor-beta3 gene cause arrhythmogenic right ventricular cardiomyopathy type 1**. *Cardiovasc Res* 2005, **65**(2):366-373.
59. van Tintelen JP, Van Gelder IC, Asimaki A, Suurmeijer AJ, Wiesfeld AC, Jongbloed JD, van den Wijngaard A, Kuks JB, van Spaendonck-Zwarts KY, Notermans N *et al*: **Severe cardiac phenotype with right ventricular predominance in a large cohort of patients with a single missense mutation in the DES gene**. *Heart Rhythm* 2009, **6**(11):1574-1583.
60. Quarta G, Syrris P, Ashworth M, Jenkins S, Zuborne Alapi K, Morgan J, Muir A, Pantazis A, McKenna WJ, Elliott PM: **Mutations in the Lamin A/C gene mimic arrhythmogenic right ventricular cardiomyopathy**. *Eur Heart J* 2012, **33**(9):1128-1136.
61. van der Zwaag PA, van Rijsingen IA, Asimaki A, Jongbloed JD, van Veldhuisen DJ, Wiesfeld AC, Cox MG, van Lochem LT, de Boer RA, Hofstra RM *et al*: **Phospholamban R14del mutation in patients diagnosed with dilated**

cardiomyopathy or arrhythmogenic right ventricular cardiomyopathy: evidence supporting the concept of arrhythmogenic cardiomyopathy. *Eur J Heart Fail* 2012, **14**(11):1199-1207.

62. Poloni G, Calore M, Rigato I, Marras E, Minervini G, Mazzotti E, Lorenzon A, Li Mura IEA, Telatin A, Zara I *et al*: **A targeted next-generation gene panel reveals a novel heterozygous nonsense variant in the TP63 gene in patients with arrhythmogenic cardiomyopathy**. *Heart Rhythm* 2019, **16**(5):773-780.
63. Brodehl A, Rezazadeh S, Williams T, Munsie NM, Liedtke D, Oh T, Ferrier R, Shen Y, Jones SJM, Stiegler AL *et al*: **Mutations in ILK, encoding integrin-linked kinase, are associated with arrhythmogenic cardiomyopathy**. *Transl Res* 2019, **208**:15-29.
64. Begay RL, Graw SL, Sinagra G, Asimaki A, Rowland TJ, Slavov DB, Gowan K, Jones KL, Brun F, Merlo M *et al*: **Filamin C Truncation Mutations Are Associated With Arrhythmogenic Dilated Cardiomyopathy and Changes in the Cell-Cell Adhesion Structures**. *JACC Clin Electrophysiol* 2018, **4**(4):504-514.
65. Notari M, Hu Y, Sutendra G, Dedeic Z, Lu M, Dupays L, Yavari A, Carr CA, Zhong S, Opel A *et al*: **iASPP, a previously unidentified regulator of desmosomes, prevents arrhythmogenic right ventricular cardiomyopathy (ARVC)-induced sudden death**. *Proc Natl Acad Sci U S A* 2015, **112**(9):E973-981.
66. Tiso N, Stephan DA, Nava A, Bagattin A, Devaney JM, Stanchi F, Larderet G, Brahmbhatt B, Brown K, Bauce B *et al*: **Identification of mutations in the cardiac ryanodine receptor gene in families affected with arrhythmogenic right ventricular cardiomyopathy type 2 (ARVD2)**. *Hum Mol Genet* 2001, **10**(3):189-194.
67. Priori SG, Napolitano C, Tiso N, Memmi M, Vignati G, Bloise R, Sorrentino V, Danieli GA: **Mutations in the cardiac ryanodine receptor gene (hRyR2) underlie catecholaminergic polymorphic ventricular tachycardia**. *Circulation* 2001, **103**(2):196-200.
68. Protonotarios N, Tsatsopoulou A, Patsourakos P, Alexopoulos D, Gezerlis P, Simitsis S, Scampardonis G: **Cardiac abnormalities in familial palmoplantar keratosis**. *Br Heart J* 1986, **56**(4):321-326.
69. Carvajal-Huerta L: **Epidermolytic palmoplantar keratoderma with woolly hair and dilated cardiomyopathy**. *Journal of the American Academy of Dermatology* 1998, **39**(3):418-421.
70. Lorenzon A, Pilichou K, Rigato I, Vazza G, De Bortoli M, Calore M, Occhi G, Carturan E, Lazzarini E, Cason M *et al*: **Homozygous Desmocollin-2 Mutations and Arrhythmogenic Cardiomyopathy**. *Am J Cardiol* 2015, **116**(8):1245-1251.
71. Al-Sabeq B, Krahn AD, Conacher S, Klein GJ, Laksman Z: **Arrhythmogenic right ventricular cardiomyopathy with recessive inheritance related to a new homozygous desmocollin-2 mutation**. *The Canadian journal of cardiology* 2014, **30**(6):696.e691-693.
72. Gerull B, Kirchner F, Chong JX, Tagoe J, Chandrasekharan K, Strohm O, Waggoner D, Ober C, Duff HJ: **Homozygous founder mutation in desmocollin-2 (DSC2) causes arrhythmogenic cardiomyopathy in the Hutterite population**. *Circ Cardiovasc Genet* 2013, **6**(4):327-336.
73. Lin Y, Zhang Q, Zhong ZA, Xu Z, He S, Rao F, Liu Y, Tang J, Wang F, Liu H *et al*: **Whole Genome Sequence Identified a Rare Homozygous Pathogenic Mutation of the DSG2 Gene in a Familial Arrhythmogenic Cardiomyopathy Involving Both Ventricles**. *Cardiology* 2017, **138**(1):41-54.

74. Qadri S, Anttonen O, Viikila J, Seppala EH, Myllykangas S, Alastalo TP, Holmstrom M, Helio T, Koskenvuo JW: **Case reports of two pedigrees with recessive arrhythmogenic right ventricular cardiomyopathy associated with homozygous Thr335Ala variant in DSG2**. *BMC Med Genet* 2017, **18**(1):86.
75. Rao M, Guo GR, Li MM, Chen S, Chen K, Chen X, Song JP, Hu SS: **The homozygous variant c.245G>A/p.G82D in PNPLA2 is associated with arrhythmogenic cardiomyopathy phenotypic manifestations**. *Clin Genet* 2019.
76. Konig E, Volpato CB, Motta BM, Blankenburg H, Picard A, Pramstaller P, Casella M, Rauhe W, Pompilio G, Meraviglia V *et al*: **Exploring digenic inheritance in arrhythmogenic cardiomyopathy**. *BMC Med Genet* 2017, **18**(1):145.
77. Rigato I, Bauce B, Rampazzo A, Zorzi A, Pilichou K, Mazzotti E, Migliore F, Marra MP, Lorenzon A, De Bortoli M *et al*: **Compound and digenic heterozygosity predicts lifetime arrhythmic outcome and sudden cardiac death in desmosomal gene-related arrhythmogenic right ventricular cardiomyopathy**. *Circ Cardiovasc Genet* 2013, **6**(6):533-542.
78. McKenna WJ, Thiene G, Nava A, Fontaliran F, Blomstrom-Lundqvist C, Fontaine G, Camerini F: **Diagnosis of arrhythmogenic right ventricular dysplasia/cardiomyopathy. Task Force of the Working Group Myocardial and Pericardial Disease of the European Society of Cardiology and of the Scientific Council on Cardiomyopathies of the International Society and Federation of Cardiology**. *Br Heart J* 1994, **71**(3):215-218.
79. Romero J, Mejia-Lopez E, Manrique C, Lucariello R: **Arrhythmogenic Right Ventricular Cardiomyopathy (ARVC/D): A Systematic Literature Review**. *Clin Med Insights Cardiol* 2013, **7**:97-114.
80. Corrado D, Basso C, Thiene G: **Comparison of United States and Italian experiences with sudden cardiac deaths in young competitive athletes: are the athletic populations comparable?** *Am J Cardiol* 2010, **105**(3):421-422; author reply 422.
81. Tandri H, Saranathan M, Rodriguez ER, Martinez C, Bomma C, Nasir K, Rosen B, Lima JA, Calkins H, Bluemke DA: **Noninvasive detection of myocardial fibrosis in arrhythmogenic right ventricular cardiomyopathy using delayed-enhancement magnetic resonance imaging**. *J Am Coll Cardiol* 2005, **45**(1):98-103.
82. Sen-Chowdhry S, Prasad SK, Syrris P, Wage R, Ward D, Merrifield R, Smith GC, Firmin DN, Pennell DJ, McKenna WJ: **Cardiovascular magnetic resonance in arrhythmogenic right ventricular cardiomyopathy revisited: comparison with task force criteria and genotype**. *J Am Coll Cardiol* 2006, **48**(10):2132-2140.
83. Asimaki A, Saffitz JE: **The role of endomyocardial biopsy in ARVC: looking beyond histology in search of new diagnostic markers**. *J Cardiovasc Electrophysiol* 2011, **22**(1):111-117.
84. Casella M, Pizzamiglio F, Dello Russo A, Carbucicchio C, Al-Mohani G, Russo E, Notarstefano P, Pieroni M, D'Amati G, Sommariva E *et al*: **Feasibility of combined unipolar and bipolar voltage maps to improve sensitivity of endomyocardial biopsy**. *Circ Arrhythm Electrophysiol* 2015, **8**(3):625-632.
85. Sen-Chowdhry S, Syrris P, McKenna WJ: **Role of genetic analysis in the management of patients with arrhythmogenic right ventricular dysplasia/cardiomyopathy**. *J Am Coll Cardiol* 2007, **50**(19):1813-1821.
86. Asimaki A, Tandri H, Huang H, Halushka MK, Gautam S, Basso C, Thiene G, Tsatsopoulou A, Protonotarios N, McKenna WJ *et al*: **A new diagnostic test for arrhythmogenic right ventricular cardiomyopathy**. *N Engl J Med* 2009, **360**(11):1075-1084.

87. Kwon YS, Park TI, Cho Y, Bae MH, Kim S: **Clinical usefulness of immunohistochemistry for plakoglobin, N-cadherin, and connexin-43 in the diagnosis of arrhythmogenic right ventricular cardiomyopathy**. *Int J Clin Exp Pathol* 2013, **6**(12):2928-2935.
88. Asimaki A, Tandri H, Duffy ER, Winterfield JR, Mackey-Bojack S, Picken MM, Cooper LT, Wilber DJ, Marcus FI, Basso C *et al*: **Altered desmosomal proteins in granulomatous myocarditis and potential pathogenic links to arrhythmogenic right ventricular cardiomyopathy**. *Circ Arrhythm Electrophysiol* 2011, **4**(5):743-752.
89. Sommariva E, D'Alessandra Y, Farina FM, Casella M, Cattaneo F, Catto V, Chiesa M, Stadiotti I, Brambilla S, Dello Russo A *et al*: **MiR-320a as a Potential Novel Circulating Biomarker of Arrhythmogenic CardioMyopathy**. *Scientific reports* 2017, **7**(1):4802.
90. Basso C, Corrado D, Marcus FI, Nava A, Thiene G: **Arrhythmogenic right ventricular cardiomyopathy**. *Lancet* 2009, **373**(9671):1289-1300.
91. Roguin A, Bomma CS, Nasir K, Tandri H, Tichnell C, James C, Rutberg J, Crosson J, Spevak PJ, Berger RD *et al*: **Implantable cardioverter-defibrillators in patients with arrhythmogenic right ventricular dysplasia/cardiomyopathy**. *J Am Coll Cardiol* 2004, **43**(10):1843-1852.
92. Hoorntje ET, Te Rijdt WP, James CA, Pilichou K, Basso C, Judge DP, Bezzina CR, van Tintelen JP: **Arrhythmogenic cardiomyopathy: pathology, genetics, and concepts in pathogenesis**. *Cardiovasc Res* 2017, **113**(12):1521-1531.
93. Lacroix D, Lions C, Klug D, Prat A: **Arrhythmogenic right ventricular dysplasia: catheter ablation, MRI, and heart transplantation**. *J Cardiovasc Electrophysiol* 2005, **16**(2):235-236.
94. Kim C, Wong J, Wen J, Wang S, Wang C, Spiering S, Kan NG, Forcales S, Puri PL, Leone TC *et al*: **Studying arrhythmogenic right ventricular dysplasia with patient-specific iPSCs**. *Nature* 2013, **494**(7435):105-110.
95. Wen JY, Wei CY, Shah K, Wong J, Wang C, Chen HS: **Maturation-Based Model of Arrhythmogenic Right Ventricular Dysplasia Using Patient-Specific Induced Pluripotent Stem Cells**. *Circ J* 2015, **79**(7):1402-1408.
96. Garcia-Gras E, Lombardi R, Giocondo MJ, Willerson JT, Schneider MD, Khoury DS, Marian AJ: **Suppression of canonical Wnt/beta-catenin signaling by nuclear plakoglobin recapitulates phenotype of arrhythmogenic right ventricular cardiomyopathy**. *J Clin Invest* 2006, **116**(7):2012-2021.
97. Ross SE, Hemati N, Longo KA, Bennett CN, Lucas PC, Erickson RL, MacDougald OA: **Inhibition of adipogenesis by Wnt signaling**. *Science* 2000, **289**(5481):950-953.
98. Takada I, Kouzmenko AP, Kato S: **Wnt and PPARgamma signaling in osteoblastogenesis and adipogenesis**. *Nat Rev Rheumatol* 2009, **5**(8):442-447.
99. Lecarpentier Y, Claes V, Duthoit G, Hebert JL: **Circadian rhythms, Wnt/beta-catenin pathway and PPAR alpha/gamma profiles in diseases with primary or secondary cardiac dysfunction**. *Front Physiol* 2014, **5**:429.
100. Semple RK, Chatterjee VK, O'Rahilly S: **PPAR gamma and human metabolic disease**. *J Clin Invest* 2006, **116**(3):581-589.
101. Caspi O, Huber I, Gepstein A, Arbel G, Maizels L, Boulos M, Gepstein L: **Modeling of arrhythmogenic right ventricular cardiomyopathy with human induced pluripotent stem cells**. *Circ Cardiovasc Genet* 2013, **6**(6):557-568.
102. Oxford EM, Danko CG, Fox PR, Kornreich BG, Moise NS: **Change in beta-catenin localization suggests involvement of the canonical Wnt pathway in**

Boxer dogs with arrhythmogenic right ventricular cardiomyopathy. *J Vet Intern Med* 2014, **28**(1):92-101.
103. Harvey KF, Pfleger CM, Hariharan IK: **The Drosophila Mst ortholog, hippo, restricts growth and cell proliferation and promotes apoptosis**. *Cell* 2003, **114**(4):457-467.
104. Meng Z, Moroishi T, Guan KL: **Mechanisms of Hippo pathway regulation**. *Genes Dev* 2016, **30**(1):1-17.
105. Zhao B, Ye X, Yu J, Li L, Li W, Li S, Yu J, Lin JD, Wang CY, Chinnaiyan AM *et al*: **TEAD mediates YAP-dependent gene induction and growth control**. *Genes Dev* 2008, **22**(14):1962-1971.
106. Boggiano JC, Vanderzalm PJ, Fehon RG: **Tao-1 phosphorylates Hippo/MST kinases to regulate the Hippo-Salvador-Warts tumor suppressor pathway**. *Dev Cell* 2011, **21**(5):888-895.
107. Praskova M, Xia F, Avruch J: **MOBKL1A/MOBKL1B phosphorylation by MST1 and MST2 inhibits cell proliferation**. *Curr Biol* 2008, **18**(5):311-321.
108. Zhao B, Wei X, Li W, Udan RS, Yang Q, Kim J, Xie J, Ikenoue T, Yu J, Li L *et al*: **Inactivation of YAP oncoprotein by the Hippo pathway is involved in cell contact inhibition and tissue growth control**. *Genes Dev* 2007, **21**(21):2747-2761.
109. Yu J, Auwerx J: **The role of sirtuins in the control of metabolic homeostasis**. *Ann N Y Acad Sci* 2009, **1173 Suppl 1**:E10-19.
110. Yin F, Yu J, Zheng Y, Chen Q, Zhang N, Pan D: **Spatial organization of Hippo signaling at the plasma membrane mediated by the tumor suppressor Merlin/NF2**. *Cell* 2013, **154**(6):1342-1355.
111. Chen SN, Gurha P, Lombardi R, Ruggiero A, Willerson JT, Marian AJ: **The hippo pathway is activated and is a causal mechanism for adipogenesis in arrhythmogenic cardiomyopathy**. *Circ Res* 2014, **114**(3):454-468.
112. Li D, Liu Y, Maruyama M, Zhu W, Chen H, Zhang W, Reuter S, Lin SF, Haneline LS, Field LJ *et al*: **Restrictive loss of plakoglobin in cardiomyocytes leads to arrhythmogenic cardiomyopathy**. *Hum Mol Genet* 2011, **20**(23):4582-4596.
113. Taniguti AP, Pertille A, Matsumura CY, Santo Neto H, Marques MJ: **Prevention of muscle fibrosis and myonecrosis in mdx mice by suramin, a TGF-beta1 blocker**. *Muscle & nerve* 2011, **43**(1):82-87.
114. Dorn T, Kornherr J, Parrotta EI, Zawada D, Ayetey H, Santamaria G, Iop L, Mastantuono E, Sinnecker D, Goedel A *et al*: **Interplay of cell-cell contacts and RhoA/MRTF-A signaling regulates cardiomyocyte identity**. *EMBO J* 2018, **37**(12).
115. Lorenzon A, Calore M, Poloni G, De Windt LJ, Braghetta P, Rampazzo A: **Wnt/beta-catenin pathway in arrhythmogenic cardiomyopathy**. *Oncotarget* 2017, **8**(36):60640-60655.
116. Droge W: **Free radicals in the physiological control of cell function**. *Physiol Rev* 2002, **82**(1):47-95.
117. Sies H, Stahl W, Sundquist AR: **Antioxidant functions of vitamins. Vitamins E and C, beta-carotene, and other carotenoids**. *Ann N Y Acad Sci* 1992, **669**:7-20.
118. Forman HJ, Zhang H, Rinna A: **Glutathione: overview of its protective roles, measurement, and biosynthesis**. *Molecular aspects of medicine* 2009, **30**(1-2):1-12.
119. Hanukoglu I, Suh BS, Himmelhoch S, Amsterdam A: **Induction and mitochondrial localization of cytochrome P450scc system enzymes in normal and transformed ovarian granulosa cells**. *J Cell Biol* 1990, **111**(4):1373-1381.

120. Sorescu D, Griendling KK: **Reactive oxygen species, mitochondria, and NAD(P)H oxidases in the development and progression of heart failure**. *Congest Heart Fail* 2002, **8**(3):132-140.
121. Imhoff BR, Hansen JM: **Differential redox potential profiles during adipogenesis and osteogenesis**. *Cell Mol Biol Lett* 2011, **16**(1):149-161.
122. Wilson-Fritch L, Burkart A, Bell G, Mendelson K, Leszyk J, Nicoloro S, Czech M, Corvera S: **Mitochondrial biogenesis and remodeling during adipogenesis and in response to the insulin sensitizer rosiglitazone**. *Mol Cell Biol* 2003, **23**(3):1085-1094.
123. Tormos KV, Anso E, Hamanaka RB, Eisenbart J, Joseph J, Kalyanaraman B, Chandel NS: **Mitochondrial complex III ROS regulate adipocyte differentiation**. *Cell Metab* 2011, **14**(4):537-544.
124. Brand MD: **The sites and topology of mitochondrial superoxide production**. *Exp Gerontol* 2010, **45**(7-8):466-472.
125. Kanda Y, Hinata T, Kang SW, Watanabe Y: **Reactive oxygen species mediate adipocyte differentiation in mesenchymal stem cells**. *Life Sci* 2011, **89**(7-8):250-258.
126. Lee H, Lee YJ, Choi H, Ko EH, Kim JW: **Reactive oxygen species facilitate adipocyte differentiation by accelerating mitotic clonal expansion**. *J Biol Chem* 2009, **284**(16):10601-10609.
127. Wang W, Zhang Y, Lu W, Liu K: **Mitochondrial reactive oxygen species regulate adipocyte differentiation of mesenchymal stem cells in hematopoietic stress induced by arabinosylcytosine**. *PLoS One* 2015, **10**(3):e0120629.
128. Friedenstein AJ, Chailakhyan RK, Gerasimov UV: **Bone marrow osteogenic stem cells: in vitro cultivation and transplantation in diffusion chambers**. *Cell Tissue Kinet* 1987, **20**(3):263-272.
129. Pontikoglou C, Deschaseaux F, Sensebe L, Papadaki HA: **Bone marrow mesenchymal stem cells: biological properties and their role in hematopoiesis and hematopoietic stem cell transplantation**. *Stem Cell Rev Rep* 2011, **7**(3):569-589.
130. Markert CD, Atala A, Cann JK, Christ G, Furth M, Ambrosio F, Childers MK: **Mesenchymal stem cells: emerging therapy for Duchenne muscular dystrophy**. *PM R* 2009, **1**(6):547-559.
131. Sun L, Akiyama K, Zhang H, Yamaza T, Hou Y, Zhao S, Xu T, Le A, Shi S: **Mesenchymal stem cell transplantation reverses multiorgan dysfunction in systemic lupus erythematosus mice and humans**. *Stem Cells* 2009, **27**(6):1421-1432.
132. Strauer BE, Schannwell CM, Brehm M: **Therapeutic potentials of stem cells in cardiac diseases**. *Minerva Cardioangiol* 2009, **57**(2):249-267.
133. Undale AH, Westendorf JJ, Yaszemski MJ, Khosla S: **Mesenchymal stem cells for bone repair and metabolic bone diseases**. *Mayo Clin Proc* 2009, **84**(10):893-902.
134. Richter W: **Mesenchymal stem cells and cartilage in situ regeneration**. *J Intern Med* 2009, **266**(4):390-405.
135. Miao C, Lei M, Hu W, Han S, Wang Q: **A brief review: the therapeutic potential of bone marrow mesenchymal stem cells in myocardial infarction**. *Stem Cell Res Ther* 2017, **8**(1):242.
136. Caplan AI: **Mesenchymal stem cells**. *J Orthop Res* 1991, **9**(5):641-650.
137. Horwitz EM, Le Blanc K, Dominici M, Mueller I, Slaper-Cortenbach I, Marini FC, Deans RJ, Krause DS, Keating A, International Society for Cellular T: **Clarification of the nomenclature for MSC: The International Society for Cellular Therapy position statement**. *Cytotherapy* 2005, **7**(5):393-395.

138. Ohishi M, Schipani E: **Bone marrow mesenchymal stem cells**. *J Cell Biochem* 2010, **109**(2):277-282.
139. Okada S, Nakauchi H, Nagayoshi K, Nishikawa S, Miura Y, Suda T: **In vivo and in vitro stem cell function of c-kit- and Sca-1-positive murine hematopoietic cells**. *Blood* 1992, **80**(12):3044-3050.
140. Thomas ED, Lochte HL, Jr., Cannon JH, Sahler OD, Ferrebee JW: **Supralethal whole body irradiation and isologous marrow transplantation in man**. *J Clin Invest* 1959, **38**:1709-1716.
141. Thomas ED, Lochte HL, Jr., Lu WC, Ferrebee JW: **Intravenous infusion of bone marrow in patients receiving radiation and chemotherapy**. *N Engl J Med* 1957, **257**(11):491-496.
142. Zuk PA, Zhu M, Mizuno H, Huang J, Futrell JW, Katz AJ, Benhaim P, Lorenz HP, Hedrick MH: **Multilineage cells from human adipose tissue: implications for cell-based therapies**. *Tissue Eng* 2001, **7**(2):211-228.
143. Jiang Y, Vaessen B, Lenvik T, Blackstad M, Reyes M, Verfaillie CM: **Multipotent progenitor cells can be isolated from postnatal murine bone marrow, muscle, and brain**. *Exp Hematol* 2002, **30**(8):896-904.
144. Yang LJ: **Liver stem cell-derived beta-cell surrogates for treatment of type 1 diabetes**. *Autoimmun Rev* 2006, **5**(6):409-413.
145. Beltrami AP, Barlucchi L, Torella D, Baker M, Limana F, Chimenti S, Kasahara H, Rota M, Musso E, Urbanek K *et al*: **Adult cardiac stem cells are multipotent and support myocardial regeneration**. *Cell* 2003, **114**(6):763-776.
146. Dominici M, Le Blanc K, Mueller I, Slaper-Cortenbach I, Marini F, Krause D, Deans R, Keating A, Prockop D, Horwitz E: **Minimal criteria for defining multipotent mesenchymal stromal cells. The International Society for Cellular Therapy position statement**. *Cytotherapy* 2006, **8**(4):315-317.
147. Jugdutt BI: **Ventricular remodeling after infarction and the extracellular collagen matrix: when is enough enough?** *Circulation* 2003, **108**(11):1395-1403.
148. Brown RD, Ambler SK, Mitchell MD, Long CS: **The cardiac fibroblast: therapeutic target in myocardial remodeling and failure**. *Annu Rev Pharmacol Toxicol* 2005, **45**:657-687.
149. Baudino TA, Carver W, Giles W, Borg TK: **Cardiac fibroblasts: friend or foe?** *Am J Physiol Heart Circ Physiol* 2006, **291**(3):H1015-1026.
150. Gaudesius G, Miragoli M, Thomas SP, Rohr S: **Coupling of cardiac electrical activity over extended distances by fibroblasts of cardiac origin**. *Circ Res* 2003, **93**(5):421-428.
151. Nag AC: **Study of non-muscle cells of the adult mammalian heart: a fine structural analysis and distribution**. *Cytobios* 1980, **28**(109):41-61.
152. Linke A, Muller P, Nurzynska D, Casarsa C, Torella D, Nascimbene A, Castaldo C, Cascapera S, Bohm M, Quaini F *et al*: **Stem cells in the dog heart are self-renewing, clonogenic, and multipotent and regenerate infarcted myocardium, improving cardiac function**. *Proc Natl Acad Sci U S A* 2005, **102**(25):8966-8971.
153. Bolli R, Chugh AR, D'Amario D, Loughran JH, Stoddard MF, Ikram S, Beache GM, Wagner SG, Leri A, Hosoda T *et al*: **Cardiac stem cells in patients with ischaemic cardiomyopathy (SCIPIO): initial results of a randomised phase 1 trial**. *Lancet* 2011, **378**(9806):1847-1857.
154. Rossini A, Frati C, Lagrasta C, Graiani G, Scopece A, Cavalli S, Musso E, Baccarin M, Di Segni M, Fagnoni F *et al*: **Human cardiac and bone marrow stromal cells exhibit distinctive properties related to their origin**. *Cardiovasc Res* 2011, **89**(3):650-660.

155. Camelliti P, McCulloch AD, Kohl P: **Microstructured cocultures of cardiac myocytes and fibroblasts: a two-dimensional in vitro model of cardiac tissue**. *Microsc Microanal* 2005, **11**(3):249-259.
156. Kohl P, Camelliti P, Burton FL, Smith GL: **Electrical coupling of fibroblasts and myocytes: relevance for cardiac propagation**. *J Electrocardiol* 2005, **38**(4 Suppl):45-50.
157. Kohl P, Kamkin AG, Kiseleva IS, Noble D: **Mechanosensitive fibroblasts in the sino-atrial node region of rat heart: interaction with cardiomyocytes and possible role**. *Experimental physiology* 1994, **79**(6):943-956.
158. Camelliti P, Borg TK, Kohl P: **Structural and functional characterisation of cardiac fibroblasts**. *Cardiovasc Res* 2005, **65**(1):40-51.
159. Sommariva E, Brambilla S, Carbucicchio C, Gambini E, Meraviglia V, Dello Russo A, Farina FM, Casella M, Catto V, Pontone G *et al*: **Cardiac mesenchymal stromal cells are a source of adipocytes in arrhythmogenic cardiomyopathy**. *Eur Heart J* 2016, **37**(23):1835-1846.
160. Ma D, Wei H, Lu J, Ho S, Zhang G, Sun X, Oh Y, Tan SH, Ng ML, Shim W *et al*: **Generation of patient-specific induced pluripotent stem cell-derived cardiomyocytes as a cellular model of arrhythmogenic right ventricular cardiomyopathy**. *Eur Heart J* 2013, **34**(15):1122-1133.
161. Al-Amoudi A, Castano-Diez D, Devos DP, Russell RB, Johnson GT, Frangakis AS: **The three-dimensional molecular structure of the desmosomal plaque**. *Proc Natl Acad Sci U S A* 2011, **108**(16):6480-6485.
162. Pilichou K, Bezzina CR, Thiene G, Basso C: **Arrhythmogenic cardiomyopathy: transgenic animal models provide novel insights into disease pathobiology**. *Circ Cardiovasc Genet* 2011, **4**(3):318-326.
163. Cerrone M, Noorman M, Lin X, Chkourko H, Liang FX, van der Nagel R, Hund T, Birchmeier W, Mohler P, van Veen TA *et al*: **Sodium current deficit and arrhythmogenesis in a murine model of plakophilin-2 haploinsufficiency**. *Cardiovasc Res* 2012, **95**(4):460-468.
164. Krusche CA, Holthofer B, Hofe V, van de Sandt AM, Eshkind L, Bockamp E, Merx MW, Kant S, Windoffer R, Leube RE: **Desmoglein 2 mutant mice develop cardiac fibrosis and dilation**. *Basic Res Cardiol* 2011, **106**(4):617-633.
165. McCauley MD, Wehrens XH: **Animal models of arrhythmogenic cardiomyopathy**. *Dis Model Mech* 2009, **2**(11-12):563-570.
166. Pilichou K, Remme CA, Basso C, Campian ME, Rizzo S, Barnett P, Scicluna BP, Bauce B, van den Hoff MJ, de Bakker JM *et al*: **Myocyte necrosis underlies progressive myocardial dystrophy in mouse dsg2-related arrhythmogenic right ventricular cardiomyopathy**. *J Exp Med* 2009, **206**(8):1787-1802.
167. Gallicano GI, Kouklis P, Bauer C, Yin M, Vasioukhin V, Degenstein L, Fuchs E: **Desmoplakin is required early in development for assembly of desmosomes and cytoskeletal linkage**. *J Cell Biol* 1998, **143**(7):2009-2022.
168. Gallicano GI, Bauer C, Fuchs E: **Rescuing desmoplakin function in extra-embryonic ectoderm reveals the importance of this protein in embryonic heart, neuroepithelium, skin and vasculature**. *Development* 2001, **128**(6):929-941.
169. Grossmann KS, Grund C, Huelsken J, Behrend M, Erdmann B, Franke WW, Birchmeier W: **Requirement of plakophilin 2 for heart morphogenesis and cardiac junction formation**. *J Cell Biol* 2004, **167**(1):149-160.
170. Kirchhof P, Fabritz L, Zwiener M, Witt H, Schafers M, Zellerhoff S, Paul M, Athai T, Hiller KH, Baba HA *et al*: **Age- and training-dependent development of**

arrhythmogenic right ventricular cardiomyopathy in heterozygous plakoglobin-deficient mice. *Circulation* 2006, **114**(17):1799-1806.
171. Eshkind L, Tian Q, Schmidt A, Franke WW, Windoffer R, Leube RE: **Loss of desmoglein 2 suggests essential functions for early embryonic development and proliferation of embryonal stem cells**. *Eur J Cell Biol* 2002, **81**(11):592-598.
172. Asimaki A, Kapoor S, Plovie E, Karin Arndt A, Adams E, Liu Z, James CA, Judge DP, Calkins H, Churko J *et al*: **Identification of a new modulator of the intercalated disc in a zebrafish model of arrhythmogenic cardiomyopathy**. *Science translational medicine* 2014, **6**(240):240ra274.
173. Macrae CA: **Cardiac Arrhythmia: In vivo screening in the zebrafish to overcome complexity in drug discovery**. *Expert opinion on drug discovery* 2010, **5**(7):619-632.
174. Kouzarides T: **Chromatin modifications and their function**. *Cell* 2007, **128**(4):693-705.
175. Aguilera O, Fernandez AF, Munoz A, Fraga MF: **Epigenetics and environment: a complex relationship**. *J Appl Physiol (1985)* 2010, **109**(1):243-251.
176. Cheung WL, Briggs SD, Allis CD: **Acetylation and chromosomal functions**. *Curr Opin Cell Biol* 2000, **12**(3):326-333.
177. Eichten SR, Schmitz RJ, Springer NM: **Epigenetics: Beyond Chromatin Modifications and Complex Genetic Regulation**. *Plant physiology* 2014, **165**(3):933-947.
178. Haberland M, Montgomery RL, Olson EN: **The many roles of histone deacetylases in development and physiology: implications for disease and therapy**. *Nat Rev Genet* 2009, **10**(1):32-42.
179. McGinty RK, Tan S: **Nucleosome structure and function**. *Chem Rev* 2015, **115**(6):2255-2273.
180. Shahbazian MD, Grunstein M: **Functions of site-specific histone acetylation and deacetylation**. *Annu Rev Biochem* 2007, **76**:75-100.
181. Brownell JE, Zhou J, Ranalli T, Kobayashi R, Edmondson DG, Roth SY, Allis CD: **Tetrahymena histone acetyltransferase A: a homolog to yeast Gcn5p linking histone acetylation to gene activation**. *Cell* 1996, **84**(6):843-851.
182. Roth SY, Denu JM, Allis CD: **Histone acetyltransferases**. *Annu Rev Biochem* 2001, **70**:81-120.
183. Nagy Z, Tora L: **Distinct GCN5/PCAF-containing complexes function as co-activators and are involved in transcription factor and global histone acetylation**. *Oncogene* 2007, **26**(37):5341-5357.
184. Sterner DE, Berger SL: **Acetylation of histones and transcription-related factors**. *Microbiol Mol Biol Rev* 2000, **64**(2):435-459.
185. Rosen ED, MacDougald OA: **Adipocyte differentiation from the inside out**. *Nat Rev Mol Cell Biol* 2006, **7**(12):885-896.
186. Koutelou E, Hirsch CL, Dent SY: **Multiple faces of the SAGA complex**. *Curr Opin Cell Biol* 2010, **22**(3):374-382.
187. Li S, Shogren-Knaak MA: **The Gcn5 bromodomain of the SAGA complex facilitates cooperative and cross-tail acetylation of nucleosomes**. *J Biol Chem* 2009, **284**(14):9411-9417.
188. Sandoz J, Nagy Z, Catez P, Caliskan G, Geny S, Renaud JB, Concordet JP, Poterszman A, Tora L, Egly JM *et al*: **Functional interplay between TFIIH and KAT2A regulates higher-order chromatin structure and class II gene expression**. *Nat Commun* 2019, **10**(1):1288.

189. Singh N, Leduc Y, Poirier G, Cerutti P: **Non-histone chromosomal protein acceptors for poly(ADP)-ribose in phorbol-12-myristate-13-acetate treated mouse embryo fibroblasts (C3H10T1/2)**. *Carcinogenesis* 1985, **6**(10):1489-1494.
190. Sugden MC, Caton PW, Holness MJ: **PPAR control: it's SIRTainly as easy as PGC**. *J Endocrinol* 2010, **204**(2):93-104.
191. Lerin C, Rodgers JT, Kalume DE, Kim SH, Pandey A, Puigserver P: **GCN5 acetyltransferase complex controls glucose metabolism through transcriptional repression of PGC-1alpha**. *Cell Metab* 2006, **3**(6):429-438.
192. Rodgers JT, Lerin C, Haas W, Gygi SP, Spiegelman BM, Puigserver P: **Nutrient control of glucose homeostasis through a complex of PGC-1alpha and SIRT1**. *Nature* 2005, **434**(7029):113-118.
193. Moreno M, Lombardi A, Silvestri E, Senese R, Cioffi F, Goglia F, Lanni A, de Lange P: **PPARs: Nuclear Receptors Controlled by, and Controlling, Nutrient Handling through Nuclear and Cytosolic Signaling**. *PPAR Res* 2010, **2010**.
194. Yang XJ: **Lysine acetylation and the bromodomain: a new partnership for signaling**. *Bioessays* 2004, **26**(10):1076-1087.
195. Jin Q, Wang C, Kuang X, Feng X, Sartorelli V, Ying H, Ge K, Dent SY: **Gcn5 and PCAF regulate PPARgamma and Prdm16 expression to facilitate brown adipogenesis**. *Mol Cell Biol* 2014, **34**(19):3746-3753.
196. Wiper-Bergeron N, Salem HA, Tomlinson JJ, Wu D, Hache RJ: **Glucocorticoid-stimulated preadipocyte differentiation is mediated through acetylation of C/EBPbeta by GCN5**. *Proc Natl Acad Sci U S A* 2007, **104**(8):2703-2708.
197. Pilato CA, Stadiotti I, Maione AS, Saverio V, Catto V, Tundo F, Dello Russo A, Tondo C, Pompilio G, Casella M *et al*: **Isolation and Characterization of Cardiac Mesenchymal Stromal Cells from Endomyocardial Bioptic Samples of Arrhythmogenic Cardiomyopathy Patients**. *J Vis Exp* 2018(132).
198. Kim SP, Ha JM, Yun SJ, Kim EK, Chung SW, Hong KW, Kim CD, Bae SS: **Transcriptional activation of peroxisome proliferator-activated receptor-gamma requires activation of both protein kinase A and Akt during adipocyte differentiation**. *Biochem Biophys Res Commun* 2010, **399**(1):55-59.
199. Lee MJ, Fried SK: **The glucocorticoid receptor, not the mineralocorticoid receptor, plays the dominant role in adipogenesis and adipokine production in human adipocytes**. *Int J Obes (Lond)* 2014, **38**(9):1228-1233.
200. Miskiewicz EI, MacPhee DJ: **Lysis Buffer Choices Are Key Considerations to Ensure Effective Sample Solubilization for Protein Electrophoresis**. *Methods Mol Biol* 2019, **1855**:61-72.
201. Moore CB, Guthrie EH, Huang MT, Taxman DJ: **Short hairpin RNA (shRNA): design, delivery, and assessment of gene knockdown**. *Methods Mol Biol* 2010, **629**:141-158.
202. Kutter C, Svoboda P: **miRNA, siRNA, piRNA: Knowns of the unknown**. *RNA Biol* 2008, **5**(4):181-188.
203. Carradori S, Secci D, Mai A: **Epigenetic modulation of PGC-1alpha activity by GCN5 inhibitors: WO2010007085**. *Expert Opin Ther Pat* 2011, **21**(10):1651-1656.
204. Dobin A, Davis CA, Schlesinger F, Drenkow J, Zaleski C, Jha S, Batut P, Chaisson M, Gingeras TR: **STAR: ultrafast universal RNA-seq aligner**. *Bioinformatics* 2013, **29**(1):15-21.
205. Robinson MD, McCarthy DJ, Smyth GK: **edgeR: a Bioconductor package for differential expression analysis of digital gene expression data**. *Bioinformatics* 2010, **26**(1):139-140.

206. McCarthy DJ, Chen Y, Smyth GK: **Differential expression analysis of multifactor RNA-Seq experiments with respect to biological variation**. *Nucleic Acids Res* 2012, **40**(10):4288-4297.
207. Love MI, Huber W, Anders S: **Moderated estimation of fold change and dispersion for RNA-seq data with DESeq2**. *Genome Biol* 2014, **15**(12):550.
208. Chen EY, Tan CM, Kou Y, Duan Q, Wang Z, Meirelles GV, Clark NR, Ma'ayan A: **Enrichr: interactive and collaborative HTML5 gene list enrichment analysis tool**. *BMC Bioinformatics* 2013, **14**:128.
209. Kuleshov MV, Jones MR, Rouillard AD, Fernandez NF, Duan Q, Wang Z, Koplev S, Jenkins SL, Jagodnik KM, Lachmann A *et al*: **Enrichr: a comprehensive gene set enrichment analysis web server 2016 update**. *Nucleic Acids Res* 2016, **44**(W1):W90-97.
210. Kuznetsov AV, Schneeberger S, Seiler R, Brandacher G, Mark W, Steurer W, Saks V, Usson Y, Margreiter R, Gnaiger E: **Mitochondrial defects and heterogeneous cytochrome c release after cardiac cold ischemia and reperfusion**. *Am J Physiol Heart Circ Physiol* 2004, **286**(5):H1633-1641.
211. Gemayel C, Pelliccia A, Thompson PD: **Arrhythmogenic right ventricular cardiomyopathy**. *J Am Coll Cardiol* 2001, **38**(7):1773-1781.
212. Noorman M, Groeneweg JA, Asimaki A, Rizzo S, Papegaaij M, van Stuijvenberg L, de Jonge N, Dooijes D, Basso C, Saffitz JE *et al*: **End stage of arrhythmogenic cardiomyopathy with severe involvement of the interventricular septum**. *Heart Rhythm* 2013, **10**(2):283-289.
213. Corrado D, Wichter T, Link MS, Hauer R, Marchlinski F, Anastasakis A, Bauce B, Basso C, Brunckhorst C, Tsatsopoulou A *et al*: **Treatment of arrhythmogenic right ventricular cardiomyopathy/dysplasia: an international task force consensus statement**. *Eur Heart J* 2015, **36**(46):3227-3237.
214. Wichter T, Paul M, Wollmann C, Acil T, Gerdes P, Ashraf O, Tjan TD, Soeparwata R, Block M, Borggrefe M *et al*: **Implantable cardioverter/defibrillator therapy in arrhythmogenic right ventricular cardiomyopathy: single-center experience of long-term follow-up and complications in 60 patients**. *Circulation* 2004, **109**(12):1503-1508.
215. Verma A, Kilicaslan F, Schweikert RA, Tomassoni G, Rossillo A, Marrouche NF, Ozduran V, Wazni OM, Elayi SC, Saenz LC *et al*: **Short- and long-term success of substrate-based mapping and ablation of ventricular tachycardia in arrhythmogenic right ventricular dysplasia**. *Circulation* 2005, **111**(24):3209-3216.
216. Asimaki A, Saffitz JE: **Remodeling of cell-cell junctions in arrhythmogenic cardiomyopathy**. *Cell Commun Adhes* 2014, **21**(1):13-23.
217. Chelko SP, Asimaki A, Andersen P, Bedja D, Amat-Alarcon N, DeMazumder D, Jasti R, MacRae CA, Leber R, Kleber AG *et al*: **Central role for GSK3beta in the pathogenesis of arrhythmogenic cardiomyopathy**. *JCI insight* 2016, **1**(5).
218. Corrado D, Basso C, Judge DP: **Arrhythmogenic Cardiomyopathy**. *Circ Res* 2017, **121**(7):784-802.
219. Vallee A, Lecarpentier Y: **Crosstalk Between Peroxisome Proliferator-Activated Receptor Gamma and the Canonical WNT/beta-Catenin Pathway in Chronic Inflammation and Oxidative Stress During Carcinogenesis**. *Frontiers in immunology* 2018, **9**:745.
220. Lopaschuk GD, Ussher JR, Folmes CD, Jaswal JS, Stanley WC: **Myocardial fatty acid metabolism in health and disease**. *Physiol Rev* 2010, **90**(1):207-258.
221. Kim EY, Kim WK, Kang HJ, Kim JH, Chung SJ, Seo YS, Park SG, Lee SC, Bae KH: **Acetylation of malate dehydrogenase 1 promotes adipogenic**

differentiation via activating its enzymatic activity. *J Lipid Res* 2012, **53**(9):1864-1876.
222. Nolte RT, Wisely GB, Westin S, Cobb JE, Lambert MH, Kurokawa R, Rosenfeld MG, Willson TM, Glass CK, Milburn MV: **Ligand binding and co-activator assembly of the peroxisome proliferator-activated receptor-gamma**. *Nature* 1998, **395**(6698):137-143.
223. Lai B, Lee JE, Jang Y, Wang L, Peng W, Ge K: **MLL3/MLL4 are required for CBP/p300 binding on enhancers and super-enhancer formation in brown adipogenesis**. *Nucleic Acids Res* 2017, **45**(11):6388-6403.
224. Takahashi N, Kawada T, Yamamoto T, Goto T, Taimatsu A, Aoki N, Kawasaki H, Taira K, Yokoyama KK, Kamei Y *et al*: **Overexpression and ribozyme-mediated targeting of transcriptional coactivators CREB-binding protein and p300 revealed their indispensable roles in adipocyte differentiation through the regulation of peroxisome proliferator-activated receptor gamma**. *J Biol Chem* 2002, **277**(19):16906-16912.
225. Yamauchi T, Oike Y, Kamon J, Waki H, Komeda K, Tsuchida A, Date Y, Li MX, Miki H, Akanuma Y *et al*: **Increased insulin sensitivity despite lipodystrophy in Crebbp heterozygous mice**. *Nat Genet* 2002, **30**(2):221-226.
226. Selvarajan S, Lund LR, Takeuchi T, Craik CS, Werb Z: **A plasma kallikrein-dependent plasminogen cascade required for adipocyte differentiation**. *Nat Cell Biol* 2001, **3**(3):267-275.
227. Smas CM, Sul HS: **Control of adipocyte differentiation**. *Biochem J* 1995, **309 (Pt 3)**:697-710.
228. Gilpin BJ, Loechel F, Mattei MG, Engvall E, Albrechtsen R, Wewer UM: **A novel, secreted form of human ADAM 12 (meltrin alpha) provokes myogenesis in vivo**. *J Biol Chem* 1998, **273**(1):157-166.
229. Kawaguchi N, Xu X, Tajima R, Kronqvist P, Sundberg C, Loechel F, Albrechtsen R, Wewer UM: **ADAM 12 protease induces adipogenesis in transgenic mice**. *Am J Pathol* 2002, **160**(5):1895-1903.
230. Yagami-Hiromasa T, Sato T, Kurisaki T, Kamijo K, Nabeshima Y, Fujisawa-Sehara A: **A metalloprotease-disintegrin participating in myoblast fusion**. *Nature* 1995, **377**(6550):652-656.
231. Kawaguchi N, Sundberg C, Kveiborg M, Moghadaszadeh B, Asmar M, Dietrich N, Thodeti CK, Nielsen FC, Moller P, Mercurio AM *et al*: **ADAM12 induces actin cytoskeleton and extracellular matrix reorganization during early adipocyte differentiation by regulating beta1 integrin function**. *J Cell Sci* 2003, **116**(Pt 19):3893-3904.
232. Young DA, Ibrahim DO, Hu D, Christman KL: **Injectable hydrogel scaffold from decellularized human lipoaspirate**. *Acta Biomater* 2011, **7**(3):1040-1049.
233. Bonnans C, Chou J, Werb Z: **Remodelling the extracellular matrix in development and disease**. *Nat Rev Mol Cell Biol* 2014, **15**(12):786-801.
234. Mariman EC, Wang P: **Adipocyte extracellular matrix composition, dynamics and role in obesity**. *Cellular and molecular life sciences : CMLS* 2010, **67**(8):1277-1292.
235. Chen CH, Ferreira JC, Gross ER, Mochly-Rosen D: **Targeting aldehyde dehydrogenase 2: new therapeutic opportunities**. *Physiol Rev* 2014, **94**(1):1-34.
236. Pang J, Wang J, Zhang Y, Xu F, Chen Y: **Targeting acetaldehyde dehydrogenase 2 (ALDH2) in heart failure-Recent insights and perspectives**. *Biochim Biophys Acta Mol Basis Dis* 2017, **1863**(8):1933-1941.

237. Budas GR, Disatnik MH, Mochly-Rosen D: **Aldehyde dehydrogenase 2 in cardiac protection: a new therapeutic target?** *Trends Cardiovasc Med* 2009, **19**(5):158-164.
238. Zhao X, Hua Y, Chen H, Yang H, Zhang T, Huang G, Fan H, Tan Z, Huang X, Liu B *et al*: **Aldehyde dehydrogenase-2 protects against myocardial infarction-related cardiac fibrosis through modulation of the Wnt/beta-catenin signaling pathway**. *Ther Clin Risk Manag* 2015, **11**:1371-1381.
239. Gomes KM, Campos JC, Bechara LR, Queliconi B, Lima VM, Disatnik MH, Magno P, Chen CH, Brum PC, Kowaltowski AJ *et al*: **Aldehyde dehydrogenase 2 activation in heart failure restores mitochondrial function and improves ventricular function and remodelling**. *Cardiovasc Res* 2014, **103**(4):498-508.
240. Doser TA, Turdi S, Thomas DP, Epstein PN, Li SY, Ren J: **Transgenic overexpression of aldehyde dehydrogenase-2 rescues chronic alcohol intake-induced myocardial hypertrophy and contractile dysfunction**. *Circulation* 2009, **119**(14):1941-1949.
241. Yuan Q, Cao S, Dong Q, Wang Z, Xu Y, Han Q, Ma J, Wei S, Pang J, Yang F *et al*: **ALDH2 Activation Inhibited Cardiac Fibroblast-to-Myofibroblast Transformation Via the TGF-beta1/Smad Signaling Pathway**. *J Cardiovasc Pharmacol* 2019, **73**(4):248-256.
242. Barski OA, Tipparaju SM, Bhatnagar A: **The aldo-keto reductase superfamily and its role in drug metabolism and detoxification**. *Drug Metab Rev* 2008, **40**(4):553-624.
243. Gaupel AC, Begley TJ, Tenniswood M: **Gcn5 Modulates the Cellular Response to Oxidative Stress and Histone Deacetylase Inhibition**. *J Cell Biochem* 2015, **116**(9):1982-1992.
244. Lee O-H, Kwon Y-I, Hong H-D, Park C-S, Lee B-Y, Kim Y-C: **Production of Reactive Oxygen Species and Changes in Antioxidant Enzyme Activities during Differentiation of 3T3-L1 Adipocyte**. *Journal of the Korean Society for Applied Biological Chemistry* 2009, **52**(1):70-75.
245. Ducluzeau PH, Priou M, Weitheimer M, Flamment M, Duluc L, Iacobazi F, Soleti R, Simard G, Durand A, Rieusset J *et al*: **Dynamic regulation of mitochondrial network and oxidative functions during 3T3-L1 fat cell differentiation**. *J Physiol Biochem* 2011, **67**(3):285-296.
246. Meerson FZ, Belkina LM, Sazontova TG, Saltykova VA, Arkhipenko Yu V: **The role of lipid peroxidation in pathogenesis of arrhythmias and prevention of cardiac fibrillation with antioxidants**. *Basic Res Cardiol* 1987, **82**(2):123-137.
247. Savelieva I, Camm J: **Statins and polyunsaturated fatty acids for treatment of atrial fibrillation**. *Nat Clin Pract Cardiovasc Med* 2008, **5**(1):30-41.
248. Plotnikov EY, Silachev DN, Popkov VA, Zorova LD, Pevzner IB, Zorov SD, Jankauskas SS, Babenko VA, Sukhikh GT, Zorov DB: **Intercellular Signalling Cross-Talk: To Kill, To Heal and To Rejuvenate**. *Heart Lung Circ* 2017, **26**(7):648-659.
249. Casado-Diaz A, Anter J, Muller S, Winter P, Quesada-Gomez JM, Dorado G: **Transcriptomic Analyses of Adipocyte Differentiation From Human Mesenchymal Stromal-Cells (MSC)**. *J Cell Physiol* 2017, **232**(4):771-784.
250. d'Amati G, di Gioia CR, Giordano C, Gallo P: **Myocyte transdifferentiation: a possible pathogenetic mechanism for arrhythmogenic right ventricular cardiomyopathy**. *Arch Pathol Lab Med* 2000, **124**(2):287-290.
251. Cerrone M, Delmar M: **Desmosomes and the sodium channel complex: implications for arrhythmogenic cardiomyopathy and Brugada syndrome**. *Trends Cardiovasc Med* 2014, **24**(5):184-190.

252. Krenning G, Zeisberg EM, Kalluri R: **The origin of fibroblasts and mechanism of cardiac fibrosis**. *J Cell Physiol* 2010, **225**(3):631-637.
253. Kohl P, Camelliti P: **Fibroblast-myocyte connections in the heart**. *Heart Rhythm* 2012, **9**(3):461-464.
254. Xie Y, Garfinkel A, Weiss JN, Qu Z: **Cardiac alternans induced by fibroblast-myocyte coupling: mechanistic insights from computational models**. *Am J Physiol Heart Circ Physiol* 2009, **297**(2):H775-784.
255. Burridge PW, Matsa E, Shukla P, Lin ZC, Churko JM, Ebert AD, Lan F, Diecke S, Huber B, Mordwinkin NM *et al*: **Chemically defined generation of human cardiomyocytes**. *Nat Methods* 2014, **11**(8):855-860.
256. Wen Q, Gandhi K, Capel RA, Hao G, O'Shea C, Neagu G, Pearcey S, Pavlovic D, Terrar DA, Wu J *et al*: **Transverse cardiac slicing and optical imaging for analysis of transmural gradients in membrane potential and Ca(2+) transients in murine heart**. *J Physiol* 2018, **596**(17):3951-3965.
257. Issa ZF, Miller JM, Zipes DP: **22 - Ventricular Arrhythmias in Ischemic Heart Disease**. In: *Clinical Arrhythmology and Electrophysiology (Third Edition).* edn. Edited by Issa ZF, Miller JM, Zipes DP. Philadelphia: Content Repository Only!; 2019: 748-815.
258. Fabritz L, Kirchhof P, Franz MR, Eckardt L, Monnig G, Milberg P, Breithardt G, Haverkamp W: **Prolonged action potential durations, increased dispersion of repolarization, and polymorphic ventricular tachycardia in a mouse model of proarrhythmia**. *Basic Res Cardiol* 2003, **98**(1):25-32.
259. Camm AJ, Janse MJ, Roden DM, Rosen MR, Cinca J, Cobbe SM: **Congenital and acquired long QT syndrome**. *Eur Heart J* 2000, **21**(15):1232-1237.
260. Morita H, Wu J, Zipes DP: **The QT syndromes: long and short**. *Lancet* 2008, **372**(9640):750-763.
261. King JH, Huang CL, Fraser JA: **Determinants of myocardial conduction velocity: implications for arrhythmogenesis**. *Front Physiol* 2013, **4**:154.
262. Laughner JI, Ng FS, Sulkin MS, Arthur RM, Efimov IR: **Processing and analysis of cardiac optical mapping data obtained with potentiometric dyes**. *Am J Physiol Heart Circ Physiol* 2012, **303**(7):H753-765.

9 Acknowledgements

Dopo un percorso cosi´ lungo, alcuni ringraziamenti sono d'obbligo e sinceramente sentiti.

Vorrei ringraziare la Professoressa Donatella Stilli, che nonostante la distanza è sempre stata disponibile a fornirmi tutto il supporto necessario. Ringrazio la Prof. Costanza Lagrasta, la Dott. Caterina Frati e la Dott. Angela Falco per aver processato al microscopio a trasmissione i miei campioni; il Prof. Corradi per le immunoistochimiche, e il Dott. Silvano Piazza e la Dott. Veronica De Sanctis per aver eseguito l'analisi trascrittomica: tutti questi esperimenti sono stati di grande rilievo per la mia tesi. Ringrazio la Dott. Elena Sommariva e il Dott. Giulio Pompilio del Centro Cardiologico Monzino di Milano per avermi fornito i campioni cellulari e per la loro estrema disponibilità e competenza.

Ringrazio il gruppo di malattie cardiovascolari, guidato da Alessandra Rossini, a cui va un grande ringraziamento per la fiducia dimostratami in questi tre anni, che spero possa rafforzarsi ancora di più nei prossimi mesi con l'inizio di questo nuovo percorso che ci aspetta. La ringrazio soprattutto per il sostegno e l'estrema pazienza mostratami durante la stesura della tesi. Non posso non ringraziare Marzia, arrivata da poco più di un anno, ma già parte integrante del nostro gruppo: vorrei ringraziarla non solo per l'attenzione e i suggerimenti che mi ha dato durante la preparazione della tesi, ma soprattutto per essere sempre pronta ad ascoltarmi: i confronti quotidiani con lei, sia in ambito scientifico che personale, sono per me motivo di grande crescita. Ringrazio Benedetta, per tutti i consigli che mi ha dato in questi tre anni e per la sua estrema disponibilità. Ringrazio Chiara per il suo prezioso contributo per esperimenti di respirometria e, soprattutto, per il grande entusiasmo che mette nel fare ricerca, è davvero stimolante per me. Come dimenticare Theresa, master student modello e ormai anche cara amica: il suo contributo in laboratorio si è rivelato essenziale soprattutto durante il mio soggiorno all'estero. E poi ringrazio Giada, non solo collega, ma ormai amica da ben tre anni: la sua simpatia, dolcezza ed esuberanza mi hanno aiutato ad affrontare con il sorriso tante giornate. La ringrazio perché´, soprattutto in questi ultimi mesi, mi è saputa stare vicino, dandomi un po´ di quella sana leggerezza e allegria che ogni tanto mi sono mancate: è in assoluto una delle persone piu´ belle che questa esperienza mi ha regalato. Anche se ormai non più parte del nostro gruppo, non posso dimenticare Betta, inizialmente collega e ormai grande amica. Tante volte confrontarmi con lei, mi ha permesso di guardare le situazioni in modo diverso, e non posso essere che contenta della bella e sincera amicizia che ancora oggi ci lega: nonostante i quotidiani impegni che ci tengono lontane, so di poter sempre contare su di lei. Un ringraziamento speciale va anche a

Viviana, con cui ho iniziato questo percorso: non posso non ringraziarla per tutto ciò che mi ha insegnato in laboratorio, ma soprattutto per avermi mostrato quanto la determinazione e la dedizione siano fondamentali per fare della buona ricerca.

Un ringraziamento va poi a tutto l'Istituto di Biomedicina, un ambiente stimolante professionalmente, e pieno di persone pronte a condividere le proprie conoscenze. In particolare, ringrazio Luisa per l'infinita pazienza mostratami e per l'attenzione che ha avuto nel fare gran parti delle analisi statistiche riportate nel mio lavoro di dottorato. Ringrazio Anne, per il supporto tecnico nell'eseguire esperimenti di espressione genica. Un grazie di cuore va poi a Corrado e Mattia che, oltre ad essere sempre stati disponibili a risolvere i miei tanti dubbi quotidiani, con la loro simpatia hanno anche allietato tante mie lunghe giornate di laboratorio. Ringrazio Clemens, uomo dotato di pazienza fuori dal comune e con un´ esperienza unica nel campo dell'informatica: grazie non solo per aver dato il tocco finale alla formattazione della mia tesi, ma per tutta la disponibilità e il sostegno dimostrato in questi tre anni. Ringrazio Johannes e Cristina, altre due figure sempre presenti durante questo mio percorso. Un pensiero speciale va poi a Julia e Paulina, due persone fantastiche che ho imparato a conoscere pian piano, ma che ad oggi posso dire essere sicuramente tra i miei punti di riferimento qui a Bolzano; non posso che ringraziarle per le tante risate, per gli innumerevoli consigli di laboratorio e non solo, ma soprattutto per il grande affetto che ogni giorno sono in grado di dimostrarmi.

Ringrazio ancora tutte le persone con cui lavoro fianco a fianco ogni giorno: Claudia, Valentina, Giovanna, Amparo, Sara, Giulia, Vladimir, Federica e tutti gli altri, da cui ho sempre tanto da imparare e che non mi hanno mai risparmiato un sorriso e una parola di conforto. Ringrazio anche Serena, Chiara, Giulia, Monica, Christa che ormai hanno intrapreso strade diverse, ma che hanno lasciato un segno indelebile in questo mio percorso.

Ringrazio la Dott. Patrizia Camelliti, che mi ha ospitato nel suo laboratorio per tre mesi: questa esperienza mi ha davvero lasciato tanto dal punto di vista professionale e soprattutto la ringrazio per l'estrema fiducia mostratami in così pochi mesi: spero vivamente che la nostra collaborazione possa andare avanti a lungo ed essere fruttuosa. Ringrazio anche la EMBO per aver supportato il mio soggiorno all´estero, finanziandomi con una Short-Term fellowship. Come dimenticare tutti i ragazzi incontrati nell'Università del Surrey. Valeria, una delle persone più dolci che abbia mai conosciuto, compagna di tante confidenze; Rolando, sempre attento nei miei confronti e pronto ad aiutarmi in qualsiasi problema; Paula, così premurosa e sempre disposta ad ascoltarmi; Davide, compagno dell´ultimo "Pig day" e

complice fino all´ultimo giorno; Andria e Anastasis, due persone con un cuore immenso che mi hanno mostrato affetto dal primo secondo e, last but not least, Robert, a cui non potrò mai smettere di dire grazie per la pazienza che ha avuto con me in quei mesi e per tutto il supporto che anche a distanza è ancora in grado di mostrarmi. E ancora grazie a Theo, Lucinda, Matt, Phil, Mafalda, Emma, Lisie, John e Anne che mi hanno accolto nella loro stupenda famiglia: ognuno di loro ha saputo rendere la mia esperienza indimenticabile, regalandomi una nuova sincera amicizia.

Un ringraziamento particolare a mamma e papa´, colonne portanti della mia vita. So che starmi vicino nonostante i tanti chilometri di distanza non è affatto semplice, eppure sono riusciti anche in questi anni a farmi sentire tutto il loro supporto e infinito affetto. Non sarebbero sufficienti pagine di belle parole per mostrar loro tutta la mia riconoscenza, ma spero davvero di averli resi ancora una volta fieri di me, e di poter vedere di nuovo i loro occhi colmi di gioia e orgoglio. Ringrazio la mia piccola Claudia, la sorella migliore che potessi desiderare e che riesce sempre a suo modo a mostrarmi tutto l'amore che prova per me: per lei mi auguro di poter essere quella persona su cui poter sempre contare.

Ringrazio le tre donne, nonna Antonietta, zia Adele e zia Vita, che mi hanno insegnato cosa vuol dire voler bene in modo incondizionato e che a qualsiasi distanza trovano il modo di essere presenti: non potrò mai ringraziarvi abbastanza per tutto l'amore che mi avete dato e ancora oggi mi dimostrate.

Ringrazio Erica e Bruna, presenze costanti nella mi vita. Sono state la mia forza più grande in tanti momenti e saperle vicine mi ha dato la grinta giusta per proseguire. Il regalo più grande che mi hanno fatto è stato farmi riscoprire più forte di quanto io stessa avessi mai potuto immaginare, e probabilmente per questo non potrò mai ringraziarle abbastanza.

Ringrazio tutti i fantastici ragazzi conosciuti qui a Bolzano: Stefano, Emanuela, Elisa, Giulio, Sarah, Elena, Diana, Lena hanno allietato tante giornate e spero ancora di poterli avere vicino a lungo. Un grazie speciale a Gabriella e Cristiana, conosciute in modo casuale, ma diventate due presenze costanti della mia quotidianità.

Grazie a Eliana, Silvia, Letizia, Manfredi, Veronica, Serena, Giuseppe, che mi hanno fatto sentire a casa tutte le volte che sono tornata a Parma e a Giulia e Chiara, preziose amicizie regalatemi dall´ Erasmus, e che ancora oggi sono presenti nella mia vita.

10 Appendix 1

List of differentially expressed genes in ACM CStCs in adipogenic medium in presence of MB-3.

log2FoldChange	pvalue	padj	external_gene_name	description
-5.870230674	2.86E-12	3.33E-09	AKR1B10	aldo-keto reductase family 1 member B10 [Source:HGNC Symbol;Acc:HGNC:382]
-4.912144089	4.25E-05	0.003115	ADH4	alcohol dehydrogenase 4 (class II), pi polypeptide [Source:HGNC Symbol;Acc:HGNC:252]
-4.722425676	0.000864	0.026157	AKAP3	A-kinase anchoring protein 3 [Source:HGNC Symbol;Acc:HGNC:373]
-4.422376916	3.21E-06	0.000427	EVI2B	ecotropic viral integration site 2B [Source:HGNC Symbol;Acc:HGNC:3500]
-4.274882301	4.10E-05	0.003039	TFEC	transcription factor EC [Source:HGNC Symbol;Acc:HGNC:11754]
-3.679643555	0.000107	0.006429	AC137932.2	uncharacterized LOC100287036 [Source:NCBI gene;Acc:100287036]
-3.624710612	0.000499	0.017697	ENHO	energy homeostasis associated [Source:HGNC Symbol;Acc:HGNC:24838]
-3.608151261	1.20E-11	1.11E-08	AKR1C2	aldo-keto reductase family 1 member C2 [Source:HGNC Symbol;Acc:HGNC:385]
-3.555233125	0.002211	0.04912	AP001596.1	novel transcript
-3.497348288	0.00176	0.042167	SNHG31	small nucleolar RNA host gene 31 [Source:HGNC Symbol;Acc:HGNC:54196]
-3.463963181	7.39E-05	0.004771	HKDC1	hexokinase domain containing 1 [Source:HGNC Symbol;Acc:HGNC:23302]
-3.420700699	0.000799	0.024604	CEBPA-DT	CEBPA divergent transcript [Source:HGNC Symbol;Acc:HGNC:25710]
-3.411434874	1.52E-06	0.000243	CLCA2	chloride channel accessory 2 [Source:HGNC Symbol;Acc:HGNC:2016]
-3.322953875	9.25E-08	2.60E-05	CACNA1G	calcium voltage-gated channel subunit alpha1 G [Source:HGNC Symbol;Acc:HGNC:1394]
-3.321606434	0.000151	0.008055	FCGBP	Fc fragment of IgG binding protein [Source:HGNC Symbol;Acc:HGNC:13572]
-3.303243701	4.81E-07	9.64E-05	COLEC12	collectin subfamily member 12 [Source:HGNC Symbol;Acc:HGNC:16016]
-3.297439873	3.38E-19	1.47E-15	OSGIN1	oxidative stress induced growth inhibitor 1 [Source:HGNC Symbol;Acc:HGNC:30093]
-3.2276145	1.37E-10	1.04E-07	AKR1C1	aldo-keto reductase family 1 member C1 [Source:HGNC Symbol;Acc:HGNC:384]
-3.085476958	3.62E-05	0.00277	AFP	alpha fetoprotein [Source:HGNC Symbol;Acc:HGNC:317]
-3.028407775	0.002241	0.049578	RNU5B-1	RNA, U5B small nuclear 1 [Source:HGNC Symbol;Acc:HGNC:10212]
-2.913570546	0.000587	0.019784	CFHR1	complement factor H related 1 [Source:HGNC Symbol;Acc:HGNC:4888]
-2.824787509	3.14E-06	0.000425	ATP8A1	ATPase phospholipid transporting 8A1 [Source:HGNC Symbol;Acc:HGNC:13531]
-2.822298108	0.002225	0.049358	AL022341.1	novel transcript

log2FoldChange	pvalue	padj	external_gene_name	description
-2.811832188	3.99E-12	4.09E-09	NMRAL2P	NmrA like redox sensor 2, pseudogene [Source:HGNC Symbol;Acc:HGNC:52332]
-2.797727381	0.000789	0.024424	CLU	clusterin [Source:HGNC Symbol;Acc:HGNC:2095]
-2.732650354	0.000459	0.016812	CCL26	C-C motif chemokine ligand 26 [Source:HGNC Symbol;Acc:HGNC:10625]
-2.631581666	0.000135	0.007427	BATF2	basic leucine zipper ATF-like transcription factor 2 [Source:HGNC Symbol;Acc:HGNC:25163]
-2.620777386	0.000108	0.006444	RASD1	ras related dexamethasone induced 1 [Source:HGNC Symbol;Acc:HGNC:15828]
-2.615433264	1.67E-05	0.001503	GNAL	G protein subunit alpha L [Source:HGNC Symbol;Acc:HGNC:4388]
-2.530641958	0.001973	0.045472	LINC02062	long intergenic non-protein coding RNA 2062 [Source:HGNC Symbol;Acc:HGNC:52907]
-2.511576181	0.000594	0.019898	ADH1B	alcohol dehydrogenase 1B (class I), beta polypeptide [Source:HGNC Symbol;Acc:HGNC:250]
-2.481404474	2.11E-06	0.000309	TMEM37	transmembrane protein 37 [Source:HGNC Symbol;Acc:HGNC:18216]
-2.480604963	0.000658	0.021284	SERPINA5	serpin family A member 5 [Source:HGNC Symbol;Acc:HGNC:8723]
-2.479621711	1.17E-05	0.001171	GPAT3	glycerol-3-phosphate acyltransferase 3 [Source:HGNC Symbol;Acc:HGNC:28157]
-2.478913551	5.20E-12	5.04E-09	TRIM16L	tripartite motif containing 16 like [Source:HGNC Symbol;Acc:HGNC:32670]
-2.387315521	0.001742	0.042005	LAMB3	laminin subunit beta 3 [Source:HGNC Symbol;Acc:HGNC:6490]
-2.344824556	0.000992	0.028883	RBM47	RNA binding motif protein 47 [Source:HGNC Symbol;Acc:HGNC:30358]
-2.335853328	0.000517	0.018127	LINC02340	long intergenic non-protein coding RNA 2340 [Source:HGNC Symbol;Acc:HGNC:53260]
-2.335675081	0.000209	0.010023	AL513534.1	
-2.305941859	1.00E-04	0.006114	PCOLCE2	procollagen C-endopeptidase enhancer 2 [Source:HGNC Symbol;Acc:HGNC:8739]
-2.292311319	1.99E-05	0.001734	CHST1	carbohydrate sulfotransferase 1 [Source:HGNC Symbol;Acc:HGNC:1969]
-2.289759806	2.43E-15	6.04E-12	PTGR1	prostaglandin reductase 1 [Source:HGNC Symbol;Acc:HGNC:18429]
-2.275131859	8.05E-05	0.005104	RAB11FIP4	RAB11 family interacting protein 4 [Source:HGNC Symbol;Acc:HGNC:30267]
-2.272185275	0.001654	0.041131	PTPN22	protein tyrosine phosphatase non-receptor type 22 [Source:HGNC Symbol;Acc:HGNC:9652]
-2.268459572	3.42E-07	7.19E-05	IGFBP6	insulin like growth factor binding protein 6 [Source:HGNC Symbol;Acc:HGNC:5475]
-2.26501273	1.73E-06	0.000272	HMOX1	heme oxygenase 1 [Source:HGNC Symbol;Acc:HGNC:5013]
-2.232604546	0.001271	0.034365	ARMH1	armadillo like helical domain containing 1 [Source:HGNC Symbol;Acc:HGNC:34345]
-2.215422345	4.73E-05	0.003424	EFCAB5	EF-hand calcium binding domain 5 [Source:HGNC Symbol;Acc:HGNC:24801]

log2FoldChange	pvalue	padj	external_gene_name	description
-2.194365166	0.000182	0.009215	BDKRB2	bradykinin receptor B2 [Source:HGNC Symbol;Acc:HGNC:1030]
-2.148663321	1.14E-05	0.001154	KITLG	KIT ligand [Source:HGNC Symbol;Acc:HGNC:6343]
-2.146300092	0.001955	0.045281	SNORA11	small nucleolar RNA, H/ACA box 11 [Source:HGNC Symbol;Acc:HGNC:32599]
-2.143343881	0.001292	0.034766	KLF15	Kruppel like factor 15 [Source:HGNC Symbol;Acc:HGNC:14536]
-2.12613554	0.000516	0.018127	AL031666.1	novel transcript, antisense to ZMYND8
-2.120769472	0.001496	0.038368	AF038458.2	novel transcript
-2.111049812	8.43E-08	2.41E-05	AKR1B1	aldo-keto reductase family 1 member B [Source:HGNC Symbol;Acc:HGNC:381]
-2.108010606	0.000368	0.014849	AC132872.2	novel transcript, antisense CCDC57
-2.091019495	0.000467	0.017051	STIM2-AS1	STIM2 antisense RNA 1 [Source:HGNC Symbol;Acc:HGNC:40879]
-2.08838845	0.000555	0.019011	ID1	inhibitor of DNA binding 1, HLH protein [Source:HGNC Symbol;Acc:HGNC:5360]
-2.082363027	0.000592	0.019863	HSD11B1	hydroxysteroid 11-beta dehydrogenase 1 [Source:HGNC Symbol;Acc:HGNC:5208]
-2.073216494	0.000369	0.014849	F2RL2	coagulation factor II thrombin receptor like 2 [Source:HGNC Symbol;Acc:HGNC:3539]
-2.065762589	0.000992	0.028883	AC080013.1	novel transcript, antisense to RARRES1
-2.032671965	0.000459	0.016812	SLC7A8	solute carrier family 7 member 8 [Source:HGNC Symbol;Acc:HGNC:11066]
-2.02853559	1.25E-06	0.000205	PIR	pirin [Source:HGNC Symbol;Acc:HGNC:30048]
-2.017672682	0.001322	0.035422	ITPKA	inositol-trisphosphate 3-kinase A [Source:HGNC Symbol;Acc:HGNC:6178]
-2.011480109	0.00183	0.043236	LTB	lymphotoxin beta [Source:HGNC Symbol;Acc:HGNC:6711]
-2.002695074	2.75E-10	1.64E-07	GCLM	glutamate-cysteine ligase modifier subunit [Source:HGNC Symbol;Acc:HGNC:4312]
-1.97367427	2.57E-06	0.000362	GABRE	gamma-aminobutyric acid type A receptor epsilon subunit [Source:HGNC Symbol;Acc:HGNC:4085]
-1.959741313	6.57E-05	0.004357	CTSL	cathepsin L [Source:HGNC Symbol;Acc:HGNC:2537]
-1.959328602	0.001724	0.041866	SPARCL1	SPARC like 1 [Source:HGNC Symbol;Acc:HGNC:11220]
-1.910360576	0.000284	0.01252	COA6-AS1	COA6 antisense RNA 1 [Source:HGNC Symbol;Acc:HGNC:40825]
-1.903690071	0.00076	0.023747	RAB7B	RAB7B, member RAS oncogene family [Source:HGNC Symbol;Acc:HGNC:30513]
-1.903326191	0.001579	0.03996	AC021752.1	novel transcript
-1.899780551	8.50E-06	0.000945	ZBED5-AS1	ZBED5 antisense RNA 1 [Source:HGNC Symbol;Acc:HGNC:48646]
-1.894852447	6.17E-08	1.96E-05	IL6R	interleukin 6 receptor [Source:HGNC Symbol;Acc:HGNC:6019]

log2FoldChange	pvalue	padj	external_gene_name	description
-1.855991563	3.40E-05	0.002663	ABCA9	ATP binding cassette subfamily A member 9 [Source:HGNC Symbol;Acc:HGNC:39]
-1.823064433	7.07E-05	0.004619	EPHX1	epoxide hydrolase 1 [Source:HGNC Symbol;Acc:HGNC:3401]
-1.782157093	5.56E-05	0.003879	AC008267.5	novel transcript
-1.776621114	0.000121	0.006969	SULF2	sulfatase 2 [Source:HGNC Symbol;Acc:HGNC:20392]
-1.767001282	0.000677	0.021787	AKR1C3	aldo-keto reductase family 1 member C3 [Source:HGNC Symbol;Acc:HGNC:386]
-1.761729574	5.36E-05	0.003786	CTH	cystathionine gamma-lyase [Source:HGNC Symbol;Acc:HGNC:2501]
-1.755328872	1.39E-06	0.000226	TBXAS1	thromboxane A synthase 1 [Source:HGNC Symbol;Acc:HGNC:11609]
-1.754268761	5.01E-05	0.003578	SLC2A12	solute carrier family 2 member 12 [Source:HGNC Symbol;Acc:HGNC:18067]
-1.741370977	0.000264	0.011816	AC137767.1	novel transcript
-1.724173545	1.75E-10	1.22E-07	SLC7A11	solute carrier family 7 member 11 [Source:HGNC Symbol;Acc:HGNC:11059]
-1.709328744	3.35E-05	0.002645	AC005076.1	novel transcript, antisense to DMTF1
-1.707333793	5.70E-05	0.003943	NSUN3	NOP2/Sun RNA methyltransferase 3 [Source:HGNC Symbol;Acc:HGNC:26208]
-1.694516605	9.91E-05	0.006085	NQO1	NAD(P)H quinone dehydrogenase 1 [Source:HGNC Symbol;Acc:HGNC:2874]
-1.692843779	1.90E-08	7.54E-06	NAMPT	nicotinamide phosphoribosyltransferase [Source:HGNC Symbol;Acc:HGNC:30092]
-1.691447356	3.38E-05	0.002652	ZNF436-AS1	ZNF436 antisense RNA 1 [Source:HGNC Symbol;Acc:HGNC:25122]
-1.68373126	0.002181	0.048865	LOXL4	lysyl oxidase like 4 [Source:HGNC Symbol;Acc:HGNC:17171]
-1.671780455	3.12E-06	0.000425	TYMSOS	TYMS opposite strand [Source:HGNC Symbol;Acc:HGNC:29553]
-1.658951031	0.00053	0.018408	APOL3	apolipoprotein L3 [Source:HGNC Symbol;Acc:HGNC:14868]
-1.637126006	0.001607	0.040319	PRRT1	proline rich transmembrane protein 1 [Source:HGNC Symbol;Acc:HGNC:13943]
-1.61184586	1.09E-05	0.001114	TMEM99	transmembrane protein 99 [Source:HGNC Symbol;Acc:HGNC:28305]
-1.605634826	1.24E-06	0.000205	BNC2-AS1	BNC2 antisense RNA 1 [Source:HGNC Symbol;Acc:HGNC:53727]
-1.601797355	5.05E-05	0.003594	CEBPA	CCAAT enhancer binding protein alpha [Source:HGNC Symbol;Acc:HGNC:1833]
-1.596944687	0.00013	0.007271	AC087741.1	novel transcript, antisense to CARD14
-1.590292225	2.37E-05	0.001993	IQCH-AS1	IQCH antisense RNA 1 [Source:HGNC Symbol;Acc:HGNC:44104]
-1.580462855	0.000195	0.009586	DNAJC27-AS1	DNAJC27 antisense RNA 1 [Source:HGNC Symbol;Acc:HGNC:42943]
-1.575116742	3.78E-05	0.00286	FTL	ferritin light chain [Source:HGNC Symbol;Acc:HGNC:3999]
-1.566922142	7.07E-08	2.16E-05	ENOX1	ecto-NOX disulfide-thiol exchanger 1 [Source:HGNC Symbol;Acc:HGNC:25474]

log2FoldChange	pvalue	padj	external_gene_name	description
-1.562518445	0.001659	0.041131	GCHFR	GTP cyclohydrolase I feedback regulator [Source:HGNC Symbol;Acc:HGNC:4194]
-1.554655365	6.00E-05	0.00409	CHI3L2	chitinase 3 like 2 [Source:HGNC Symbol;Acc:HGNC:1933]
-1.530610722	1.95E-05	0.001724	AP001972.5	TEC
-1.527241074	1.36E-05	0.001283	LINC01094	long intergenic non-protein coding RNA 1094 [Source:HGNC Symbol;Acc:HGNC:49219]
-1.516857209	3.46E-05	0.002693	AP002387.2	novel transcript
-1.510419943	4.34E-05	0.003168	LINC02019	long intergenic non-protein coding RNA 2019 [Source:HGNC Symbol;Acc:HGNC:52854]
-1.506976515	0.001453	0.037874	LXN	latexin [Source:HGNC Symbol;Acc:HGNC:13347]
-1.499347151	1.28E-05	0.001247	PGD	phosphogluconate dehydrogenase [Source:HGNC Symbol;Acc:HGNC:8891]
-1.486236696	1.53E-05	0.001397	MFSD13A	major facilitator superfamily domain containing 13A [Source:HGNC Symbol;Acc:HGNC:26196]
-1.481266562	0.000558	0.019059	HIST1H1C	histone cluster 1 H1 family member c [Source:HGNC Symbol;Acc:HGNC:4716]
-1.475582456	1.38E-05	0.001297	PTGFR	prostaglandin F receptor [Source:HGNC Symbol;Acc:HGNC:9600]
-1.475418969	0.001533	0.038912	IFI44L	interferon induced protein 44 like [Source:HGNC Symbol;Acc:HGNC:17817]
-1.469834337	2.00E-06	0.000301	PPM1K	protein phosphatase, Mg2+/Mn2+ dependent 1K [Source:HGNC Symbol;Acc:HGNC:25415]
-1.467706942	2.48E-05	0.00206	ALDH3A2	aldehyde dehydrogenase 3 family member A2 [Source:HGNC Symbol;Acc:HGNC:403]
-1.465067171	0.000216	0.01028	LYNX1	Ly6/neurotoxin 1 [Source:HGNC Symbol;Acc:HGNC:29604]
-1.46193912	1.15E-07	3.08E-05	SAT1	spermidine/spermine N1-acetyltransferase 1 [Source:HGNC Symbol;Acc:HGNC:10540]
-1.45080161	2.55E-07	5.78E-05	TMCC1-AS1	TMCC1 antisense RNA 1 (head to head) [Source:HGNC Symbol;Acc:HGNC:49060]
-1.4259041	0.000499	0.017697	AC084824.5	novel transcript, antisense to DNM1L
-1.411942025	0.001496	0.038368	CA11	carbonic anhydrase 11 [Source:HGNC Symbol;Acc:HGNC:1370]
-1.402539252	0.002063	0.046776	SRPX	sushi repeat containing protein X-linked [Source:HGNC Symbol;Acc:HGNC:11309]
-1.387933883	0.0012	0.033275	NONOP2	non-POU domain containing, octamer-binding pseudogene 2 [Source:HGNC Symbol;Acc:HGNC:42032]
-1.379499516	2.68E-05	0.002173	P2RX6	purinergic receptor P2X 6 [Source:HGNC Symbol;Acc:HGNC:8538]
-1.376958492	0.001744	0.042005	ARG2	arginase 2 [Source:HGNC Symbol;Acc:HGNC:664]
-1.364962096	0.000415	0.016048	DOCK4	dedicator of cytokinesis 4 [Source:HGNC Symbol;Acc:HGNC:19192]
-1.344650682	1.16E-06	0.000195	TIMP1	TIMP metallopeptidase inhibitor 1 [Source:HGNC Symbol;Acc:HGNC:11820]

log2FoldChange	pvalue	padj	external_gene_name	description
-1.328088347	2.50E-07	5.78E-05	SQSTM1	sequestosome 1 [Source:HGNC Symbol;Acc:HGNC:11280]
-1.32194901	0.000252	0.011494	AC096921.2	novel transcript, overlapping to TGFBR2
-1.32034283	0.000128	0.007203	FAM171B	family with sequence similarity 171 member B [Source:HGNC Symbol;Acc:HGNC:29412]
-1.316381	0.000928	0.027487	EBF1	EBF transcription factor 1 [Source:HGNC Symbol;Acc:HGNC:3126]
-1.31159128	0.000438	0.016479	TDP2	tyrosyl-DNA phosphodiesterase 2 [Source:HGNC Symbol;Acc:HGNC:17768]
-1.30626689	0.000173	0.008885	C9orf72	C9orf72-SMCR8 complex subunit [Source:HGNC Symbol;Acc:HGNC:28337]
-1.300079976	8.83E-07	0.000164	MHENCR	melanoma highly expressed competing endogenous lncRNA for miR-425 and miR-489 [Source:HGNC Symbol;Acc:HGNC:53110]
-1.296893084	9.40E-06	0.001005	FAH	fumarylacetoacetate hydrolase [Source:HGNC Symbol;Acc:HGNC:3579]
-1.295501815	0.000246	0.01124	ENSG00000265263	ENSG00000265263
-1.277337188	5.73E-05	0.00395	SMPD1	sphingomyelin phosphodiesterase 1 [Source:HGNC Symbol;Acc:HGNC:11120]
-1.272099464	0.001823	0.043132	ABCA6	ATP binding cassette subfamily A member 6 [Source:HGNC Symbol;Acc:HGNC:36]
-1.26348019	3.04E-05	0.002422	ROM1	retinal outer segment membrane protein 1 [Source:HGNC Symbol;Acc:HGNC:10254]
-1.260471761	0.000206	0.009933	DLGAP1-AS1	DLGAP1 antisense RNA 1 [Source:HGNC Symbol;Acc:HGNC:31676]
-1.256591355	0.001016	0.029441	AL441992.1	novel transcript
-1.254078917	0.001817	0.043103	STEAP1	STEAP family member 1 [Source:HGNC Symbol;Acc:HGNC:11378]
-1.241449836	7.70E-06	0.000872	DUSP6	dual specificity phosphatase 6 [Source:HGNC Symbol;Acc:HGNC:3072]
-1.234126407	0.000204	0.00989	AC012146.1	novel transcript, antisense to ZNF232
-1.23327392	0.000182	0.009215	TMEM144	transmembrane protein 144 [Source:HGNC Symbol;Acc:HGNC:25633]
-1.217401566	0.001659	0.041131	DUSP5	dual specificity phosphatase 5 [Source:HGNC Symbol;Acc:HGNC:3071]
-1.21399171	0.000516	0.018127	GBA	glucosylceramidase beta [Source:HGNC Symbol;Acc:HGNC:4177]
-1.212913908	5.52E-06	0.000677	MAP3K14	mitogen-activated protein kinase kinase kinase 14 [Source:HGNC Symbol;Acc:HGNC:6853]
-1.212195548	0.001865	0.043589	LRRK2	leucine rich repeat kinase 2 [Source:HGNC Symbol;Acc:HGNC:18618]
-1.209721039	0.000742	0.023444	ALDH6A1	aldehyde dehydrogenase 6 family member A1 [Source:HGNC Symbol;Acc:HGNC:7179]
-1.208312162	8.25E-05	0.005212	GSEC	G-quadruplex forming sequence containing lncRNA [Source:HGNC Symbol;Acc:HGNC:48645]
-1.20560436	2.01E-06	0.000301	FGGY	FGGY carbohydrate kinase domain containing [Source:HGNC Symbol;Acc:HGNC:25610]

log2FoldChange	pvalue	padj	external_gene_name	description
-1.205415404	0.001489	0.038358	CCDC69	coiled-coil domain containing 69 [Source:HGNC Symbol;Acc:HGNC:24487]
-1.204554089	0.00055	0.018928	POPDC3	popeye domain containing 3 [Source:HGNC Symbol;Acc:HGNC:17649]
-1.201268896	9.41E-07	0.000173	DISP1	dispatched RND transporter family member 1 [Source:HGNC Symbol;Acc:HGNC:19711]
-1.199253858	0.000315	0.013441	AASS	aminoadipate-semialdehyde synthase [Source:HGNC Symbol;Acc:HGNC:17366]
-1.187240639	0.000442	0.016571	GSR	glutathione-disulfide reductase [Source:HGNC Symbol;Acc:HGNC:4623]
-1.178261505	0.000334	0.01403	SLC19A3	solute carrier family 19 member 3 [Source:HGNC Symbol;Acc:HGNC:16266]
-1.177802169	0.001471	0.038195	TCN2	transcobalamin 2 [Source:HGNC Symbol;Acc:HGNC:11653]
-1.173656798	0.00177	0.042219	AC124798.1	antisense to KCNJ11 and overlapping to a novel gene
-1.169642297	4.20E-05	0.003088	AC017002.3	novel transcript
-1.162559523	0.00049	0.017571	AC021097.1	novel transcript, antisense to SMARCD3
-1.162023042	0.00026	0.011757	PACRGL	parkin coregulated like [Source:HGNC Symbol;Acc:HGNC:28442]
-1.158062018	0.000431	0.016319	AC011445.2	novel transcript
-1.156652459	0.000409	0.015884	MEGF9	multiple EGF like domains 9 [Source:HGNC Symbol;Acc:HGNC:3234]
-1.154076357	4.50E-08	1.55E-05	SRP14-AS1	SRP14 antisense RNA1 (head to head) [Source:HGNC Symbol;Acc:HGNC:48619]
-1.152549698	1.41E-05	0.001304	HIPK2	homeodomain interacting protein kinase 2 [Source:HGNC Symbol;Acc:HGNC:14402]
-1.152287018	5.64E-07	0.000112	ACOT13	acyl-CoA thioesterase 13 [Source:HGNC Symbol;Acc:HGNC:20999]
-1.148153399	0.00126	0.034231	C5	complement C5 [Source:HGNC Symbol;Acc:HGNC:1331]
-1.146690874	2.22E-09	1.04E-06	PPIF	peptidylprolyl isomerase F [Source:HGNC Symbol;Acc:HGNC:9259]
-1.136161741	2.43E-05	0.002037	ASPH	aspartate beta-hydroxylase [Source:HGNC Symbol;Acc:HGNC:757]
-1.135919685	0.000233	0.010764	MMD	monocyte to macrophage differentiation associated [Source:HGNC Symbol;Acc:HGNC:7153]
-1.124575627	4.15E-06	0.000524	BLVRB	biliverdin reductase B [Source:HGNC Symbol;Acc:HGNC:1063]
-1.118350424	1.13E-06	0.000194	ALDH2	aldehyde dehydrogenase 2 family member [Source:HGNC Symbol;Acc:HGNC:404]
-1.110375216	0.000485	0.017456	INPP4B	inositol polyphosphate-4-phosphatase type II B [Source:HGNC Symbol;Acc:HGNC:6075]
-1.092127326	0.001084	0.030753	MTSS1	MTSS I-BAR domain containing 1 [Source:HGNC Symbol;Acc:HGNC:20443]
-1.090077486	0.000657	0.021284	LHFPL2	LHFPL tetraspan subfamily member 2 [Source:HGNC Symbol;Acc:HGNC:6588]
-1.082852471	0.000659	0.021284	DIRAS3	DIRAS family GTPase 3 [Source:HGNC Symbol;Acc:HGNC:687]

log2FoldChange	pvalue	padj	external_gene_name	description
-1.074435207	0.000371	0.014866	LINC00467	long intergenic non-protein coding RNA 467 [Source:HGNC Symbol;Acc:HGNC:28227]
-1.065250667	7.56E-05	0.004846	AC022400.8	TEC
-1.060842181	0.000384	0.015242	TTC32	tetratricopeptide repeat domain 32 [Source:HGNC Symbol;Acc:HGNC:32954]
-1.060286575	0.001587	0.040049	AC108673.3	novel transcript
-1.06015902	5.64E-05	0.003919	ADI1	acireductone dioxygenase 1 [Source:HGNC Symbol;Acc:HGNC:30576]
-1.056822466	7.88E-06	0.000886	SNHG9	small nucleolar RNA host gene 9 [Source:HGNC Symbol;Acc:HGNC:33102]
-1.04927222	0.001582	0.039977	OGFRL1	opioid growth factor receptor like 1 [Source:HGNC Symbol;Acc:HGNC:21378]
-1.048974878	0.000338	0.014114	ZBTB21	zinc finger and BTB domain containing 21 [Source:HGNC Symbol;Acc:HGNC:13083]
-1.040818083	0.000867	0.026189	ENG	endoglin [Source:HGNC Symbol;Acc:HGNC:3349]
-1.040694595	0.000164	0.008544	G6PD	glucose-6-phosphate dehydrogenase [Source:HGNC Symbol;Acc:HGNC:4057]
-1.0330635	1.05E-06	0.000183	C5orf30	chromosome 5 open reading frame 30 [Source:HGNC Symbol;Acc:HGNC:25052]
-1.031696877	0.000184	0.009246	FAM217B	family with sequence similarity 217 member B [Source:HGNC Symbol;Acc:HGNC:16170]
-1.031688631	1.22E-05	0.001206	TRIM16	tripartite motif containing 16 [Source:HGNC Symbol;Acc:HGNC:17241]
-1.030867636	1.11E-06	0.000192	LY96	lymphocyte antigen 96 [Source:HGNC Symbol;Acc:HGNC:17156]
-1.026907179	0.001199	0.033275	CDC37L1-DT	CDC37L1 divergent transcript [Source:HGNC Symbol;Acc:HGNC:49735]
-1.016224169	0.001063	0.030476	YTHDF3-AS1	YTHDF3 antisense RNA 1 (head to head) [Source:HGNC Symbol;Acc:HGNC:48728]
-1.007416531	0.001654	0.041131	IL1R1	interleukin 1 receptor type 1 [Source:HGNC Symbol;Acc:HGNC:5993]
-1.007017847	5.95E-07	0.000117	MDM2	MDM2 proto-oncogene [Source:HGNC Symbol;Acc:HGNC:6973]
-1.002168864	0.000785	0.024383	OSGIN2	oxidative stress induced growth inhibitor family member 2 [Source:HGNC Symbol;Acc:HGNC:1355]
1.000016106	0.000407	0.015852	AL590867.2	60S ribosomal protein L27a (RPL27A) pseudogene
1.000720363	0.000335	0.014032	RPL13P12	ribosomal protein L13 pseudogene 12 [Source:HGNC Symbol;Acc:HGNC:35701]
1.007734024	4.97E-05	0.003566	BRWD1	bromodomain and WD repeat domain containing 1 [Source:HGNC Symbol;Acc:HGNC:12760]
1.007778717	7.80E-05	0.004966	RPL37P2	ribosomal protein L37 pseudogene 2 [Source:HGNC Symbol;Acc:HGNC:17092]
1.012531793	0.000329	0.0139	CARHSP1	calcium regulated heat stable protein 1 [Source:HGNC Symbol;Acc:HGNC:17150]
1.014724732	0.000293	0.012718	RPL34P27	ribosomal protein L34 pseudogene 27 [Source:HGNC Symbol;Acc:HGNC:36369]

log2FoldChange	pvalue	padj	external_gene_name	description
1.019100678	0.001083	0.030753	PCGF5	polycomb group ring finger 5 [Source:HGNC Symbol;Acc:HGNC:28264]
1.024041148	0.00017	0.008755	ADAMTS1	ADAM metallopeptidase with thrombospondin type 1 motif 1 [Source:HGNC Symbol;Acc:HGNC:217]
1.025181528	0.000123	0.006999	GJC2	gap junction protein gamma 2 [Source:HGNC Symbol;Acc:HGNC:17494]
1.027435596	0.000206	0.009933	LASP1	LIM and SH3 protein 1 [Source:HGNC Symbol;Acc:HGNC:6513]
1.03279323	0.001843	0.043444	SPTLC2	serine palmitoyltransferase long chain base subunit 2 [Source:HGNC Symbol;Acc:HGNC:11278]
1.03325452	0.000848	0.025803	SLC25A4	solute carrier family 25 member 4 [Source:HGNC Symbol;Acc:HGNC:10990]
1.041271997	3.01E-07	6.41E-05	ENAH	ENAH actin regulator [Source:HGNC Symbol;Acc:HGNC:18271]
1.045372156	0.002036	0.046487	RPL26P19	ribosomal protein L26 pseudogene 19 [Source:HGNC Symbol;Acc:HGNC:36393]
1.052336095	9.76E-05	0.006012	CRYBG3	crystallin beta-gamma domain containing 3 [Source:HGNC Symbol;Acc:HGNC:34427]
1.052607387	6.08E-07	0.000118	PLEKHG2	pleckstrin homology and RhoGEF domain containing G2 [Source:HGNC Symbol;Acc:HGNC:29515]
1.056010952	0.001071	0.030627	AC005262.1	ribosomal protein L35 (RPL35) pseudogene
1.057370682	0.001442	0.037693	LOXL2	lysyl oxidase like 2 [Source:HGNC Symbol;Acc:HGNC:6666]
1.059094994	0.00176	0.042167	C14orf28	chromosome 14 open reading frame 28 [Source:HGNC Symbol;Acc:HGNC:19834]
1.062102156	0.001236	0.033879	RPL12P47	ribosomal protein L12 pseudogene 47 [Source:HGNC Symbol;Acc:HGNC:51939]
1.066527139	0.000187	0.009365	CCSAP	centriole, cilia and spindle associated protein [Source:HGNC Symbol;Acc:HGNC:29578]
1.067874178	0.001422	0.03723	MICAL1	microtubule associated monooxygenase, calponin and LIM domain containing 1 [Source:HGNC Symbol;Acc:HGNC:20619]
1.072148037	0.000494	0.01766	FLNC	filamin C [Source:HGNC Symbol;Acc:HGNC:3756]
1.080443614	0.002232	0.049464	RTKN2	rhotekin 2 [Source:HGNC Symbol;Acc:HGNC:19364]
1.084979228	9.71E-07	0.000176	MIEF2	mitochondrial elongation factor 2 [Source:HGNC Symbol;Acc:HGNC:17920]
1.086542995	2.78E-05	0.002234	RPS23P8	ribosomal protein S23 pseudogene 8 [Source:HGNC Symbol;Acc:HGNC:35982]
1.096335554	0.000365	0.014804	CHML	CHM like Rab escort protein [Source:HGNC Symbol;Acc:HGNC:1941]
1.113029719	0.000659	0.021284	ZNF788P	zinc finger family member 788, pseudogene [Source:HGNC Symbol;Acc:HGNC:33112]
1.114263542	0.000282	0.0125	AC073861.1	ribosomal protein S18 (RPS18) pseudogene
1.115460621	0.000247	0.011275	AC021016.3	novel transcript, antisense to CTDSP1

log2FoldChange	pvalue	padj	external_gene_name	description
1.118135728	0.001763	0.042167	AL135905.1	novel transcript, antisense to PTP4A1
1.125961884	0.000221	0.010427	COL5A2	collagen type V alpha 2 chain [Source:HGNC Symbol;Acc:HGNC:2210]
1.128859499	1.34E-05	0.001278	SNHG29	small nucleolar RNA host gene 29 [Source:HGNC Symbol;Acc:HGNC:28619]
1.131022119	0.000414	0.016035	FOXP1-IT1	FOXP1 intronic transcript 1 [Source:HGNC Symbol;Acc:HGNC:41335]
1.136611284	0.000339	0.014114	CILP2	cartilage intermediate layer protein 2 [Source:HGNC Symbol;Acc:HGNC:24213]
1.136832696	0.000115	0.006723	VASP	vasodilator stimulated phosphoprotein [Source:HGNC Symbol;Acc:HGNC:12652]
1.143577178	7.08E-06	0.000807	FARP1	FERM, ARH/RhoGEF and pleckstrin domain protein 1 [Source:HGNC Symbol;Acc:HGNC:3591]
1.14363417	0.000355	0.014488	AL391422.4	novel transcript, antisense to PXDC1
1.146541199	0.000216	0.01028	HTRA1	HtrA serine peptidase 1 [Source:HGNC Symbol;Acc:HGNC:9476]
1.147263161	0.001146	0.03212	WSB1	WD repeat and SOCS box containing 1 [Source:HGNC Symbol;Acc:HGNC:19221]
1.149172138	3.98E-06	0.000507	HAGH	hydroxyacylglutathione hydrolase [Source:HGNC Symbol;Acc:HGNC:4805]
1.149901603	1.96E-05	0.001724	REEP4	receptor accessory protein 4 [Source:HGNC Symbol;Acc:HGNC:26176]
1.151477529	0.000423	0.016124	HOMER1	homer scaffold protein 1 [Source:HGNC Symbol;Acc:HGNC:17512]
1.157554339	4.60E-05	0.003345	NOP14-AS1	NOP14 antisense RNA 1 [Source:HGNC Symbol;Acc:HGNC:20205]
1.158012703	0.000628	0.020768	SLC25A6	solute carrier family 25 member 6 [Source:HGNC Symbol;Acc:HGNC:10992]
1.158065842	3.07E-06	0.000425	SLC43A2	solute carrier family 43 member 2 [Source:HGNC Symbol;Acc:HGNC:23087]
1.167042306	0.000104	0.006297	TUBB6	tubulin beta 6 class V [Source:HGNC Symbol;Acc:HGNC:20776]
1.167183964	0.000132	0.007329	LINC00324	long intergenic non-protein coding RNA 324 [Source:HGNC Symbol;Acc:HGNC:26628]
1.167868465	4.86E-06	0.000601	AOPEP	aminopeptidase O (putative) [Source:HGNC Symbol;Acc:HGNC:1361]
1.171487367	2.23E-05	0.001906	VIM	vimentin [Source:HGNC Symbol;Acc:HGNC:12692]
1.173387363	0.000633	0.020861	SAMD4A	sterile alpha motif domain containing 4A [Source:HGNC Symbol;Acc:HGNC:23023]
1.174637019	0.000227	0.010598	RPL18AP3	ribosomal protein L18a pseudogene 3 [Source:HGNC Symbol;Acc:HGNC:31387]
1.176816822	7.13E-05	0.004641	MYH9	myosin heavy chain 9 [Source:HGNC Symbol;Acc:HGNC:7579]
1.189387343	0.00036	0.014615	TEAD3	TEA domain transcription factor 3 [Source:HGNC Symbol;Acc:HGNC:11716]
1.192130433	0.001858	0.043553	OSBPL10	oxysterol binding protein like 10 [Source:HGNC Symbol;Acc:HGNC:16395]
1.196548938	4.20E-08	1.52E-05	ACTB	actin beta [Source:HGNC Symbol;Acc:HGNC:132]

log2FoldChange	pvalue	padj	external_gene_name	description
1.204614403	1.70E-05	0.001523	FERMT2	fermitin family member 2 [Source:HGNC Symbol;Acc:HGNC:15767]
1.206256584	1.76E-06	0.000275	TRNP1	TMF1 regulated nuclear protein 1 [Source:HGNC Symbol;Acc:HGNC:34348]
1.210375934	1.48E-05	0.001362	MFAP3L	microfibril associated protein 3 like [Source:HGNC Symbol;Acc:HGNC:29083]
1.210677231	0.000195	0.009586	ATP8B1	ATPase phospholipid transporting 8B1 [Source:HGNC Symbol;Acc:HGNC:3706]
1.217524377	0.000121	0.006967	AL355309.1	ribosomal protein L28 pseudogene
1.2178202	0.001923	0.04481	AC027237.4	novel transcript, antisense to PAQR5
1.224487847	0.000179	0.009144	SNX30	sorting nexin family member 30 [Source:HGNC Symbol;Acc:HGNC:23685]
1.226457934	0.00019	0.009454	CYTOR	cytoskeleton regulator RNA [Source:HGNC Symbol;Acc:HGNC:28717]
1.233253406	7.54E-05	0.004846	INSIG2	insulin induced gene 2 [Source:HGNC Symbol;Acc:HGNC:20452]
1.234620398	0.000269	0.012043	ADAM12	ADAM metallopeptidase domain 12 [Source:HGNC Symbol;Acc:HGNC:190]
1.236853602	0.000447	0.016598	CDT1	chromatin licensing and DNA replication factor 1 [Source:HGNC Symbol;Acc:HGNC:24576]
1.244863847	9.22E-06	0.000994	RNY1	RNA, Ro60-associated Y1 [Source:HGNC Symbol;Acc:HGNC:10242]
1.251168863	3.11E-06	0.000425	PLP2	proteolipid protein 2 [Source:HGNC Symbol;Acc:HGNC:9087]
1.253039818	2.66E-10	1.64E-07	NEXN	nexilin F-actin binding protein [Source:HGNC Symbol;Acc:HGNC:29557]
1.254918541	0.001531	0.038912	C12orf75	chromosome 12 open reading frame 75 [Source:HGNC Symbol;Acc:HGNC:35164]
1.256466881	3.69E-06	0.00048	FBLIM1	filamin binding LIM protein 1 [Source:HGNC Symbol;Acc:HGNC:24686]
1.269494428	0.001609	0.040319	RGS5	regulator of G protein signaling 5 [Source:HGNC Symbol;Acc:HGNC:10001]
1.283624522	0.002024	0.046314	GRAMD2B	GRAM domain containing 2B [Source:HGNC Symbol;Acc:HGNC:24911]
1.286833456	0.000349	0.014338	MICAL2	microtubule associated monooxygenase, calponin and LIM domain containing 2 [Source:HGNC Symbol;Acc:HGNC:24693]
1.29445231	0.00148	0.038206	SPARC	secreted protein acidic and cysteine rich [Source:HGNC Symbol;Acc:HGNC:11219]
1.297807229	0.000581	0.0197	ADAMTS6	ADAM metallopeptidase with thrombospondin type 1 motif 6 [Source:HGNC Symbol;Acc:HGNC:222]
1.299236683	0.000498	0.017697	FHL2	four and a half LIM domains 2 [Source:HGNC Symbol;Acc:HGNC:3703]
1.300291165	0.000164	0.008544	GYS1	glycogen synthase 1 [Source:HGNC Symbol;Acc:HGNC:4706]
1.302079273	2.26E-06	0.000323	TPM1	tropomyosin 1 [Source:HGNC Symbol;Acc:HGNC:12010]
1.30462895	9.31E-05	0.005784	SLC1A4	solute carrier family 1 member 4 [Source:HGNC Symbol;Acc:HGNC:10942]

log2FoldChange	pvalue	padj	external_gene_name	description
1.323382555	3.85E-05	0.002893	LINC00672	long intergenic non-protein coding RNA 672 [Source:HGNC Symbol;Acc:HGNC:44353]
1.327633628	0.000842	0.025671	CDH2	cadherin 2 [Source:HGNC Symbol;Acc:HGNC:1759]
1.332164101	4.95E-05	0.003565	RPL10P16	ribosomal protein L10 pseudogene 16 [Source:HGNC Symbol;Acc:HGNC:36882]
1.333089747	1.02E-06	0.000181	TRAF5	TNF receptor associated factor 5 [Source:HGNC Symbol;Acc:HGNC:12035]
1.336831375	0.000244	0.011236	PCSK4	proprotein convertase subtilisin/kexin type 4 [Source:HGNC Symbol;Acc:HGNC:8746]
1.337791364	0.000148	0.007943	TNS1	tensin 1 [Source:HGNC Symbol;Acc:HGNC:11973]
1.341763504	0.000444	0.016576	AC025280.1	novel transcript, sense intronic to CRISPLD2
1.342486659	0.00184	0.043417	DPYSL3	dihydropyrimidinase like 3 [Source:HGNC Symbol;Acc:HGNC:3015]
1.343499317	0.000723	0.023015	CDC42EP3	CDC42 effector protein 3 [Source:HGNC Symbol;Acc:HGNC:16943]
1.351766376	0.000144	0.0078	RRAD	RRAD, Ras related glycolysis inhibitor and calcium channel regulator [Source:HGNC Symbol;Acc:HGNC:10446]
1.357523407	8.74E-07	0.000164	FSTL1	follistatin like 1 [Source:HGNC Symbol;Acc:HGNC:3972]
1.357722081	0.001815	0.043103	DIAPH3	diaphanous related formin 3 [Source:HGNC Symbol;Acc:HGNC:15480]
1.370734853	0.000166	0.008575	CCDC80	coiled-coil domain containing 80 [Source:HGNC Symbol;Acc:HGNC:30649]
1.372893479	1.40E-07	3.65E-05	FANK1	fibronectin type III and ankyrin repeat domains 1 [Source:HGNC Symbol;Acc:HGNC:23527]
1.374530911	0.00198	0.045492	RNF217-AS1	RNF217 antisense RNA 1 (head to head) [Source:HGNC Symbol;Acc:HGNC:50866]
1.383206571	0.000297	0.012794	MT-TP	mitochondrially encoded tRNA-Pro (CCN) [Source:HGNC Symbol;Acc:HGNC:7494]
1.383959031	1.78E-12	2.38E-09	CAVIN1	caveolae associated protein 1 [Source:HGNC Symbol;Acc:HGNC:9688]
1.39329275	0.000288	0.01264	CHAC1	ChaC glutathione specific gamma-glutamylcyclotransferase 1 [Source:HGNC Symbol;Acc:HGNC:28680]
1.398368237	0.001738	0.041988	ARL4A	ADP ribosylation factor like GTPase 4A [Source:HGNC Symbol;Acc:HGNC:695]
1.398609695	1.15E-06	0.000195	BOK	BCL2 family apoptosis regulator BOK [Source:HGNC Symbol;Acc:HGNC:1087]
1.399416247	3.75E-07	7.78E-05	MT-ND6	mitochondrially encoded NADH:ubiquinone oxidoreductase core subunit 6 [Source:HGNC Symbol;Acc:HGNC:7462]
1.402733197	0.000558	0.019059	SLC7A5	solute carrier family 7 member 5 [Source:HGNC Symbol;Acc:HGNC:11063]
1.404638189	3.50E-05	0.002715	COL1A2	collagen type I alpha 2 chain [Source:HGNC Symbol;Acc:HGNC:2198]
1.410411444	0.000169	0.008706	AC093535.2	tec
1.410691271	0.000285	0.012535	DPF1	double PHD fingers 1 [Source:HGNC Symbol;Acc:HGNC:20225]

log2FoldChange	pvalue	padj	external_gene_name	description
1.411646183	1.09E-05	0.001114	PPME1	protein phosphatase methylesterase 1 [Source:HGNC Symbol;Acc:HGNC:30178]
1.418313829	8.34E-05	0.005254	DISC1	DISC1 scaffold protein [Source:HGNC Symbol;Acc:HGNC:2888]
1.419332904	0.000154	0.00815	CCDC189	coiled-coil domain containing 189 [Source:HGNC Symbol;Acc:HGNC:28078]
1.41951524	0.000297	0.012794	RNY4	RNA, Ro60-associated Y4 [Source:HGNC Symbol;Acc:HGNC:10244]
1.421041338	0.000497	0.017697	MYEF2	myelin expression factor 2 [Source:HGNC Symbol;Acc:HGNC:17940]
1.421929911	0.000626	0.02075	NEDD9	neural precursor cell expressed, developmentally down-regulated 9 [Source:HGNC Symbol;Acc:HGNC:7733]
1.42891018	6.24E-05	0.004217	ENO2	enolase 2 [Source:HGNC Symbol;Acc:HGNC:3353]
1.434661357	9.32E-05	0.005784	FST	follistatin [Source:HGNC Symbol;Acc:HGNC:3971]
1.441182465	0.001678	0.041327	PTGS2	prostaglandin-endoperoxide synthase 2 [Source:HGNC Symbol;Acc:HGNC:9605]
1.44194307	0.000104	0.006297	TUBBP1	tubulin beta pseudogene 1 [Source:HGNC Symbol;Acc:HGNC:12414]
1.442594865	0.00054	0.018695	PCDHGA5	protocadherin gamma subfamily A, 5 [Source:HGNC Symbol;Acc:HGNC:8703]
1.444167445	7.27E-07	0.000139	COL5A1	collagen type V alpha 1 chain [Source:HGNC Symbol;Acc:HGNC:2209]
1.452577065	6.07E-06	0.000726	DSP	desmoplakin [Source:HGNC Symbol;Acc:HGNC:3052]
1.460720682	0.002197	0.04894	CAMK1D	calcium/calmodulin dependent protein kinase ID [Source:HGNC Symbol;Acc:HGNC:19341]
1.47055666	1.24E-05	0.001217	EEF1A1	eukaryotic translation elongation factor 1 alpha 1 [Source:HGNC Symbol;Acc:HGNC:3189]
1.47206793	6.26E-06	0.000738	EHD1	EH domain containing 1 [Source:HGNC Symbol;Acc:HGNC:3242]
1.480405838	5.77E-06	0.000698	COBLL1	cordon-bleu WH2 repeat protein like 1 [Source:HGNC Symbol;Acc:HGNC:23571]
1.481530534	2.06E-07	4.99E-05	CTPS1	CTP synthase 1 [Source:HGNC Symbol;Acc:HGNC:2519]
1.486892955	6.12E-10	3.05E-07	FLNA	filamin A [Source:HGNC Symbol;Acc:HGNC:3754]
1.501076989	0.000123	0.006999	FRY	FRY microtubule binding protein [Source:HGNC Symbol;Acc:HGNC:20367]
1.505410747	1.97E-07	4.84E-05	FILIP1L	filamin A interacting protein 1 like [Source:HGNC Symbol;Acc:HGNC:24589]
1.507707363	0.000389	0.015399	NPR3	natriuretic peptide receptor 3 [Source:HGNC Symbol;Acc:HGNC:7945]
1.519755784	0.002073	0.046901	LINC00933	long intergenic non-protein coding RNA 933 [Source:HGNC Symbol;Acc:HGNC:48625]
1.526652925	3.64E-09	1.61E-06	PDLIM7	PDZ and LIM domain 7 [Source:HGNC Symbol;Acc:HGNC:22958]
1.53013058	1.66E-06	0.000262	SH3PXD2A	SH3 and PX domains 2A [Source:HGNC Symbol;Acc:HGNC:23664]

log2FoldChange	pvalue	padj	external_gene_name	description
1.54229007	4.13E-05	0.003051	KCTD11	potassium channel tetramerization domain containing 11 [Source:HGNC Symbol;Acc:HGNC:21302]
1.549869042	0.000919	0.027251	RASA4CP	RAS p21 protein activator 4C, pseudogene [Source:HGNC Symbol;Acc:HGNC:44185]
1.553328347	0.001475	0.038195	CCDC148	coiled-coil domain containing 148 [Source:HGNC Symbol;Acc:HGNC:25191]
1.553543947	0.000874	0.026281	EGR2	early growth response 2 [Source:HGNC Symbol;Acc:HGNC:3239]
1.561543812	4.54E-08	1.55E-05	TES	testin LIM domain protein [Source:HGNC Symbol;Acc:HGNC:14620]
1.562227696	0.001714	0.041866	AC132872.4	TEC
1.562325021	2.83E-06	0.000395	HIC1	HIC ZBTB transcriptional repressor 1 [Source:HGNC Symbol;Acc:HGNC:4909]
1.576648697	6.69E-05	0.004404	FAM129A	family with sequence similarity 129 member A [Source:HGNC Symbol;Acc:HGNC:16784]
1.582469719	1.08E-07	2.98E-05	TUBB2B	tubulin beta 2B class IIb [Source:HGNC Symbol;Acc:HGNC:30829]
1.587336831	0.000475	0.017182	C1orf198	chromosome 1 open reading frame 198 [Source:HGNC Symbol;Acc:HGNC:25900]
1.598035092	0.000139	0.00757	RAMP1	receptor activity modifying protein 1 [Source:HGNC Symbol;Acc:HGNC:9843]
1.600701638	0.00036	0.014615	ANXA2P2	annexin A2 pseudogene 2 [Source:HGNC Symbol;Acc:HGNC:539]
1.601548958	1.98E-10	1.28E-07	CALD1	caldesmon 1 [Source:HGNC Symbol;Acc:HGNC:1441]
1.610266478	2.01E-05	0.001744	VWA1	von Willebrand factor A domain containing 1 [Source:HGNC Symbol;Acc:HGNC:30910]
1.610989033	1.46E-13	2.54E-10	CSRP1	cysteine and glycine rich protein 1 [Source:HGNC Symbol;Acc:HGNC:2469]
1.618458132	3.67E-11	3.20E-08	HSPB1	heat shock protein family B (small) member 1 [Source:HGNC Symbol;Acc:HGNC:5246]
1.628147321	0.000726	0.023073	ROR1	receptor tyrosine kinase like orphan receptor 1 [Source:HGNC Symbol;Acc:HGNC:10256]
1.653498124	2.81E-14	6.13E-11	TGFB1I1	transforming growth factor beta 1 induced transcript 1 [Source:HGNC Symbol;Acc:HGNC:11767]
1.655353841	0.000289	0.01264	ADAM19	ADAM metallopeptidase domain 19 [Source:HGNC Symbol;Acc:HGNC:197]
1.656780308	0.0011	0.031142	SPINT2	serine peptidase inhibitor, Kunitz type 2 [Source:HGNC Symbol;Acc:HGNC:11247]
1.665838657	5.14E-10	2.72E-07	EDIL3	EGF like repeats and discoidin domains 3 [Source:HGNC Symbol;Acc:HGNC:3173]
1.667528361	1.71E-10	1.22E-07	ACTN1	actinin alpha 1 [Source:HGNC Symbol;Acc:HGNC:163]
1.671941062	1.18E-15	3.42E-12	SNHG32	small nucleolar RNA host gene 32 [Source:HGNC Symbol;Acc:HGNC:19078]
1.683125052	7.33E-05	0.004752	NALCN	sodium leak channel, non-selective [Source:HGNC Symbol;Acc:HGNC:19082]
1.687632289	0.000909	0.027111	EFHD1	EF-hand domain family member D1 [Source:HGNC Symbol;Acc:HGNC:29556]

log2FoldChange	pvalue	padj	external_gene_name	description
1.701210177	0.000588	0.019784	CHADL	chondroadherin like [Source:HGNC Symbol;Acc:HGNC:25165]
1.703208823	0.001134	0.031853	ENSG00000280551	ENSG00000280551
1.705486478	0.000183	0.009246	ZSWIM4	zinc finger SWIM-type containing 4 [Source:HGNC Symbol;Acc:HGNC:25704]
1.721743871	0.00014	0.007626	COL3A1	collagen type III alpha 1 chain [Source:HGNC Symbol;Acc:HGNC:2201]
1.739165767	0.000405	0.015825	AC048380.2	TEC
1.754606481	0.000219	0.010332	MPP2	membrane palmitoylated protein 2 [Source:HGNC Symbol;Acc:HGNC:7220]
1.754665893	0.000653	0.021238	SHROOM3	shroom family member 3 [Source:HGNC Symbol;Acc:HGNC:30422]
1.761736512	0.00196	0.045325	SCAND2P	SCAN domain containing 2 pseudogene [Source:HGNC Symbol;Acc:HGNC:10567]
1.782533976	0.00071	0.022646	WNT5A	Wnt family member 5A [Source:HGNC Symbol;Acc:HGNC:12784]
1.784555432	0.000115	0.006723	GPM6B	glycoprotein M6B [Source:HGNC Symbol;Acc:HGNC:4461]
1.785606115	0.000156	0.0082	THBS2	thrombospondin 2 [Source:HGNC Symbol;Acc:HGNC:11786]
1.792243827	0.000959	0.02811	ADM2	adrenomedullin 2 [Source:HGNC Symbol;Acc:HGNC:28898]
1.795496104	1.34E-07	3.55E-05	MT-TS1	mitochondrially encoded tRNA-Ser (UCN) 1 [Source:HGNC Symbol;Acc:HGNC:7497]
1.808146098	0.000195	0.009586	PDLIM3	PDZ and LIM domain 3 [Source:HGNC Symbol;Acc:HGNC:20767]
1.815313843	0.001054	0.030324	CARMN	cardiac mesoderm enhancer-associated non-coding RNA [Source:HGNC Symbol;Acc:HGNC:42872]
1.838604265	6.63E-08	2.06E-05	MBNL1-AS1	MBNL1 antisense RNA 1 [Source:HGNC Symbol;Acc:HGNC:44584]
1.839002969	0.000245	0.01124	CRISPLD2	cysteine rich secretory protein LCCL domain containing 2 [Source:HGNC Symbol;Acc:HGNC:25248]
1.839227118	0.001721	0.041866	AC130371.2	novel transcript
1.843282934	0.000807	0.024809	DPYSL4	dihydropyrimidinase like 4 [Source:HGNC Symbol;Acc:HGNC:3016]
1.848454976	2.88E-21	1.67E-17	MYL9	myosin light chain 9 [Source:HGNC Symbol;Acc:HGNC:15754]
1.85073635	2.50E-06	0.000354	AC002350.1	novel transcript
1.852994146	1.35E-12	1.96E-09	ALDH1B1	aldehyde dehydrogenase 1 family member B1 [Source:HGNC Symbol;Acc:HGNC:407]
1.856424274	6.09E-05	0.00413	MIR1915HG	MIR1915 host gene [Source:HGNC Symbol;Acc:HGNC:31448]
1.856503373	0.000327	0.013836	ICAM5	intercellular adhesion molecule 5 [Source:HGNC Symbol;Acc:HGNC:5348]
1.86204635	8.64E-06	0.000952	YPEL1	yippee like 1 [Source:HGNC Symbol;Acc:HGNC:12845]

log2FoldChange	pvalue	padj	external_gene_name	description
1.868099191	9.19E-05	0.005745	SCN3A	sodium voltage-gated channel alpha subunit 3 [Source:HGNC Symbol;Acc:HGNC:10590]
1.906037796	0.000224	0.010493	FGF1	fibroblast growth factor 1 [Source:HGNC Symbol;Acc:HGNC:3665]
1.913684272	7.66E-07	0.000145	LRRC75A	leucine rich repeat containing 75A [Source:HGNC Symbol;Acc:HGNC:32403]
1.940687655	0.000233	0.010764	COL4A4	collagen type IV alpha 4 chain [Source:HGNC Symbol;Acc:HGNC:2206]
1.940838901	9.54E-05	0.005898	NPAS1	neuronal PAS domain protein 1 [Source:HGNC Symbol;Acc:HGNC:7894]
1.971961984	0.000131	0.007271	LMCD1	LIM and cysteine rich domains 1 [Source:HGNC Symbol;Acc:HGNC:6633]
1.98698804	0.002191	0.048879	ZNF853	zinc finger protein 853 [Source:HGNC Symbol;Acc:HGNC:21767]
1.994695977	2.61E-05	0.002133	PLCB4	phospholipase C beta 4 [Source:HGNC Symbol;Acc:HGNC:9059]
1.995354408	2.75E-12	3.33E-09	COL4A2	collagen type IV alpha 2 chain [Source:HGNC Symbol;Acc:HGNC:2203]
2.006306967	1.67E-05	0.001503	INHBA	inhibin subunit beta A [Source:HGNC Symbol;Acc:HGNC:6066]
2.014379878	3.74E-09	1.61E-06	PRKCZ-AS1	PRKCZ antisense RNA 1 [Source:HGNC Symbol;Acc:HGNC:40477]
2.018325556	3.31E-08	1.23E-05	MT-TQ	mitochondrially encoded tRNA-Gln (CAA/G) [Source:HGNC Symbol;Acc:HGNC:7495]
2.025930345	0.000449	0.016606	HSD17B6	hydroxysteroid 17-beta dehydrogenase 6 [Source:HGNC Symbol;Acc:HGNC:23316]
2.02942752	0.001732	0.041953	HLA-L	major histocompatibility complex, class I, L (pseudogene) [Source:HGNC Symbol;Acc:HGNC:4970]
2.050174385	0.001198	0.033275	CCDC144NL-AS1	CCDC144NL antisense RNA 1 [Source:HGNC Symbol;Acc:HGNC:51340]
2.056453882	5.18E-14	1.00E-10	TPM2	tropomyosin 2 [Source:HGNC Symbol;Acc:HGNC:12011]
2.067607339	0.001846	0.043456	AC106820.2	novel transcript, antisense to C16orf59
2.084521959	0.000919	0.027251	AC136604.3	novel transcript
2.09710204	0.000396	0.015542	EXTL1	exostosin like glycosyltransferase 1 [Source:HGNC Symbol;Acc:HGNC:3515]
2.1008013	0.00013	0.007271	DACT1	dishevelled binding antagonist of beta catenin 1 [Source:HGNC Symbol;Acc:HGNC:17748]
2.132624334	1.80E-06	0.000275	AC116917.1	pseudogene similar to part of tropomyosin 2 (beta) TPM2
2.14127347	0.000346	0.014293	4-Mar	membrane associated ring-CH-type finger 4 [Source:HGNC Symbol;Acc:HGNC:29269]
2.147110489	0.000379	0.015072	KIRREL3	kirre like nephrin family adhesion molecule 3 [Source:HGNC Symbol;Acc:HGNC:23204]
2.158148032	0.000503	0.017788	HAPLN1	hyaluronan and proteoglycan link protein 1 [Source:HGNC Symbol;Acc:HGNC:2380]
2.161336501	3.82E-06	0.000494	MUC1	mucin 1, cell surface associated [Source:HGNC Symbol;Acc:HGNC:7508]
2.169741858	0.000103	0.006279	TFR2	transferrin receptor 2 [Source:HGNC Symbol;Acc:HGNC:11762]

log2FoldChange	pvalue	padj	external_gene_name	description
2.172594395	1.80E-06	0.000275	CPNE5	copine 5 [Source:HGNC Symbol;Acc:HGNC:2318]
2.190899379	1.33E-05	0.001271	LINC00702	long intergenic non-protein coding RNA 702 [Source:HGNC Symbol;Acc:HGNC:44676]
2.194056357	0.000707	0.022589	P2RY6	pyrimidinergic receptor P2Y6 [Source:HGNC Symbol;Acc:HGNC:8543]
2.198656053	0.000157	0.008259	ABLIM2	actin binding LIM protein family member 2 [Source:HGNC Symbol;Acc:HGNC:19195]
2.199734424	1.97E-07	4.84E-05	NUAK1	NUAK family kinase 1 [Source:HGNC Symbol;Acc:HGNC:14311]
2.243296437	0.001229	0.033741	MEX3B	mex-3 RNA binding family member B [Source:HGNC Symbol;Acc:HGNC:25297]
2.248477642	2.76E-05	0.00223	CACNB4	calcium voltage-gated channel auxiliary subunit beta 4 [Source:HGNC Symbol;Acc:HGNC:1404]
2.257775575	4.49E-07	9.11E-05	CCDC81	coiled-coil domain containing 81 [Source:HGNC Symbol;Acc:HGNC:26281]
2.273389261	0.000903	0.026978	NCKAP1L	NCK associated protein 1 like [Source:HGNC Symbol;Acc:HGNC:4862]
2.27551113	0.001683	0.041327	ISM2	isthmin 2 [Source:HGNC Symbol;Acc:HGNC:23176]
2.295859188	0.000833	0.02554	IGFBP7-AS1	IGFBP7 antisense RNA 1 [Source:HGNC Symbol;Acc:HGNC:40296]
2.304284896	0.001074	0.030653	AC087164.1	novel transcript
2.307428503	1.89E-10	1.27E-07	COL4A1	collagen type IV alpha 1 chain [Source:HGNC Symbol;Acc:HGNC:2202]
2.318545561	3.80E-07	7.80E-05	LMOD1	leiomodin 1 [Source:HGNC Symbol;Acc:HGNC:6647]
2.333397431	0.002243	0.049578	ATG9B	autophagy related 9B [Source:HGNC Symbol;Acc:HGNC:21899]
2.349813058	0.000472	0.017129	PDZD4	PDZ domain containing 4 [Source:HGNC Symbol;Acc:HGNC:21167]
2.350178327	0.000569	0.019356	FBXL22	F-box and leucine rich repeat protein 22 [Source:HGNC Symbol;Acc:HGNC:27537]
2.36476176	3.00E-08	1.14E-05	COL12A1	collagen type XII alpha 1 chain [Source:HGNC Symbol;Acc:HGNC:2188]
2.371620968	0.000591	0.019863	PDZK1IP1	PDZK1 interacting protein 1 [Source:HGNC Symbol;Acc:HGNC:16887]
2.378263144	0.001382	0.036501	HLA-J	major histocompatibility complex, class I, J (pseudogene) [Source:HGNC Symbol;Acc:HGNC:4967]
2.380651948	8.68E-06	0.000952	OXTR	oxytocin receptor [Source:HGNC Symbol;Acc:HGNC:8529]
2.387113074	6.14E-06	0.000729	NREP	neuronal regeneration related protein [Source:HGNC Symbol;Acc:HGNC:16834]
2.415137546	6.57E-05	0.004357	NANOS3	nanos C2HC-type zinc finger 3 [Source:HGNC Symbol;Acc:HGNC:22048]
2.421918197	1.19E-18	4.14E-15	AP000892.3	novel transcript
2.426682996	5.88E-06	0.000707	VTRNA1-3	vault RNA 1-3 [Source:HGNC Symbol;Acc:HGNC:12656]

log2FoldChange	pvalue	padj	external_gene_name	description
2.448143685	0.000137	0.007471	RASGRP1	RAS guanyl releasing protein 1 [Source:HGNC Symbol;Acc:HGNC:9878]
2.449621076	0.000145	0.007819	SHROOM2	shroom family member 2 [Source:HGNC Symbol;Acc:HGNC:630]
2.457298216	1.95E-08	7.57E-06	PPP1R14A	protein phosphatase 1 regulatory inhibitor subunit 14A [Source:HGNC Symbol;Acc:HGNC:14871]
2.457372575	1.65E-28	2.87E-24	TAGLN	transgelin [Source:HGNC Symbol;Acc:HGNC:11553]
2.506825647	1.30E-05	0.001264	CTXN1	cortexin 1 [Source:HGNC Symbol;Acc:HGNC:31108]
2.52721223	0.000131	0.007271	ARFGEF3	ARFGEF family member 3 [Source:HGNC Symbol;Acc:HGNC:21213]
2.53748301	1.02E-06	0.000181	CCDC184	coiled-coil domain containing 184 [Source:HGNC Symbol;Acc:HGNC:33749]
2.552219613	0.00185	0.04348	NOS1	nitric oxide synthase 1 [Source:HGNC Symbol;Acc:HGNC:7872]
2.553545499	7.07E-06	0.000807	COL1A1	collagen type I alpha 1 chain [Source:HGNC Symbol;Acc:HGNC:2197]
2.572457146	0.000564	0.01921	CX3CL1	C-X3-C motif chemokine ligand 1 [Source:HGNC Symbol;Acc:HGNC:10647]
2.595623593	0.001476	0.038195	AL121749.1	novel transcript
2.609010211	1.15E-05	0.001154	TSPAN2	tetraspanin 2 [Source:HGNC Symbol;Acc:HGNC:20659]
2.623678495	0.001167	0.03258	FAM43B	family with sequence similarity 43 member B [Source:HGNC Symbol;Acc:HGNC:31791]
2.629808933	0.001223	0.033698	SAA1	serum amyloid A1 [Source:HGNC Symbol;Acc:HGNC:10513]
2.650453722	0.001403	0.036866	WIPF3	WAS/WASL interacting protein family member 3 [Source:HGNC Symbol;Acc:HGNC:22004]
2.677232651	0.000826	0.025347	JAM2	junctional adhesion molecule 2 [Source:HGNC Symbol;Acc:HGNC:14686]
2.695337757	0.000212	0.010145	LINC01583	long intergenic non-protein coding RNA 1583 [Source:HGNC Symbol;Acc:HGNC:51425]
2.706634382	0.000476	0.017182	AL021392.1	novel transcript
2.715572876	5.04E-08	1.66E-05	COL4A3	collagen type IV alpha 3 chain [Source:HGNC Symbol;Acc:HGNC:2204]
2.725578882	7.17E-08	2.16E-05	JPH2	junctophilin 2 [Source:HGNC Symbol;Acc:HGNC:14202]
2.752066866	0.001808	0.043003	AMZ1	archaelysin family metallopeptidase 1 [Source:HGNC Symbol;Acc:HGNC:22231]
2.793492749	0.000786	0.024383	SAA2	serum amyloid A2 [Source:HGNC Symbol;Acc:HGNC:10514]
2.808210849	0.000127	0.007182	PITX2	paired like homeodomain 2 [Source:HGNC Symbol;Acc:HGNC:9005]
2.820699723	2.33E-05	0.001973	AC004151.1	Rho GTPase activating protein 45 [Source:NCBI gene;Acc:23526]
2.830121968	0.001767	0.042209	COL17A1	collagen type XVII alpha 1 chain [Source:HGNC Symbol;Acc:HGNC:2194]
2.840593221	4.62E-08	1.55E-05	ANKRD1	ankyrin repeat domain 1 [Source:HGNC Symbol;Acc:HGNC:15819]

log2FoldChange	pvalue	padj	external_gene_name	description
2.885447697	0.001324	0.035422	CA8	carbonic anhydrase 8 [Source:HGNC Symbol;Acc:HGNC:1382]
2.889825377	0.00137	0.036324	FAM110C	family with sequence similarity 110 member C [Source:HGNC Symbol;Acc:HGNC:33340]
2.954822876	0.001052	0.030324	AC131649.1	novel transcript
2.972517439	0.001274	0.034405	PCSK9	proprotein convertase subtilisin/kexin type 9 [Source:HGNC Symbol;Acc:HGNC:20001]
2.977768153	0.000638	0.020943	SPRN	shadow of prion protein [Source:HGNC Symbol;Acc:HGNC:16871]
2.981300739	5.97E-10	3.05E-07	LIMS2	LIM zinc finger domain containing 2 [Source:HGNC Symbol;Acc:HGNC:16084]
3.064402516	6.40E-06	0.000744	NOG	noggin [Source:HGNC Symbol;Acc:HGNC:7866]
3.082056384	0.000472	0.017129	NRXN3	neurexin 3 [Source:HGNC Symbol;Acc:HGNC:8010]
3.089054362	0.000334	0.01403	AL356417.2	novel transcript, antisense to FNDC1
3.096517045	1.72E-23	1.50E-19	MYLK	myosin light chain kinase [Source:HGNC Symbol;Acc:HGNC:7590]
3.139023861	2.00E-13	3.16E-10	SYNPO2	synaptopodin 2 [Source:HGNC Symbol;Acc:HGNC:17732]
3.152594814	2.44E-05	0.002037	TMEM74B	transmembrane protein 74B [Source:HGNC Symbol;Acc:HGNC:15893]
3.174439257	0.001248	0.034013	FAM71F1	family with sequence similarity 71 member F1 [Source:HGNC Symbol;Acc:HGNC:30704]
3.175447308	6.73E-11	5.59E-08	AL590004.3	novel transcript
3.194742549	1.12E-07	3.05E-05	BCYRN1	brain cytoplasmic RNA 1 [Source:HGNC Symbol;Acc:HGNC:1022]
3.287287189	1.92E-09	9.28E-07	ACTA2	actin alpha 2, smooth muscle [Source:HGNC Symbol;Acc:HGNC:130]
3.288208667	2.87E-10	1.64E-07	AC023449.2	novel transcript, sense intronic to ATP10A
3.299670654	0.000106	0.006377	CELSR1	cadherin EGF LAG seven-pass G-type receptor 1 [Source:HGNC Symbol;Acc:HGNC:1850]
3.328106127	0.000123	0.006999	RF01210	
3.427440601	1.90E-05	0.001693	RNF165	ring finger protein 165 [Source:HGNC Symbol;Acc:HGNC:31696]
3.497878846	8.17E-08	2.37E-05	SORBS1	sorbin and SH3 domain containing 1 [Source:HGNC Symbol;Acc:HGNC:14565]
3.50882249	0.000192	0.009507	KCNH6	potassium voltage-gated channel subfamily H member 6 [Source:HGNC Symbol;Acc:HGNC:18862]
3.551004498	0.000342	0.014216	C15orf48	chromosome 15 open reading frame 48 [Source:HGNC Symbol;Acc:HGNC:29898]
3.568724472	0.001217	0.033625	LMF1-AS1	LMF1 antisense RNA 1 [Source:HGNC Symbol;Acc:HGNC:50469]
3.578588552	3.86E-12	4.09E-09	CNN1	calponin 1 [Source:HGNC Symbol;Acc:HGNC:2155]
3.612165727	0.001295	0.034798	TRIM31	tripartite motif containing 31 [Source:HGNC Symbol;Acc:HGNC:16289]

log2FoldChange	pvalue	padj	external_gene_name	description
3.682469322	0.002268	0.049868	AL021707.8	novel transcript, sense intronic to SUN2
3.725716695	0.000118	0.006861	FAM153B	family with sequence similarity 153 member B [Source:HGNC Symbol;Acc:HGNC:27323]
3.773958124	0.000118	0.006877	KLC3	kinesin light chain 3 [Source:HGNC Symbol;Acc:HGNC:20717]
3.820256854	0.001085	0.030753	BEND5	BEN domain containing 5 [Source:HGNC Symbol;Acc:HGNC:25668]
3.848812039	0.000935	0.027538	AC007608.1	novel transcript, antisense to NKD1
3.851257269	0.000836	0.02554	LINC00547	long intergenic non-protein coding RNA 547 [Source:HGNC Symbol;Acc:HGNC:43682]
3.854946481	5.29E-08	1.71E-05	ENTPD1	ectonucleoside triphosphate diphosphohydrolase 1 [Source:HGNC Symbol;Acc:HGNC:3363]
3.858314201	1.89E-07	4.82E-05	CASC18	cancer susceptibility 18 [Source:HGNC Symbol;Acc:HGNC:49463]
3.961101804	0.000758	0.023729	CYP26C1	cytochrome P450 family 26 subfamily C member 1 [Source:HGNC Symbol;Acc:HGNC:20577]
4.229639411	2.53E-07	5.78E-05	L1CAM	L1 cell adhesion molecule [Source:HGNC Symbol;Acc:HGNC:6470]
4.260908104	2.50E-05	0.002064	COL11A1	collagen type XI alpha 1 chain [Source:HGNC Symbol;Acc:HGNC:2186]
4.508222167	7.78E-08	2.30E-05	IGF1	insulin like growth factor 1 [Source:HGNC Symbol;Acc:HGNC:5464]
4.519847248	0.001717	0.041866	FOXQ1	forkhead box Q1 [Source:HGNC Symbol;Acc:HGNC:20951]
4.590532126	1.06E-05	0.001098	SLAMF8	SLAM family member 8 [Source:HGNC Symbol;Acc:HGNC:21391]
4.613106918	0.001703	0.041781	AC090377.1	novel transcript
4.638564149	1.91E-07	4.82E-05	NPPB	natriuretic peptide B [Source:HGNC Symbol;Acc:HGNC:7940]
4.655607431	2.73E-07	6.03E-05	ACTG2	actin gamma 2, smooth muscle [Source:HGNC Symbol;Acc:HGNC:145]
4.658907623	1.01E-05	0.001053	NPTX1	neuronal pentraxin 1 [Source:NCBI gene;Acc:4884]
4.711081864	0.000524	0.018285	AL691449.1	ribosomal protein L26 pseudogene (RPL26)
4.769092033	0.00013	0.007271	HOXA13	homeobox A13 [Source:HGNC Symbol;Acc:HGNC:5102]
4.789088417	0.00085	0.025812	AL138787.1	implantation-associated protein (DKFZp564K142) pseudogene
4.92772323	0.000531	0.018408	FAM153A	family with sequence similarity 153 member A [Source:HGNC Symbol;Acc:HGNC:29940]
5.087730169	2.48E-09	1.14E-06	KIAA0040	KIAA0040 [Source:HGNC Symbol;Acc:HGNC:28950]
5.170450992	2.55E-07	5.78E-05	CADM3	cell adhesion molecule 3 [Source:HGNC Symbol;Acc:HGNC:17601]
5.241424714	2.02E-06	0.000301	AC010976.2	novel transcript, antisense to MYO7B

log2FoldChange	pvalue	padj	external_gene_name	description
5.302968086	4.98E-10	2.72E-07	EPPK1	epiplakin 1 [Source:HGNC Symbol;Acc:HGNC:15577]
5.392749407	1.36E-10	1.04E-07	KRT34	keratin 34 [Source:HGNC Symbol;Acc:HGNC:6452]
5.410349352	2.26E-05	0.001919	ACKR1	atypical chemokine receptor 1 (Duffy blood group) [Source:HGNC Symbol;Acc:HGNC:4035]
5.902515175	3.58E-06	0.000472	ESPN	espin [Source:HGNC Symbol;Acc:HGNC:13281]